Budker Institute of Nuclear Physics

Conceptual Design Report on Superconducting Dipole Magnet Designed for the CBM detector

Novosibirsk
August, 2019

THIS WORK HAS BEEN DONE UNDER SPECIFIC CONSULTANCY AGREEMENT BETWEEN FAIR FROM ONE SIDE AND BINP FROM THE OTHER SIDE FOR A FEASABILITY STUDY AND A CONCEPTUAL DESIGN OF A SUPERCONDUCTING DIPOLE MAGNET FOR THE CBM DETECTOR

BINP authors of the report are:

Mezentsev N.	e-mail: N.A.Mezentsev@inp.nsk.su
Bragin A.	e-mail: A.V.Bragin@inp.nsk.su
Pivovarov S.	e-mail: S.G.Pivovarov@inp.nsk.su
Shkaruba V.	e-mail: V.A.Shkaruba@inp.nsk.su
Erokhin A.	e-mail: A.I.Erokhin@inp.nsk.su
Khrushchev S.	e-mail: S.V.Khrushchev@inp.nsk.su
Tsukanov V.	e-mail: V.M.Tsukanov@inp.nsk.su
Volkov A.	e-mail: A.A.Volkov@inp.nsk.su
Tarasenko O.	e-mail: O.A.Tarasenko@inp.nsk.su
Syrovatin V	e-mail: V.M.Syrovatin@inp.nsk.su
Kholopov M.	e-mail: M.A.Kholopov@inp.nsk.su

With participation of GSI colleagues:

Peter Snger
Gebhard Moritz
Marion Kauschke

BINP director adviser,
Budker Institute of Nuclear Physics,

Mezentsev N.A.

CONTENT

1. Introduction

1.1 Content of the conceptual design

The scope of the contract is to design, manufacture, measure, deliver, install and commission the superconducting dipole magnet for CBM experiment at FAIR.

The Budker INP agrees to satisfy to the main parameters of the superconducting magnet for the CBM presented in "Collaboration Contract CBM Magnet BINP Annex3 specifications", design, prototyping, production, delivery, assembly and testing of the complete Dipole Magnet for the CBM experiment and tools necessary for its transport, storage and assembly Acceptance Test at the Customer's Site and Commissioning of the CBM superconducting magnet for the FAIR including extent of delivery, general conditions of the Contract, General mechanical requirements, general manufacturing standards, instrumentation and, documentation.

The conceptual design report should present the following items:

- Magnetic field calculations;
- Design of superconducting cable and coil;
- Quench calculations;
- Stress calculations, including all mechanical structures;
- Design of cryogenics including the cryostat, brunch box, feed box and cryogenic lines.

1.2 Preamble

The superconducting dipole magnet will be installed in the CBM detector at FAIR. The magnet provides vertical magnetic field with a magnetic field integral of 1 T*m which is needed to obtain a momentum resolution of $\Delta p/p=1$ % for track reconstruction at FAIR beam energies.

The magnet gap has a height of 144 cm and a width of 300 cm in order to accommodate the STS detector system with a polar angle acceptance of 25° and a horizontal acceptance of 30°. The magnet is of the H-type with a warm iron yoke/pole and cylindrical superconducting coils. The coil winding has 1716 turns. The wire has Nb-Ti filaments embedded into a copper matrix with a total Cu/SC ratio of about 7.1. The operating current and the maximal magnetic field in the coils are 666 A and 3.8 T, respectively. The coil winding will be embedded in a copper case. The vertical force in the coils is about 300 tons at test current of 700 A. The cold mass is suspended from the room temperature vacuum vessel by eight suspension titanium rods. Eight cylindrical support struts (or one large strut) will compensate the vertical forces. The energy stored in the magnet is about 5 MJ.

1.3 General requirements

The scope of delivery includes the following, see Fig. 1:

- Magnetic and engineering design of the magnet including all necessary tools, dimensioning calculations for stands and lifting units, etc;
- Engineering design of the Feed Box and the Branch Box incl. the cryogenic connection line;
- Production and delivery of the magnet (consisting of yoke, cold masses and cryostats, alignment components, Feed box and stand), the Branch Box, the cryogenic connection line and all tools;
- Engineering design, production and delivery of the Power Converter;
- Transportation of all components to site, complete assembly and the preparation of installation;
- Documentation.

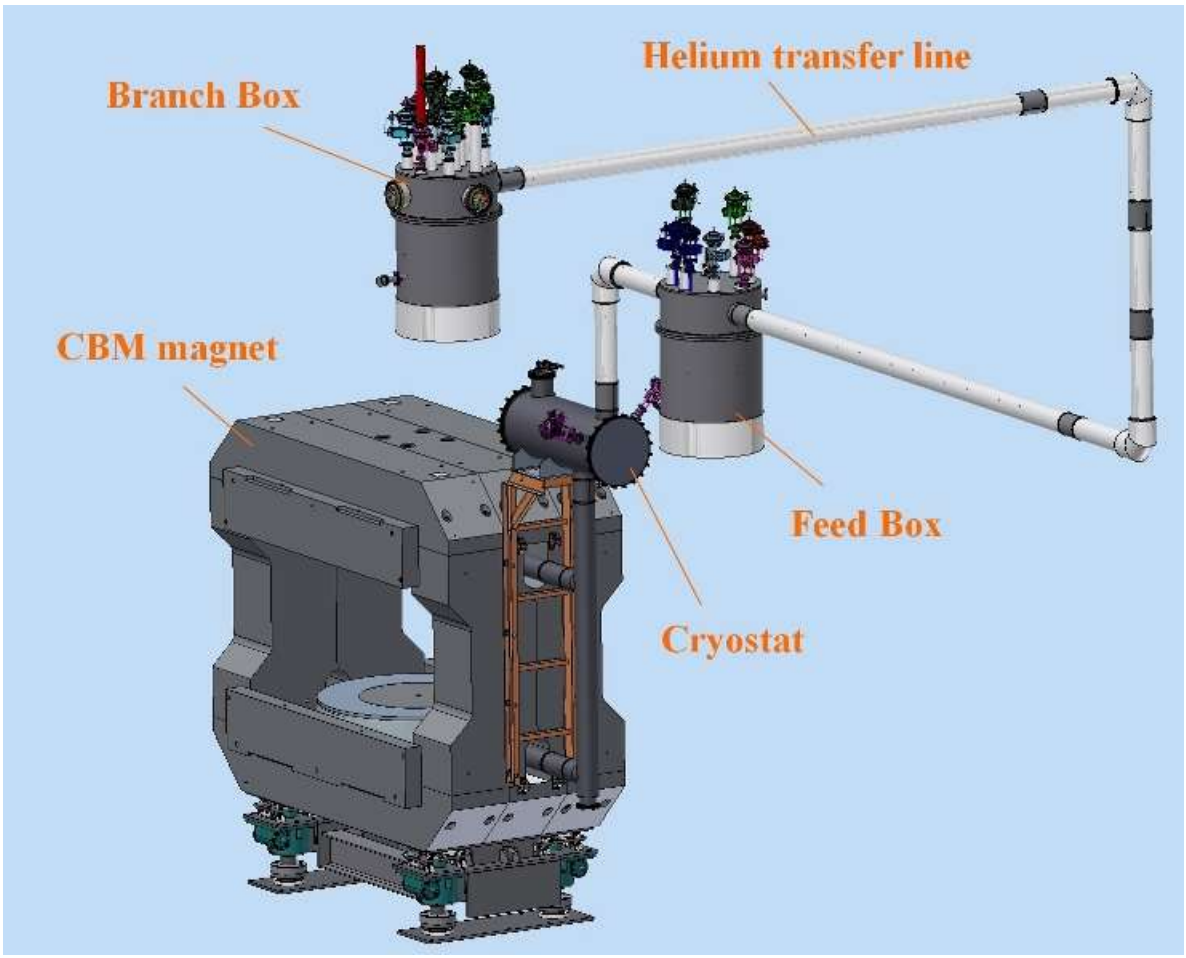

Fig. 1. General view of the CBM magnet and cryogenics supplied by BINP.

1.4 General parameters

The following list contains the mandatory required parameters of the CBM dipole magnet:

Geometry

- Opening angle: ±25° vertically, ± 30° horizontally from the target
- Free aperture: 1.44 m vertically x 3.0 m horizontally, no conical geometry.

The Silicon Tracking System (STS) and its services will occupy all available space in the aperture, from left to right vertical yoke. It requires also space between lower coil and the vertical yoke bar. Distance target- magnet core end: 1m (STS detector must fit in).

- Total length: 1.5 m
- Free space upstream of the magnet: >2 m
- Field integral within STS detector (along straight lines): 1 T*m along ± 0.5 m line around the center, and maximal field ≈ 1 T, depending on the magnet length
- Field integral variation over the whole opening angle along straight lines: ≤ 20% (± 10%)
- Fringe field downstream < reasonable value of the order of 50 to 100 Gauss at a distance of 1.6 m from the target at the position of the first RICH box (RICH only).

Operating conditions

- Operates at both polarities
- 100% duty cycle, 3 months/year, 20 years
- No real time restriction on the ramp: 1 hour up ramp
- Radiation damage (<10MG for organics): no problem
- Radiation Energy deposit in the cryogenic system: max. 1 W

Assembly

- Field clamps dismountable for MUCH
- Assembly in situ
- Weight restriction: crane 30 tons (including lifting jacks)
- Maximum floor load: 100 tons/m^2
- Beam height over magnet base: 2.7 m

Alignment

- Position accuracy: ± 0.5 mm (December 2018 meeting in GSI)
- Orientation accuracy (roll): ± 0.5 mrad

The requirements given above are mandatory.

1.5 The schedule and what is going on

The schedule milestones of the CBM magnet manufacturing are discussed here. Two conditions are important:

1. The CBM magnet should be assembled and tested on BINP site. Only iron yoke and the magnet itself will be tested. The cryogenics of the CBM magnet may be tested only in GSI site. The BINP tests may/will be performed with another equipment of cryogenics. The radiation shields will be cooled with liquid nitrogen or by evaporating helium gas from the cryostat. A cryocooler will be used in a case of using the HTS current leads in the BINP tests.

2. The GSI site will be able to accept the CBM magnet and the cryogenics not earlier than during 2022 and make the cooling down test of the CBM cryogenics not earlier than in March 2023.

So, the current conceptual study is mainly aimed on the magnet and iron yoke designs. It is desired to accomplish the CDR and the PDR stages during the 2019 year.

The bare SC cable manufacturing is manufactured in December 2018. All main parameters were measured. Up to March 2020 the SC cable will be insulated.

The contract for the iron yoke manufacturing is signed with subcontractor. The manufacturer is the same as for the PANDA detector iron yoke. The iron yoke will be manufactured by March 2020.

2. General design

2.1 The magnet design

The rough sketch of the CBM magnet showing only principal elements is presented in the Fig. 2. It consists of the iron yoke, the superconducting magnet and the cryostat.

The iron yoke serves as a construction frame for the magnet and systems of the detector. It also should suppress stray field by the RICH detector. Total mass of the iron yoke is about 150 tons. The yoke is assembled of iron blocks having masses in the range between 3 and 13.6 tons. The material of the blocks is a kind of *steel 10* in Russian specification. The cylindrical parts of the iron yoke representing the poles will be made of technically pure iron – Armco. The Armco iron has similar properties as for the Russian steel *08kp*.

Some details of the iron yoke support enabling necessary alignments are shown on the Fig. 3. The design of this support satisfies the mandatory parameters for magnet alignments including rotation around vertical axis.

The superconducting magnet is designed of two separated superconducting coils (upper and lower coils) symmetrically placed in the detector close to the top and bottom blocks of the iron yoke, as shown in Fig. 2. Such configuration represents a dipole magnet. The coils are placed around the cylindrical blocks of the iron yoke (poles). The distance between the poles is 1440 mm. The total view of the lower coil is shown on the Fig. 4.

The superconducting coil consists of the superconducting winding, copper case and stainless steel plate, Fig. 5. The coil is surrounded by copper radiation shield cooled by 50 -55 K helium, Fig. 6.

This outer surface of the coil will be covered by aluminum foils (aluminized Mylar) in order to reduce its thermal emissivity. The radiation shields will be covered by multilayer insulation up to 20 layers. The coil is suspended inside the vacuum vessel on eight titanium rods. In order to withstand huge vertical force of ~ 300 t, the support struts will be used. Two designs are being considered, first is using 8 separate struts such as in Samurai magnet, and the second is a single large strut. The last one looks more promising. The final decision on the struts design will be taken by November 2019.

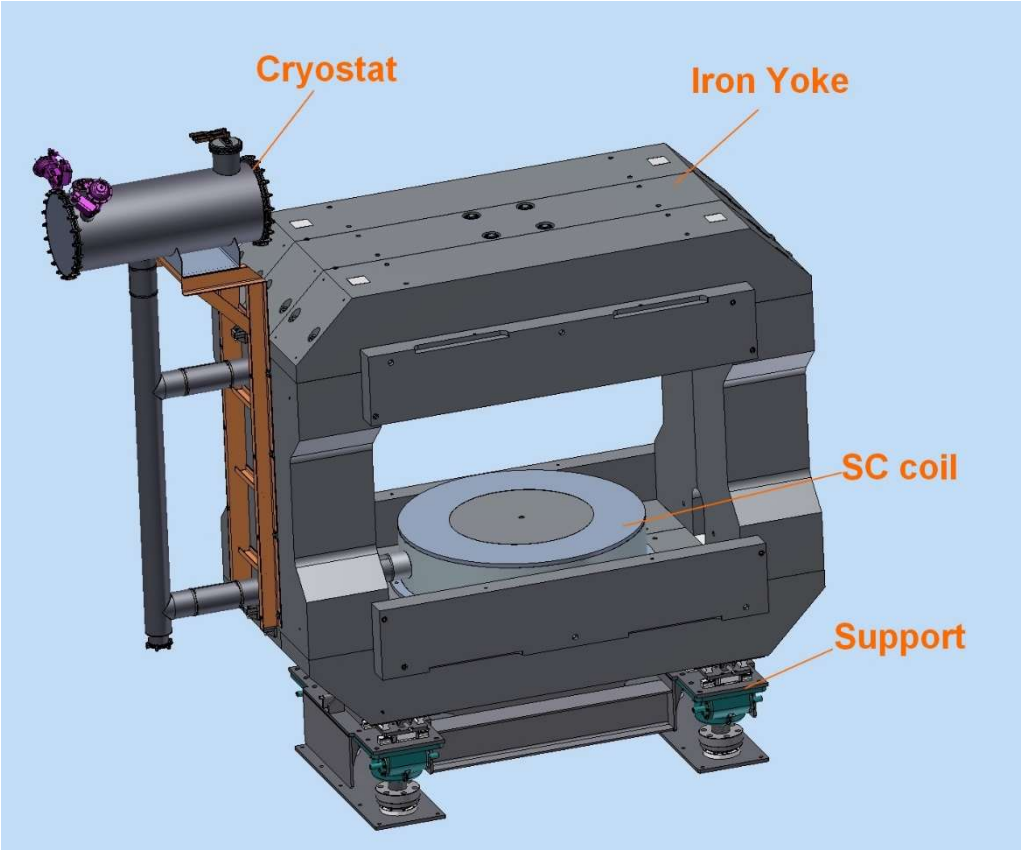

Fig. 2. The sketch of the CBM magnet of May 2017. The magnet consists of upper and lower coils. The main dimensions of the yoke are 3700 mm of height, 2000 mm (2380) of width (with field clamps) and 4400 mm of length.

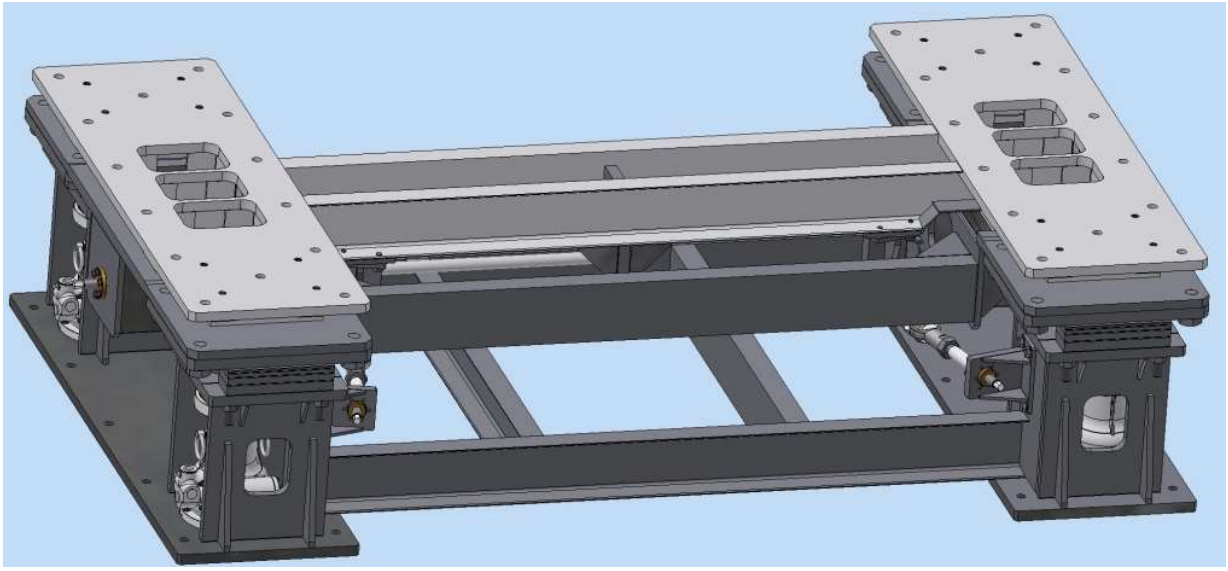

Fig. 3. The support of the iron yoke.

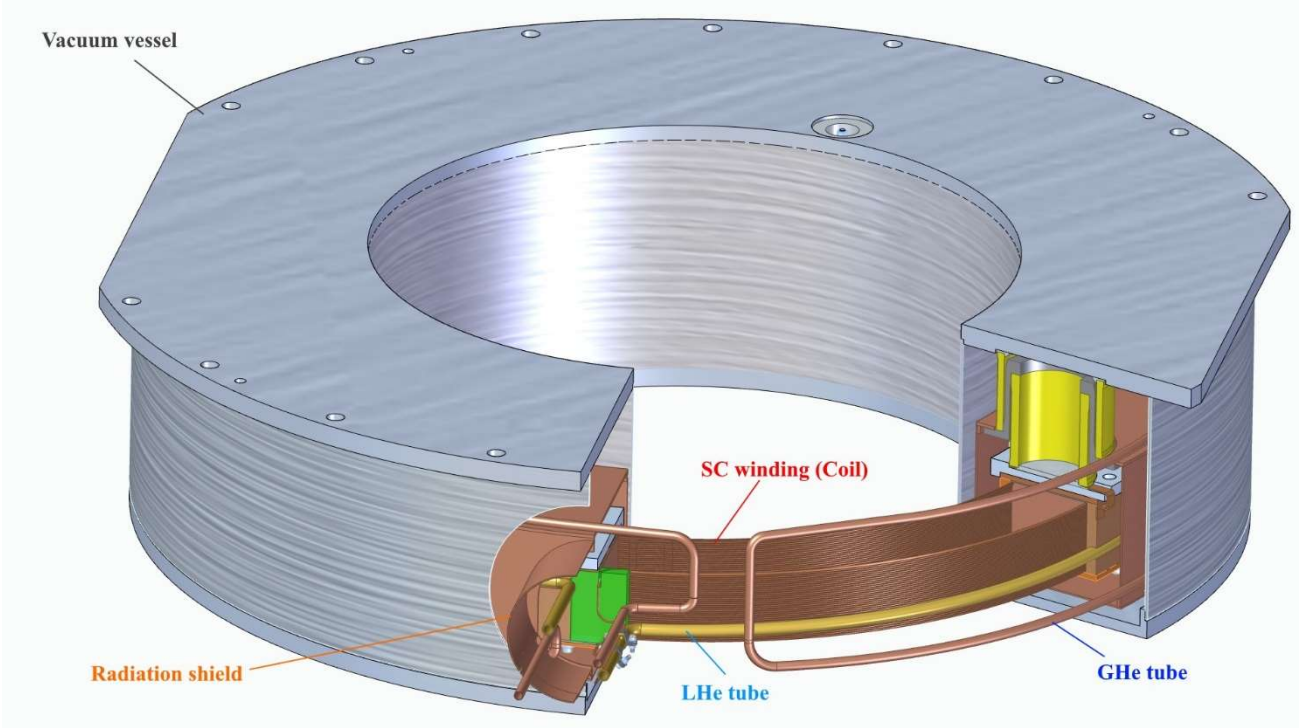

Fig. 4. The view of the upper coil placed in the vacuum vessel.

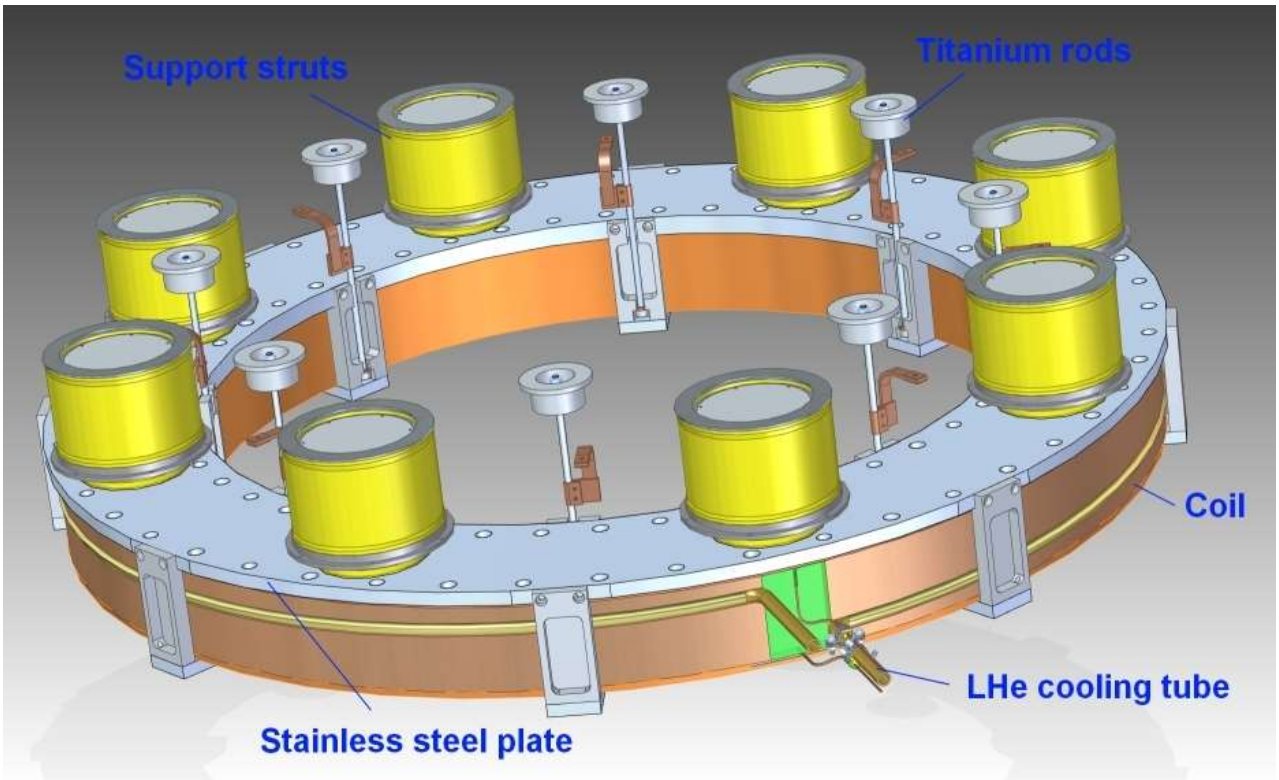

Fig. 5. The superconducting upper coil with 8 support struts. The green part is an insulator breaking thermal short-circuit in the copper cylinder harmful during cooling down.

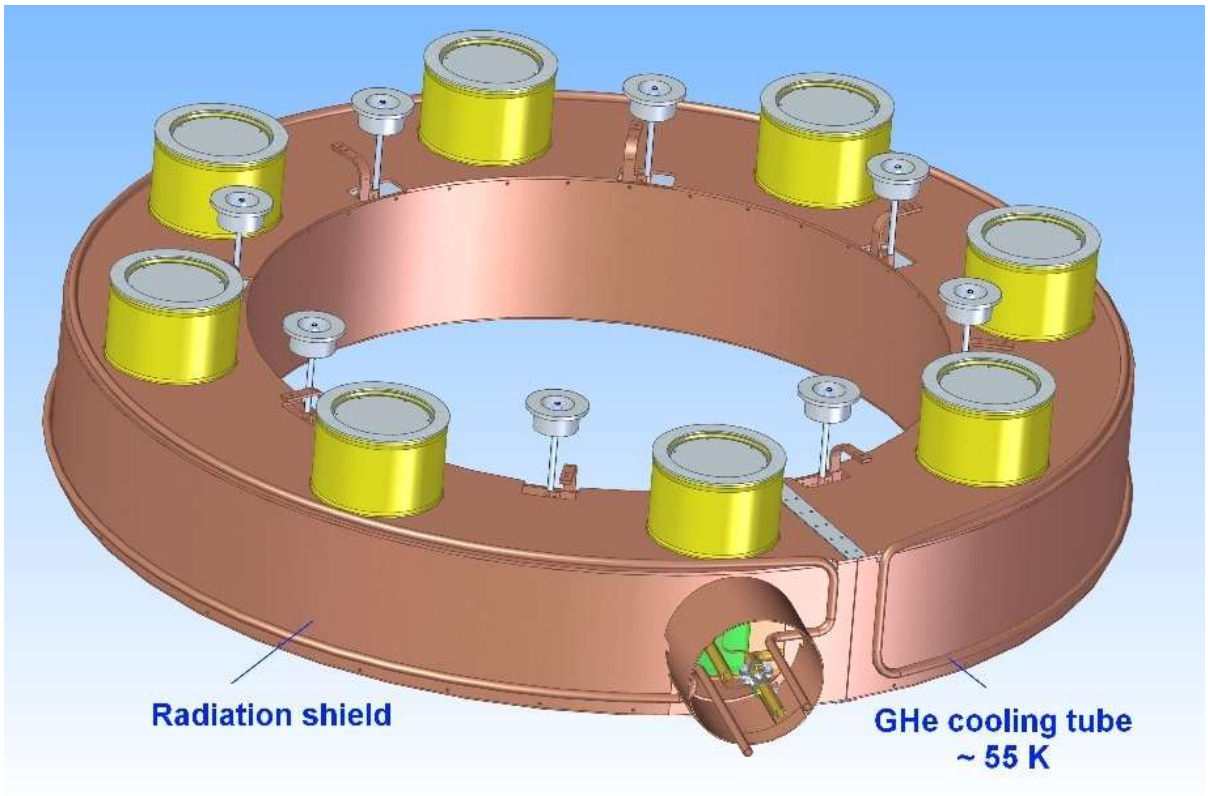

Fig. 6. The upper coil surrounded by the radiation shield.

The preliminary design one of the eight support struts is shown on the Fig. 7. Each support should withstand vertical compressive force up to 45 tons. The G-10 (G-11) cylinders of these struts are the main structural parts of the support to be optimized with respect to mechanical loads and heat in-leaks to the coils. These struts will give major part of the heat loads on the cold mass of the magnet. It will be also important to reduce emissivity of the G-10 cylinders by gluing aluminized Mylar foils on outer surfaces of the struts.

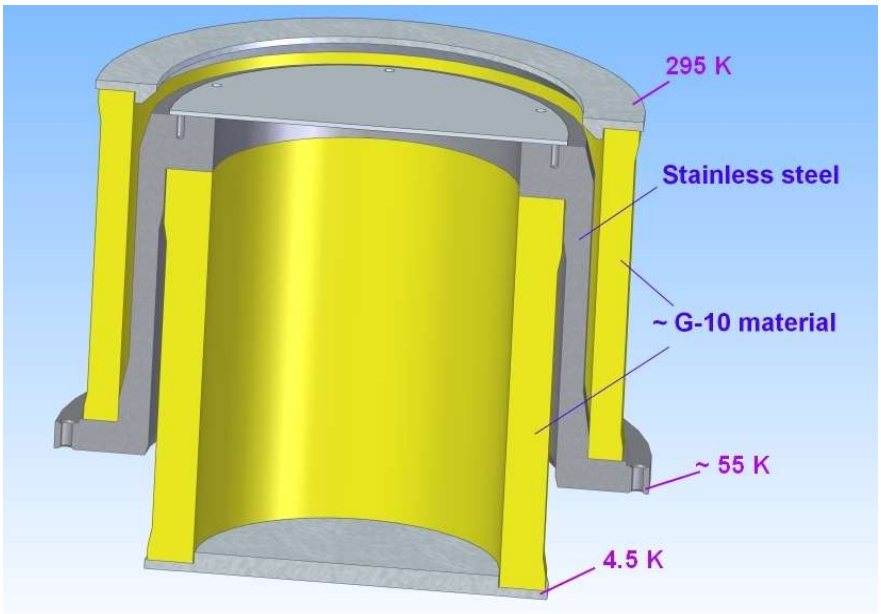

Fig. 7. Cross-section of the support struts. The plastic material is better to be made of G-11 plastic.

The design of the superconducting coils with single large strut is shown on the Fig. 8. The comparison between the two designs of the struts will be given below. The main problem of existing

two design is that they should be optimized according many parameters, such as mechanical stress and strains, shear stresses, thermal stress, thermal loads and stresses in the superconducting windings.

During cooling down procedure the coils will be shrinking radially by ~ 2 mm. This effect should be accounted in the design of the struts and the vacuum vessel. The friction movements should be avoided in the cold parts of the assembled coil to prevent heat releases. Some material with low friction coefficient will be placed between the contacting surfaces where the movement will be allowed.

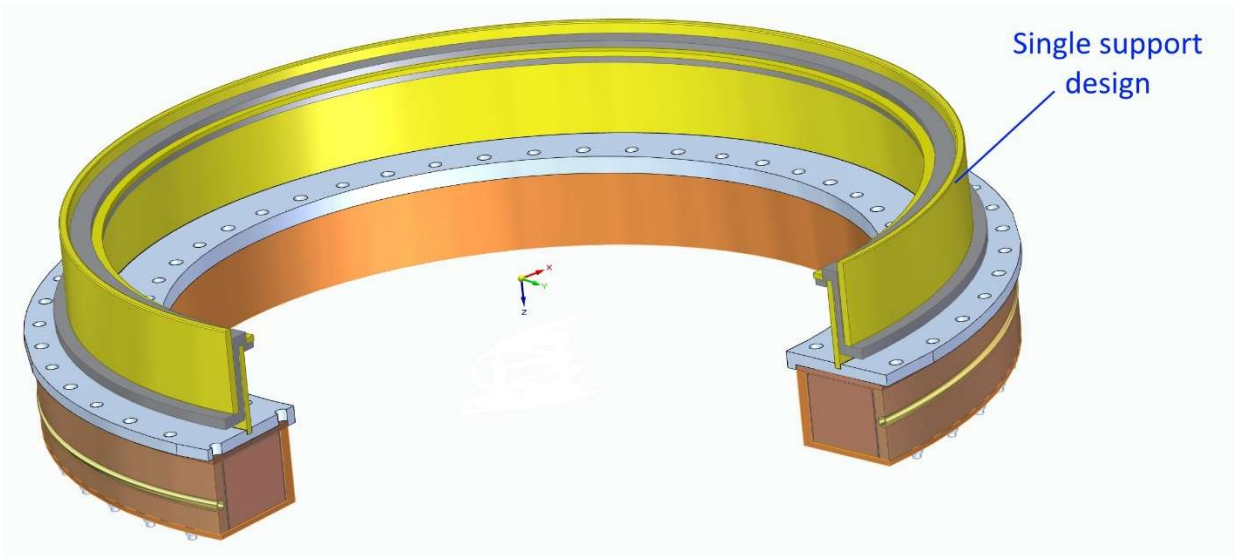

Fig. 8. The upper coil design with single large support.

2.2 Superconducting coil design

The design of the superconducting coil is based on dry winding on the copper elements which should serve as a copper case surrounding the winding. The copper case is connected with the LHe cooling tube which is soldered to the outer wall of the copper case. The technological procedure of making such winding will take two epoxy impregnations. Details of the technology steps of making such coils can be various and will be detailed later.

The total view of the superconducting winding after first impregnation is shown on the Fig. 9. Special steel plates will be used for winding and impregnation. The copper case has will be made of 99.9% technical copper (M1 as Russian standard). The current coil design has even number of layers that avoids the complications for impregnation and assembling of such coils, as shown on the Fig. 10 demanding of G-10 insertions. The LHe cooling tube will be soldered and fixed in the groove of the outer cylinder. This cylinder and the side copper ring will be bolted to the impregnated coil. After this the coil will be epoxy impregnated again. Indium foils will be placed between the bolted surfaces during the coil assembling.

The thickness of the side walls of the copper case is 8 mm, the thickness of the inner and outer walls is ~ 25 mm.

The stainless steel plates and clamps will be assembled around the copper case after finishing of the impregnating procedures. The stainless steel plate will be bolted to the copper case. The threaded holes of the copper case will be filled with Helicoil inserts.

The parameters of the superconducting coil are listed in the Table 1.

The winding will be made of two pieces of the superconducting cable having length of about 4.5÷5 km. One splicing will be made during a winding procedure of one coil using soft soldering on a base of Sn-Ag alloy. The splicing place will be positioned inside the wall of the copper case. This wall is faced towards the center of the magnet. The length of the splicing will be not less than 10 cm.

It is planned to make dry winding in special winding tools. Glass-fiber insulation having thickness

of 0.3 mm will be placed between the layers. It is worth to note here that the SC winding contains a large fraction of insulation about 45% by volume. This comes from the demands to have large safety of electrical protection and to have effective energy extraction system during a quench processes. Large amount of the winding insulation decreases the transverse velocity of normal zone propagation that consequently decreases the rate of winding resistivity built-up during a quench. So, major time during a quench the external resistor will have larger value than internal resistivity of the winding leading the stored energy to be mostly dissipated in the external resistor.

After completion of the winding procedure it will be impregnated by epoxy resin compound. Special tools will be manufactured for the vacuum impregnation procedure. The copper case walls will have several grooves for epoxy compound to be distributed as uniformly as possible. Fine powder of Al_2O_3 is often added to epoxy resin that improves thermal parameters of epoxy compound. Typical grain size of such powder is 3-5 μm and the volume content of the powder is ~ 50%. Technological tests will be performed to test more preferable powder, i.e. boron nitride (BN). Such technology of epoxy impregnation is widely used in BINP. It is well know that the filling powder decreases thermal contraction of the epoxy compound to the copper contraction value.

Practically, the current coil design can be impregnated by wet winding method. The decision on the impregnation procedure will be given on the later stage of this project.

After the impregnations and the copper case assembling the view of the coil will be as shown in the Fig. 11.

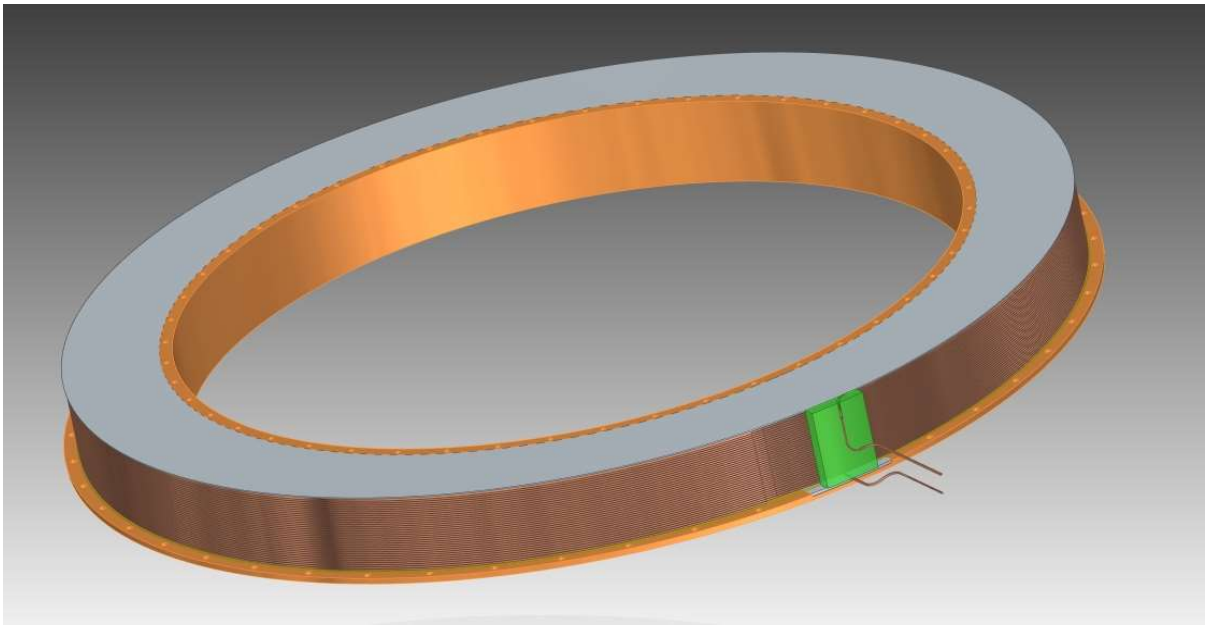

Fig. 9. The superconducting coil after the first impregnation with epoxy resin. The green part is an insertion of G-10 material.

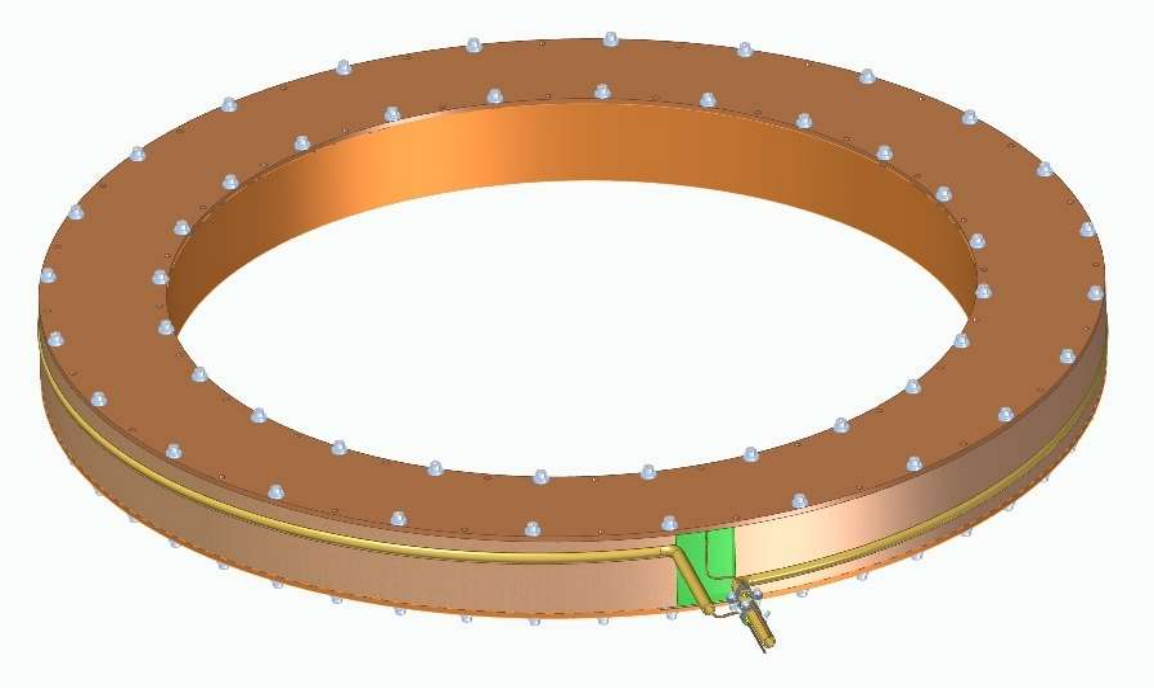

Fig. 10. The view of the coil after impregnations and assembling. The copper case is bolted.

The stainless steel plate with clamps made of 316LN stainless steel serves as a structural frame for supports connections and for rigidity of the whole coil structure. The thickness of the plate is ~ 25 mm. The yield strength of 316LN at 77 K is 1400 MPa [Iwasa, p. 638]. As a proposal, BINP may use other stainless steel material provided by Russian manufacturers. The bolts will be also used for this assembling the coil. The holes of the copper case will have thread inserts a kind of Helicoil®. The copper case plate is fixed along two circumferences to the stainless steel plate by the bolts. The view of the superconducting coil after assembling with support struts and suspension rods is shown on the Fig. 12 (this assembling is connected to the plate of the vacuum vessel which is not shown here).

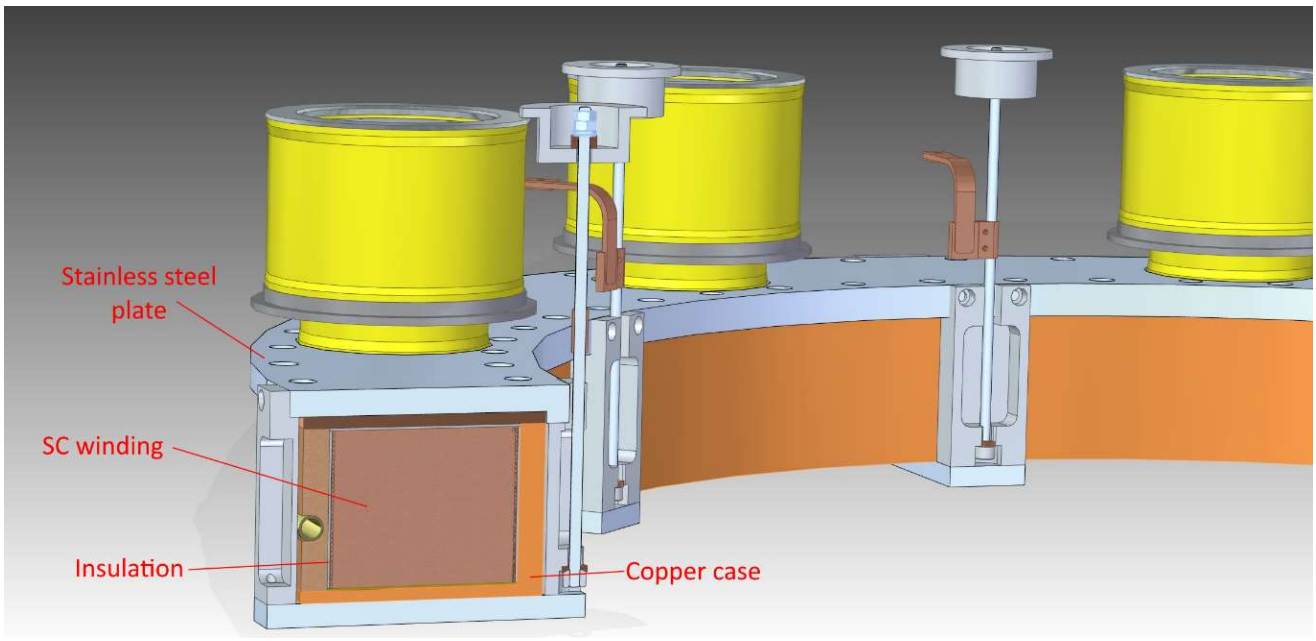

Fig. 11. The view of coil cross-section after assembling.

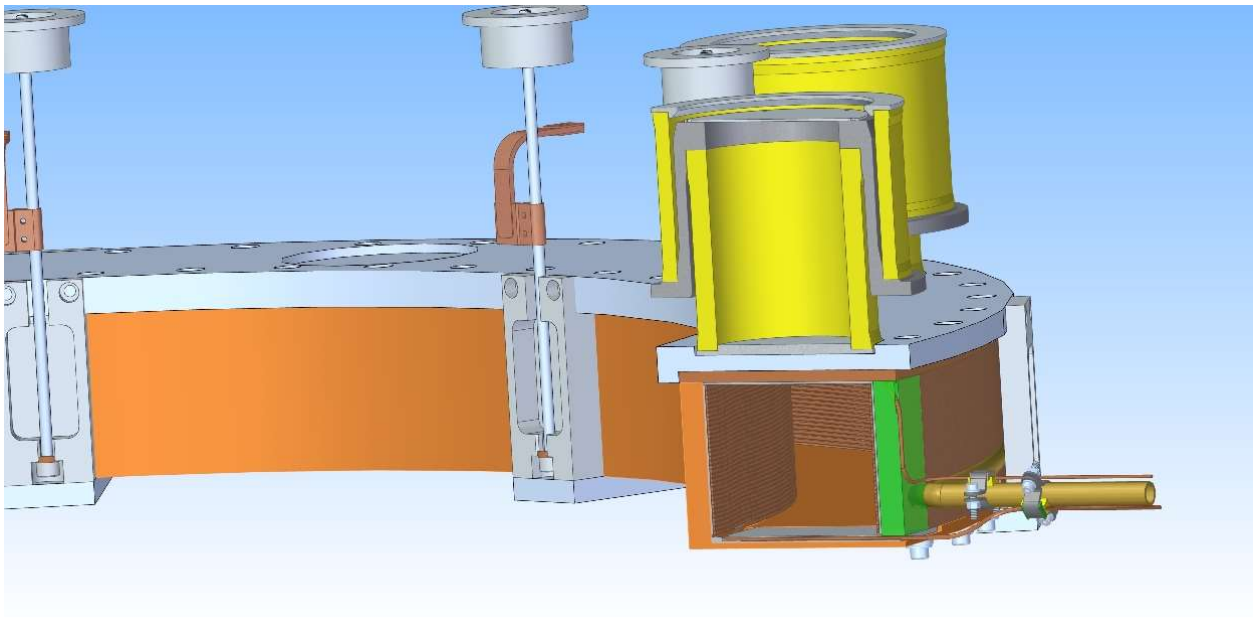

Fig. 12. The stainless steel plate and the copper case assembled by using bolts. The support struts and the suspension rods are also attached.

The thermal stabilization of the coil will be realized by flow of liquid helium at 4.5 K through the LHe cooling tube mentioned above, see Fig. 5. This tube has an internal diameter 15.8 mm and wall thickness of 2 mm. These tubes will be placed with inclination for upper and lower coils of the magnet in such a way that the exit end of the tube should be placed at higher position than the inlet end of the tube.

Table 1 Superconducting coil parameters

Coils parameters	**Values**
Inner diameter of the winding, mm	1396
Cross section sizes of the winding:	
height, mm	132
radial thickness, mm	157
Number of turns in one coil (33x52)	1716
Number of layers in one coil	52
Interlayer insulation, mm	0.3
Operating current Io, A	666[1]
Test current, Io*1.05, A	700
Magnetic field on the coil Bmax, T	3.6
Io/Ic ratio along the load line, %	~50
Io/Ic at fixed B, %	20
Helium temperature, K	4.5
Temperature of current sharing, K	6.8
Stored energy of the magnet, MJ	4.9
Cold mass of one coil, kg	~ 1800
Cold mass of one coil SC winding, kg	800
Inductance of the magnet at operating current, H	~22.1
E/M ratio for two windings, kJ/kg	3.1
Mutual inductance between the coils, H	0.21
Vertical force on one coil toward the yoke, MN	3.0

[1] The 666 A current is optimal value. The quench and the Lorentz forces calculations were done for 700 A current.

Superconducting cable

The main parameters of the superconducting cable are almost the same which were specified in the TDR except the cable length and increased amount of the NbTi. The SC wire was manufactured in December 2018. The main parameters are listed in the Table 2.

The SC winding will be made of two pieces of the cable each having a length of ~ 5 km. It will give more convenience for the production of the cable for BINP subcontractors as well as in manufacturing of the superconducting coil.

The superconducting wires, having a length of single piece of 5 km, were produced by the monolithic technology, see Fig. 13. After insulation it will be as shown on the Fig. 14.

Working point is shown on the load line of the CBM magnet, it corresponds to 3.6 T of magnetic field and 666 A of operation current, see Fig. 15.

Table 2. The main parameters of the manufactured SC wires

Cable #	Length, km	Height Width, mm	Cu/nonCu	Critical current at 8 T, A	RRR	Number of filaments	Diameter of filaments, um	Yield strength, MPa	Twist pitch, mm
1-c3-37-2-18	5.2	2.02 3.25	6.994	>764	217	713	38	115	39
1-c3-37-3-18	5.4	2.02 3.25	6.610	>820	223	713	39	145	39
1-c3-37-4-18	5.5	2.02 3.25	6.825	>786	214	713	38	122	38
1-c3-37-5-18	5.4	2.02 3.25	6.704	>800	209	713	38	138	38
1-c3-37-6-18	5.5	2.02 3.25	6.987	>779	200	713	38	122	38
1-c3-37-7-18	5.5	2.02 3.25	6.705	>799	208	713	38	123	38

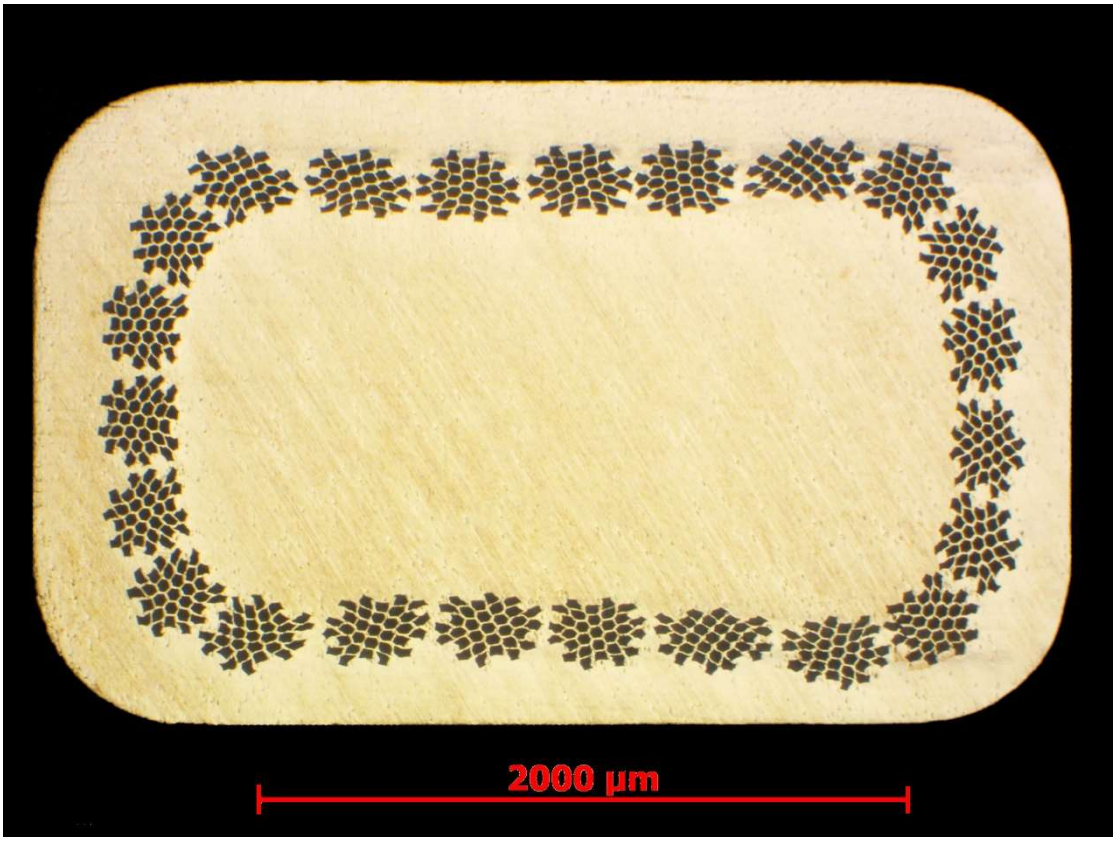

Fig. 13. The cross-section of the manufactured superconducting wire (photo).

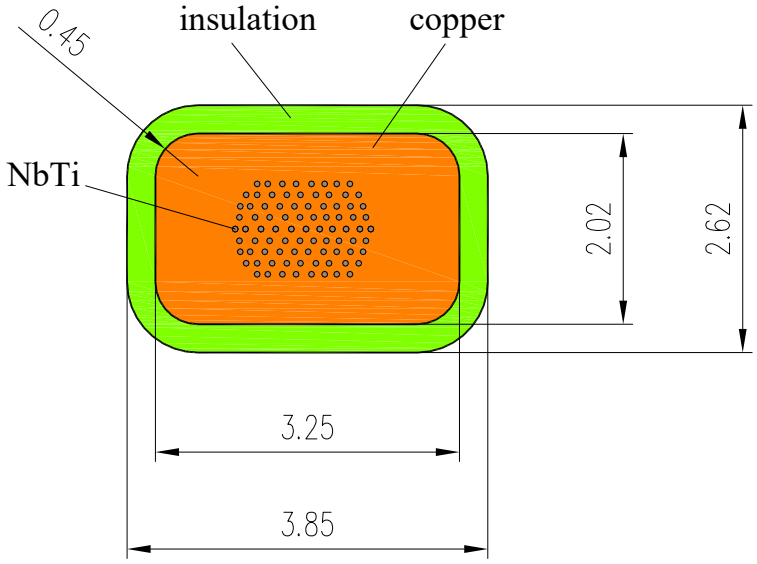

Fig. 14 The cross section of the SC cable with insulation. The cable will be covered by insulation of total thickness 0.3 mm. It will include Kevlar insulation with thickness 0.1 mm, the rest will be fiber glass cloth.

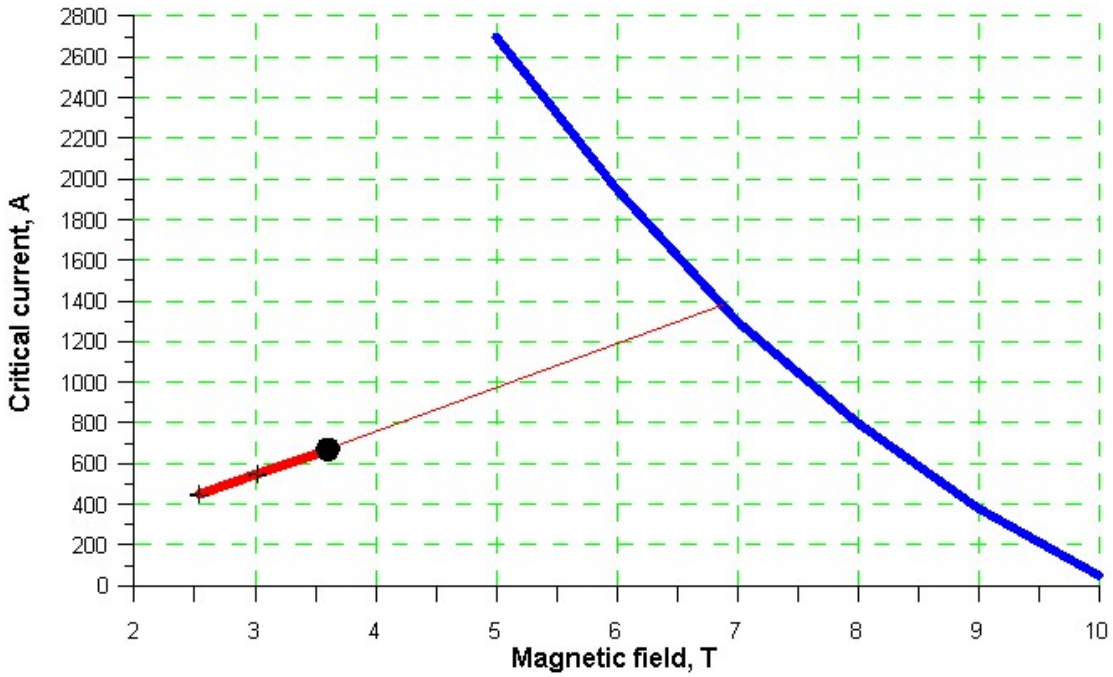

Fig. 15. Load line of the CBM magnet at 4.2 K. The blue line is the NbTi SC cable measured and fitted parameters. The black dot is a working point 666 A@ 3.6 T.

The SC wire will be insulated by March 2020. The fiber glass cloth will be Silane treated preventing undesirable water adsorption.

2.3 Cryostat design

The CBM magnet will be supplied from the external cryogenic station with *gaseous* helium of 4.6 K at 3 bar and helium of 50 K at 18 bar. The cryostat itself will be filled with 4.5 K liquid helium due to expansion after the J-T valve. The magnet will be supplied with liquid helium from the cryostat placed on the top of the iron yoke as shown on the Fig. 2. The preliminary design of the cryostat is shown on the Fig. 16. The volume of the liquid helium is proposed be about ~180 l, Fig. 17. The level of liquid helium will be controlled to contain not less than ~ 40 l of liquid helium. The LHe volume will be filled from the Feed Box via the phase separator.

The LHe volume of the cryostat will supply the coils of the magnet with liquid helium. The

cooling of the coil in ordinary operation is considered as thermosyphon cooling. The liquid helium goes from the LHe volume down to the lower coil, then it makes on turn around this coil inside copper pipe. After this helium goes up to upper coil and goes one turn around this coil in the same manner as for the lower coil. After this, helium goes to the top part of the LHe vessel. The gaseous helium returns from the LHe vessel to the cryogenic station.

The cryostat also has ports for vacuum measurement and initial pumping of the magnet and the Feed Box.

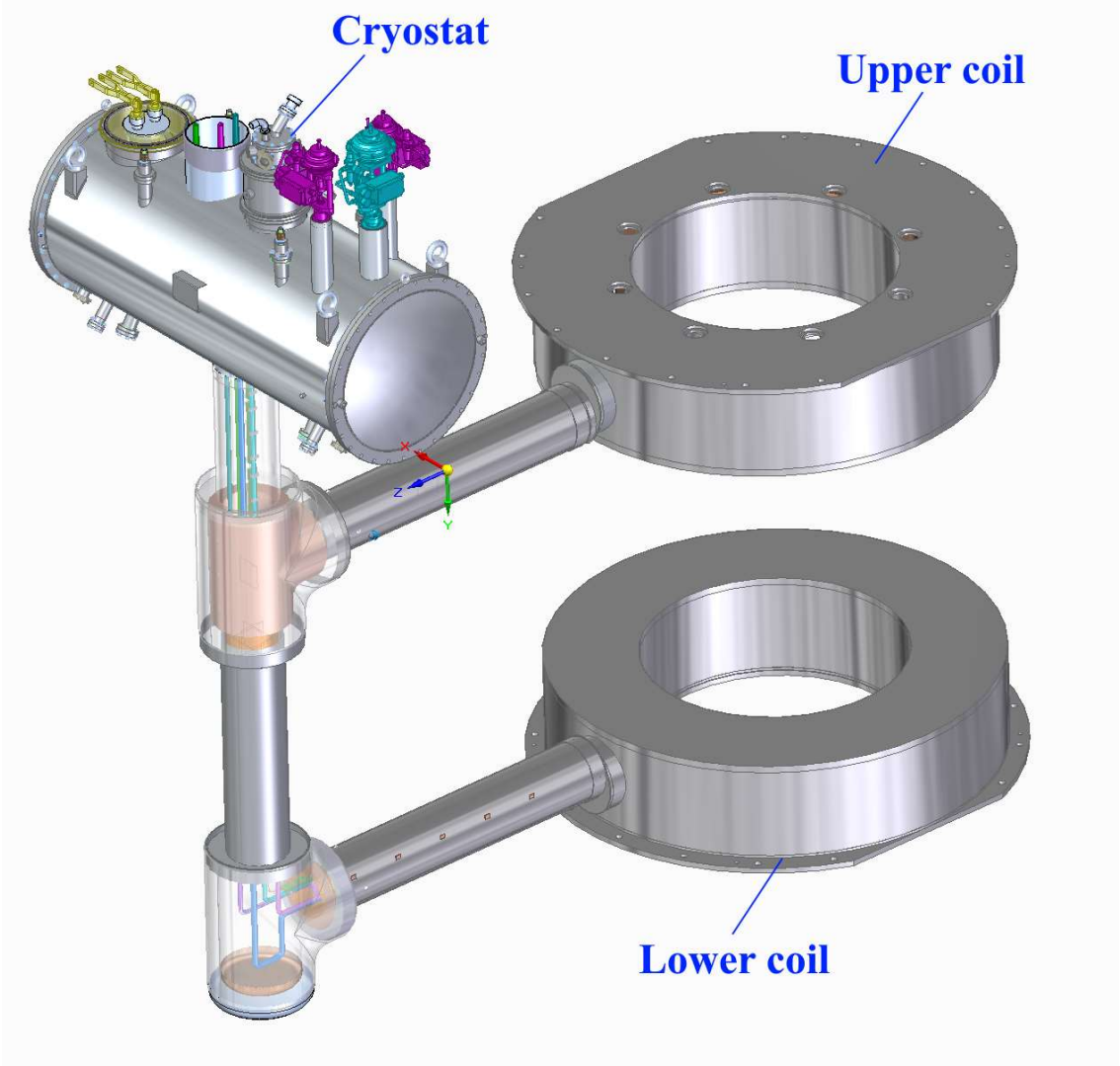

Fig. 16. View of the cryostat top of the CBM magnet.

The current leads will be designed for the current values up to 800 A. Some part of the gaseous helium entering the cryostat will cool these current leads via thermal conductivity of sapphire plates.

The design of the current leads with HTS insertions is considered here, Fig. 18. These current leads will not use 4.5 K gaseous helium for internal cooling, so the design of the cryostat and control process will be simplified. However, the operation of such current leads depends on the interception temperature cooling by 50 K helium. The heat exchanger of the current leads by 50 K helium is important in this design, this helium going from the Feed Box should cool first these current leads. The HTS current leads may be a kind of CS-1000-347 ($6000) by CryoSaver with 1000 A at 64 K critical current and 0.212 W (for pair) of conductive power to LHe temperature.

The neck of the cryostat serves for various purposes. On the warm part of it valves for connection with multipurpose line, connections for measurements and filling of liquid helium in the BINP tests will be placed. In the BINP test there the 50 K helium will be not available, so the same current leads cooled by a cryocooler, as shown on the Fig. 19.

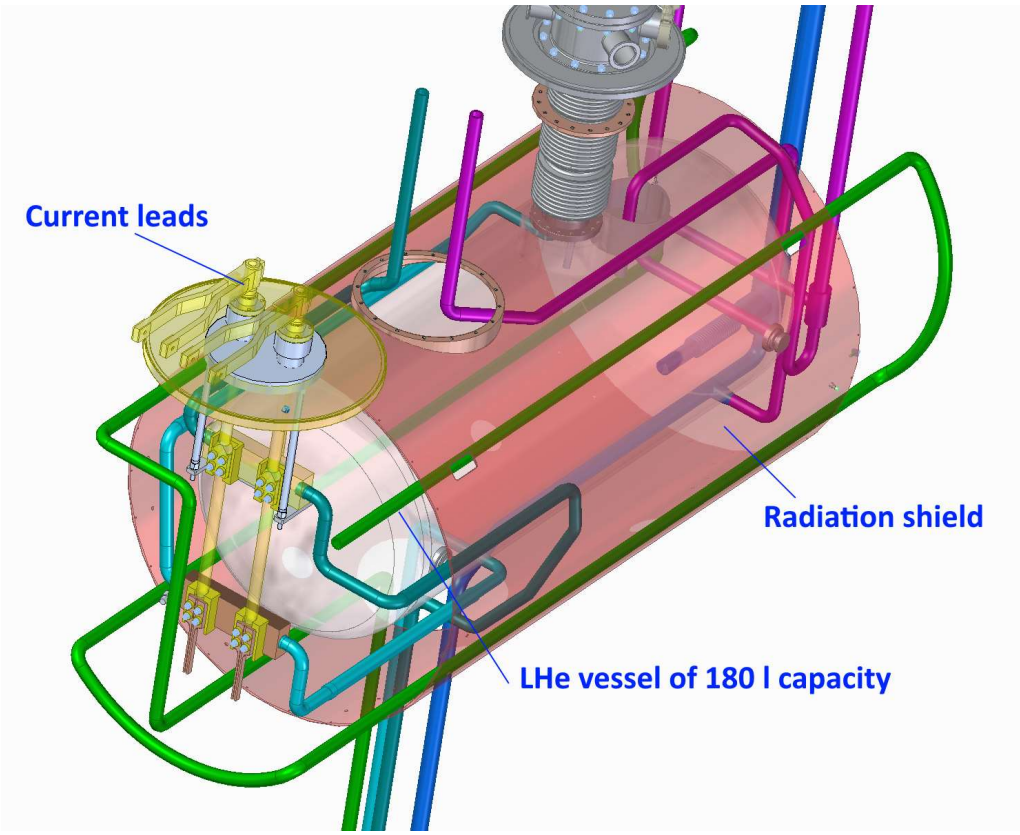

Fig. 17. Some elements of the cryostat. There are three control valves, now shown here.

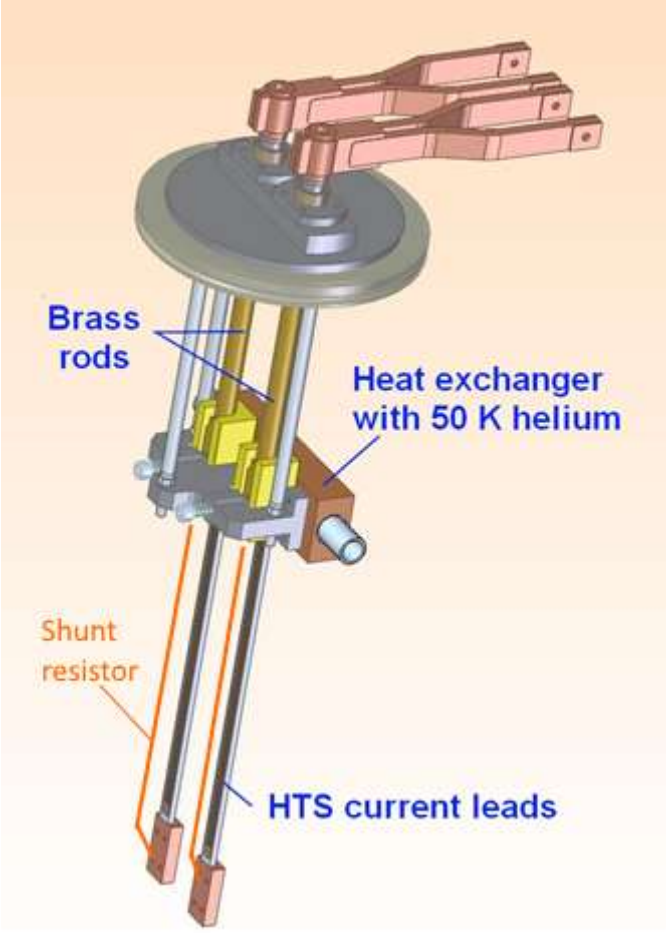

Fig. 18. The HTS current leads. The shunt resistor may be placed for protection.

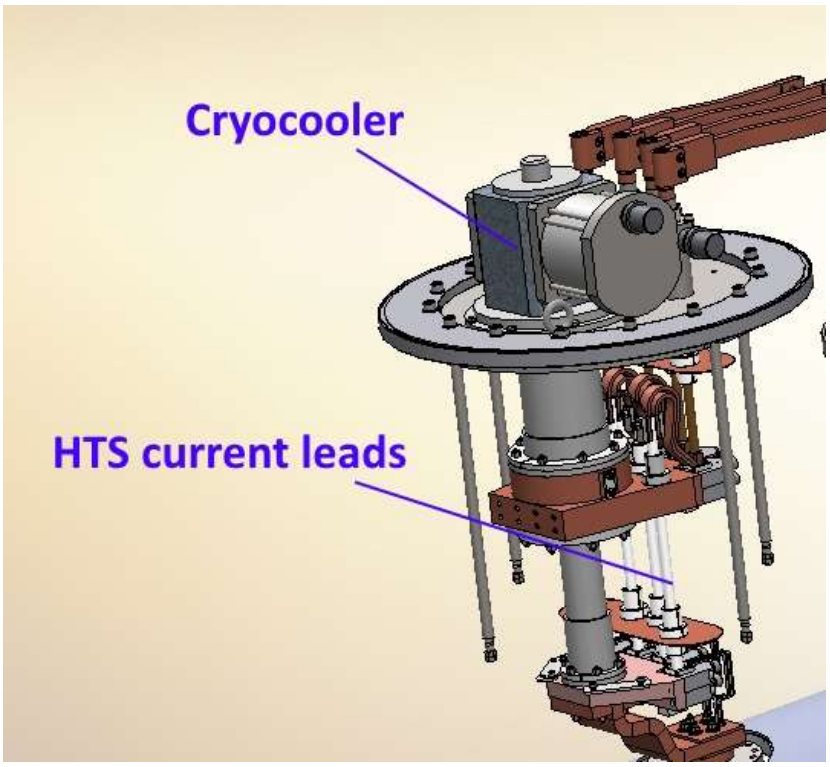

Fig. 19. The current leads block to be used in the BINP tests.

The HTS current leads need protection from burning in case of normal zone appearance while powering the magnet. It may happen, for example, by a gas condensate drops directly on these current leads or on the nearest bus bars. In the normal state, the current leads have relatively high resistance and too low mass. The shunting resistor can effectively protect such current leads.

The shunt resistor is a brass[2] foil with the following dimensions l×w×t: 300 mm ×15 mm × 1.5 mm. The heat in-leak to 4.5 K helium will be:

Q = {1040 W/m}*S/L, where {} is integrated heat conductivity in 4.2-60 K range, S and L is a cross-section and the length of the brass foil.

$Q = 1040*2.25*10^{-5}/0.3 = 0.078$ W per shunt. Total heat in-leak for two shunts will be 0.156 W.

The resistance of the shunt is $R_{sh} = \rho*L/S$, $R = 3.2*10^{-8}*0.3/2.25*10^{-5} = 4.3*10^{-4}$ Ohm. This resistance should be much low than the resistance of the HTS current lead in a normal state.

In a worst quench case, the normal zone will appear on the current lead, then is goes to the magnet to make it normal. The velocity of the normal zone propagation is ~ 7 m/s, the characteristic time of the current decay is ~ 14 s, so the total time of the current decay in the shunt is t = 3 m/ 7 (m/s) + 14/2 = 7.4 s. The energy dissipated in the shunt is:

$E = I^2*R_{sh}*t = 700^2*4.3*10^{-4}*7.4 = 1.56$ kJ.

The volume of the shunt is $V = 0.3*2.25*10^{-5} = 6.75*10^{-6}$ m^3.

The volumetric enthalpy of the shunt is $2.3*10^5$ kJ/m^3 that corresponds to ~ 120 K temperature.

The shunt resistor gives additional 0.156 W power to helium, to be compared with 0.212 W from the current leads itself. So, the total heat load will be 0.37 W to 4.5 K temperature surfaces.

Preliminary design of the bus bars fixation is shown on the Fig. 20. Such fixation enables rigid positioning of the SC cables in the grooves. The SC cables are insulated from LHe tubes while the thermal contact to these tubes is maximal. The cable splicing will be performed in these fixation by soldering along a length of 10-15 cm.

[2] The stainless steel is also possible. It will be thicker, about 6 mm.

Heat generation in one splicing is estimated about 1 mW. That is too low value.

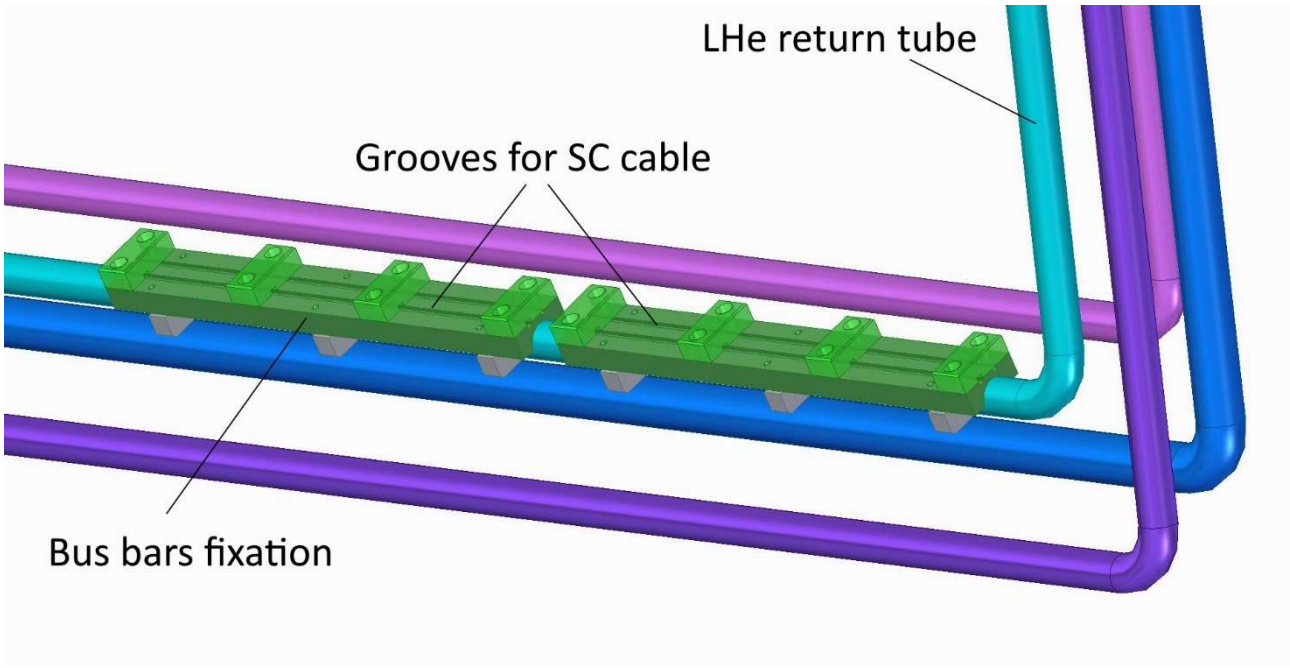

Fig. 20. The current design of the bus bars fixation. The green parts are made of G-10 material.

The radiation shield of the cryostat will be cooled by return line of the gaseous helium at about 55 K of temperature. The direct line of 50 K helium should directly go to the magnet for cooling its supports and the radiation shields.

The radiation shield of the cryostat will be suspended on ball supports made of a kind of G-10 composite. The outer surfaces of the shield will be covered by multilayer superinsulation.

The cryogenic valves in the cryostat are not shown here.

3. Design calculations

3.1 Magnetic field calculations

The magnetic field calculations were made with Mermaid and ANSYS codes. There were three models independently calculated:

1. 3D model in Mermaid code in BINP;
2. 3D model in ANSYS code by Yury Gussakov, the report was issued in March 2018;
3. 2D and 3D models in ANSYS code in BINP.

Very useful calculations were done by Stefania Farinon. That results were not completely coincided with previous possibly due to different B-H values in the materials.

The iron yoke almost in all models was slightly different. The differences were the outer cuts in the field clamps and the size of holes in the pillars.

If the codes give the results of the magnetic field with differences 1-2% then it was decided that the results are in agreement.

The Mermaid code was developed in BINP more than 25 years ago; it demonstrated good accuracy in many calculations. Mermaid 3D model had about $5*10^6$ nodes and 153 plain sections in Z direction. New 3D model of ANSYS code was used for comparison with Mermaid calculations. The Mermaid 3D code is unable to make models of real shape; the models approximated by parallelepipeds as will be seen in the figure below. So, some differences between the ANSYS and

Mermaid codes should be.

The ANSYS 3D models had $0.5 \div 1 * 10^6$ nodes. ANSYS models are more flexible with mesh sizes also ANSYS code gives more possibilities in calculation analysis, and it is linked with structural analysis.

The calculated results should demonstrate that the current design of the CBM magnet is in accordance with the desired parameters of the magnetic field listed in the specifications, and also the results of forces acting on the yoke blocks and the coil. Magnetic field on the SC coils is also very important.

The design of the iron yoke was changed with respect to the TDR. The changes are the height and the shape of the poles. Now the poles have a cylindrical shape and the height is decreased by 2 cm. The field clamps became of simple bar shape. The vertical side supports of the iron yoke are also simplified.

The 3D models of Mermaid and ANSYS codes are presented in Fig. 21 and Fig. 22 respectively. Some calculations were made in ANSYS 2D model. The iron yoke steel was chosen as Steel 1010 (as Russian specification, that corresponds to Steel 1020 of USA and Steel 1.0402 of Germany). The poles of the yoke are a kind of ARMCO Steel or Steel 08kp (as of Russian specification, which corresponds to Steel 1008 of USA and Steel 1.0322 of Germany).

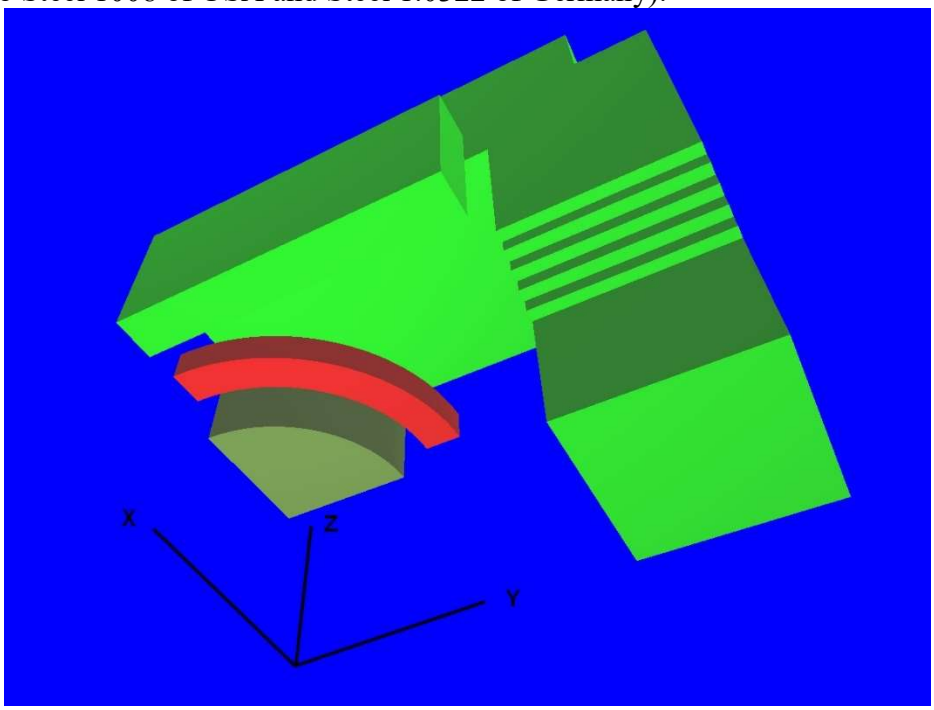

Fig. 21. The 3D model in the Mermaid code. The model contains 1/8 part of the magnet.

The magnetic properties of the steels taken into the all calculations are presented on the Table 3. The B-μ data for these steels are from the Mermaid code library. The H values were calculated as $H=B/\mu\mu_0$. The data beyond 25 kG are extrapolated by the codes own solvers.

Most calculations were done at 1749 turns and 686 A current. The last parameters are 1716 turns and 666 A which was calculated in the ANSYS 3D models. The view of the last model is 1/8 part model on the Fig. 22.

The results of the Mermaid and ANSYS calculations were very close. The magnetic field distribution calculated in Mermaid and ANSYS 3D codes along the beam line of the detector is shown on the Fig. 23.

The magnetic field values inside the SC winding were compared with Mermaid and ANSYS calculations and were very close also. The magnetic field values in the SC winding calculated in the

ANSYS 3D model are presented in Fig. 24.

Table 3. The magnetic properties of the Mermaid code library steels.

Armco			**Steel 1010**		
B, kGs	**μ**	**H, A/m**	**B, kGs**	**μ**	**H, A/m**
0.000	2500.00	0	0.000	700.00	0
1.000	2500.00	31.832	1.000	840.00	94.738
2.000	3333.00	47.753	2.000	990.00	160.767
3.000	3846.00	62.075	3.000	1120.00	213.160
4.000	4347.00	73.227	4.000	1320.00	241.151
5.000	4672.00	85.167	5.000	1500.00	265.266
6.000	4800.00	99.475	6.000	1520.00	314.131
7.000	4730.00	117.771	7.000	1500.00	371.372
8.000	4651.00	136.882	8.000	1450.00	439.061
9.000	4456.00	160.7312	9.000	1370.00	522.787
10.000	4201.00	189.4306	10.000	1270.00	626.613
11.000	3767.00	232.3807	11.000	1175.00	745.003
12.000	3154.00	302.7767	12.000	990.00	964.604
13.000	2551.00	405.542	13.000	830.00	1246.431
14.000	1919.00	580.572	14.000	660.00	1688.057
15.000	1153.00	1035.30	15.000	530.00	2252.259
16.000	615.00	2070.37	16.000	400.00	3183.19
17.000	303.00	4464.87	17.000	270.00	5010.58
18.000	146.00	9811.21	18.000	180.00	7957.98
19.000	89.00	16988.95	19.000	120.00	12600.14
20.000	61.00	26091.74	20.000	80.00	19894.95
21.000	43.00	38864.56	21.000	43.00	38864.56
22.000	30.00	58358.53	22.000	24.00	72948.17
23.000	19.00	96333.46	23.000	15.00	122022.39
24.000	12.00	159159.64	24.000	10.00	190991.56
25.000	8.00	248686.93	25.000	7.00	284213.64

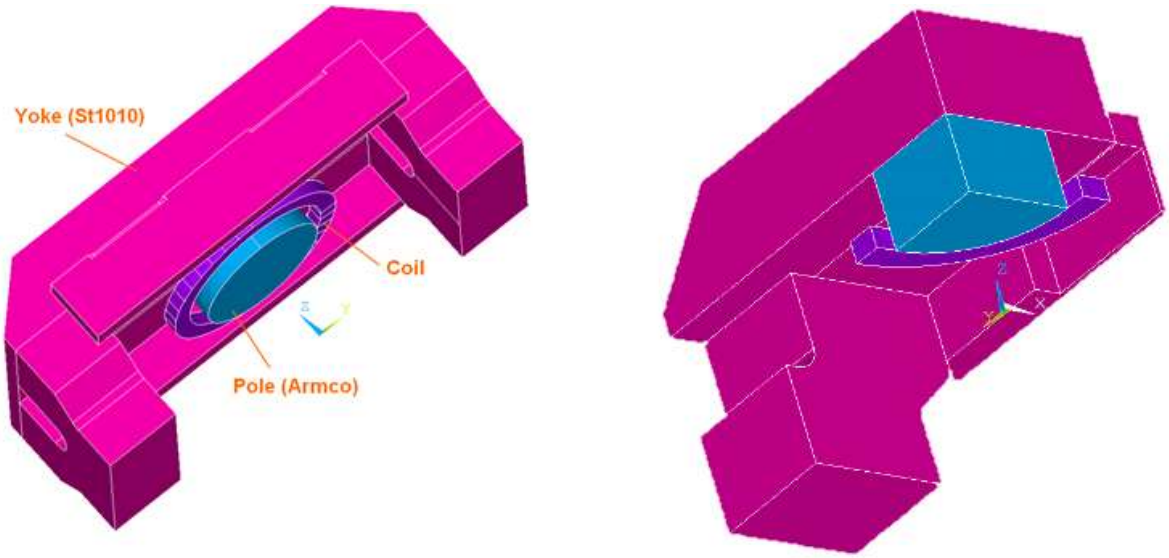

Fig. 22. The ½ part and ⅛ part of 3D models in the ANSYS code used in the calculations.

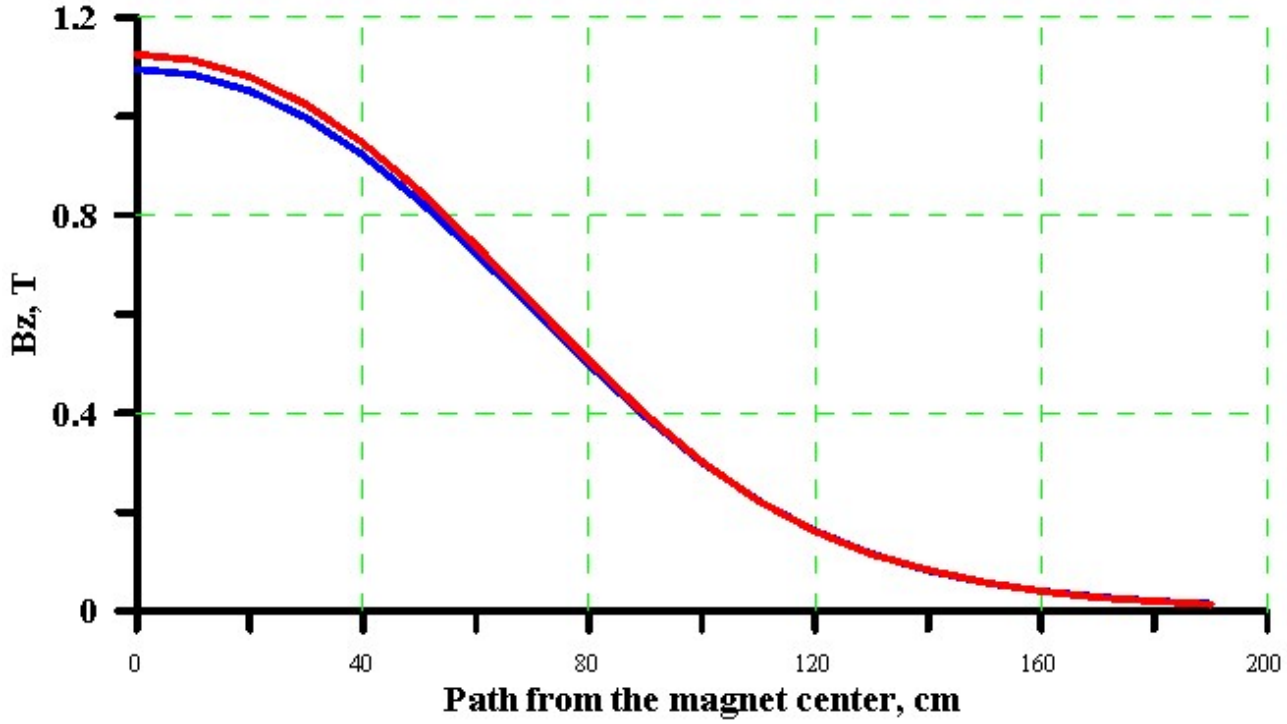

Fig. 23. Magnetic field distribution along the beam from the center of the magnet detector. Blue line is by Mermaid calculations, the red line is by ANSYS calculations. The results is for 1749 turns and 686 A current.

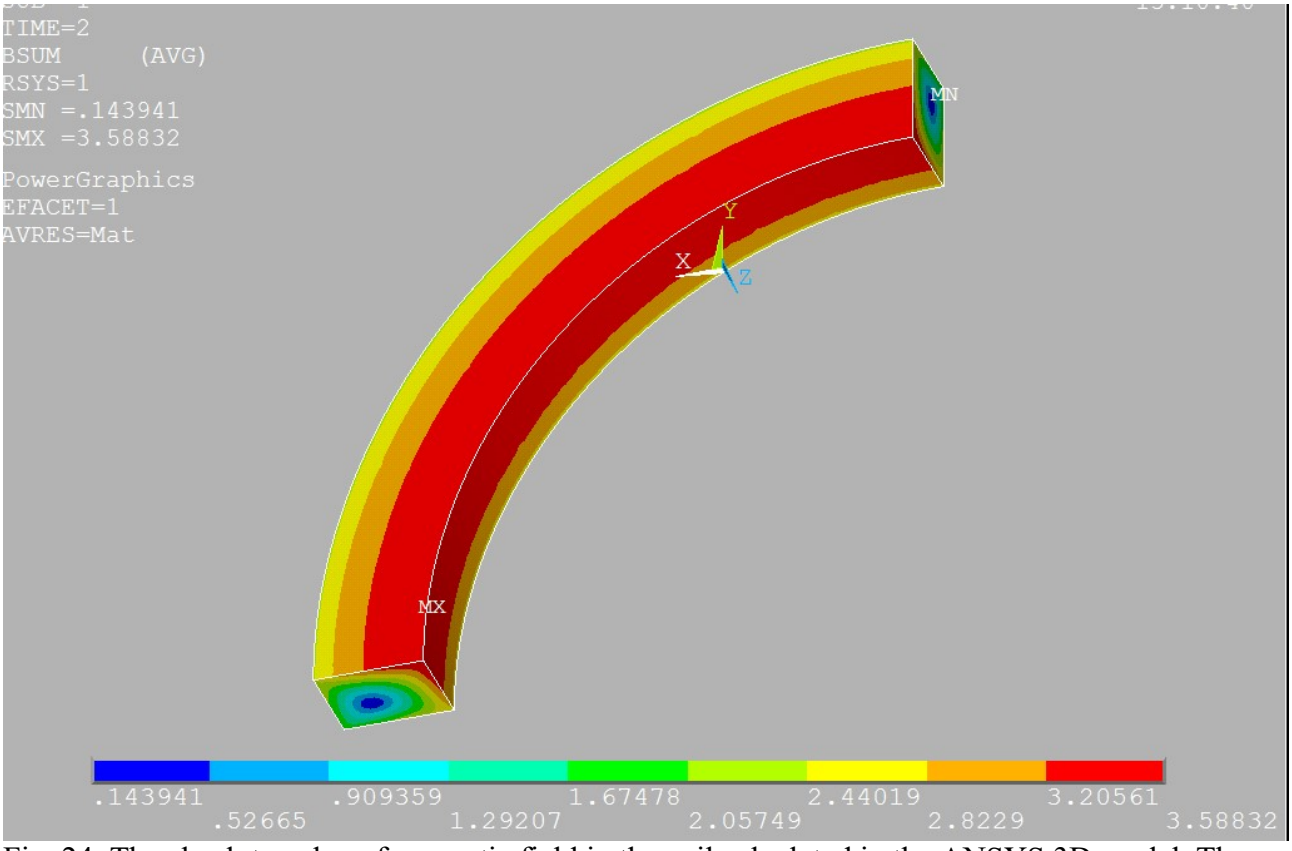

Fig. 24. The absolute value of magnetic field in the coil calculated in the ANSYS 3D model. The maximal value on the coil is 3.6 T. The result is for 1716 turns and 666 A current.

The map of the magnetic field around the RICH detector is shown in the Table 4. The presented results are from Mermaid and ANSYS calculations. Previous Mermaid results come from different

3D model, September 2017. The axis directions are shown on the Fig. 21. In this table the Y = 0 that gives largest values of the magnetic field. The filed clamp size of the iron yoke is limited by X = 119 cm. That is the widest size of the iron yoke along X direction. The ANSYS calculations with the clamps made of Armco steel were made; the magnetic field decreased in the grey region by ~ 1-3% only.

Table 4. The map of the magnetic field [T] around the RICH detector calculated by Mermaid and ANSYS 3D. The RICH detector is placed around the grey shadows within X = 1.40÷2.10 m and Z = 1.74÷1.97 m.

Z, cm	X, cm	Mer	Ans	Mer	Ans	Mer	Ans	Mer	Ans	Mer	Ans
		110		120		130		140		150	
100		1.463	1.528	0.037	0.416	0.034	0.032	0.0279	0.0266	0.022	0.021
110		1.456	1.519	0.023	0.17	0.022	0.021	0.0192	0.0187	0.016	0.016
120		1.457	1.518	0.017	0.0688	0.016	0.016	0.0138	0.0138	0.012	0.012
130		1.175	1.228	0.0131	0.0595	0.012	0.012	0.0103	0.0106	0.0091	0.0092
140		1.0074	0.613	0.0141	0.0149	0.0088	0.0093	0.0079	0.0083	0.0071	0.0073
150		0.0046	0.0057	0.0056	0.0064	0.0063	0.0067	0.0061	0.0066	0.0056	0.0060
160		0.0052	0.0062	0.0051	0.0060	0.0051	0.0059	0.0049	0.0055	0.0046	0.0050
170		0.0052	0.0063	0.0048	0.0058	0.0045	0.0053	**0.0041**	**0.0047**	**0.0038**	**0.0043**
180		0.0053	0.0068	0.0044	0.0054	0.0040	0.0047	**0.0036**	**0.0042**	**0.0033**	**0.0037**
190		0.0046	0.0060	0.0038	0.0048	0.0034	0.0042	**0.0031**	**0.0036**	**0.0029**	**0.0032**
200		0.0034	0.0046	0.0031	0.0041	0.0029	0.0036	**0.0026**	**0.0032**	**0.0024**	**0.0028**

The influences of different kind of steels of the iron yoke, of the field clamps cuts and total current on the main parameters are presented in the Table 5. The results presented in this table were calculated in ANSYS 3D model with identical mesh. As far as the magnetic field integral is the main parameter it was agreed to have ~666 A of operating current at 1716 turns (52 layers) and to have the field clamps with internal cuts. Additional result of the last design is more uniform azimuthal distribution of the forces in the winding, see Fig. 25.

Table 5. Influence of different kind of steels of the iron yoke on the main parameters of the CBM magnet.

Parameters	**Yoke: Steel 1010, Pole: Armco, *the previous design***	**The *previous design* without the field clamps**	**The *previous design* with field clamps having the cuts like in Fig. 3**	**Yoke: Steel 1010, Pole: Armco, *the* 52 layers and with FC cuts,**	**Yoke: Steel 1010, Pole: Armco, *the* 52 layers and with FC cuts, the last design**
B in the center, T	**1.125**	1.138	1.138	1.124	**1.099**
Bmax on the coil, T	**3.888**	~3.8	~3.76	3.70	**3.59**
$\int$ Bds ± 0.5 m, T*m	**1.031**	1.048	1.047	1.034	**1.012**
Operating current, A	**686**	686	686	686	**666**
Number of turns	**1749**	1749	1749	1716	**1716**
E stored energy, MJ	**5.33**	5.28	5.31	5.14	**4.90**

The forces on the coil were calculated in ANSYS 3D model and estimated in Mermaid code (at 686 A current and 1749 turns). The Mermaid 3D code does not make forces calculations. The distributions of Br and Bz (radial and axial) components were extracted from the Mermaid code and the forces were estimated by Lorentz formulas. The Mermaid estimated behavior of the Br was very close to the ANSYS direct calculations of average Br component in the nine sectors of the ¼ part of the coil, see Fig. 25. The average value of Br in the whole 90° sector of the coil is 0.564 T. So, the vertical force Fz equals Br*I*Rav = 0.564*1.2*10^6*4.86 = 3.29 MN, i.e. 330 tons.

The ANSYS 3D performs the direct calculations of the nodal forces, which were calculated in the one 90° sector having a fine mesh. The result is $8.014*10^5$ N. So, for the whole coil the **Fz** = $4*8.014*10^5$ = **3.21 MN**.

The vertical force was calculated at 700 A (test current) and 1716 turns. The result is **Fz** = **3.05 MN**.

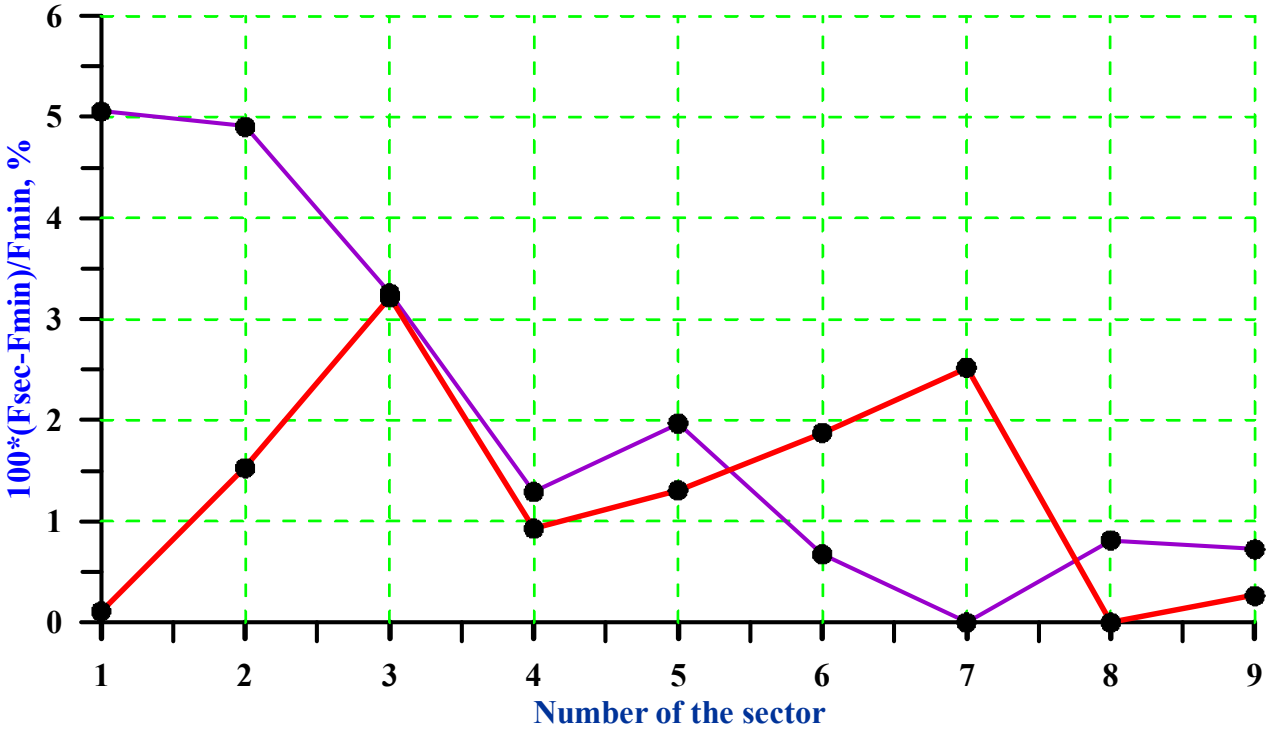

Fig. 25. The forces distribution inside the coil along the azimuth. The red line is for radial force, the purple line is for axial force acting on the struts. Fsec is the force in the sector, Fmin is the minimal force among all sectors. It looks that the accuracy of the calculations is not less than 1%.

The forces acting on the shifted one coil with its bottom positioned at Z = 0.815 m (upper coil) were calculated in ½ part ANSYS 3D model using nodal force calculations method. The results of the calculations (686 A and 1749 turns) are presented on the Table 6.

Table 6. Forces appeared after shift of the coil in various directions. The non-shifted values are Fx=Fy= 0 N, Fz = + 3.21 MN.

Shifts	Fx, N	Fy, N	Fz, N
Δz = 5 mm (opposite to the center)	~ 0	~ 0	$3.21*10^6$
Δz = -5 mm (to the center)	~ 0	~ 0	$3.07*10^6$
Δx = 5 mm	$2.56*10^4$	~ 0	$3.207*10^6$
Δx = 10 mm	$4.77*10^4$	~ 0	$3.12*10^6$
Δy = 5 mm	~ 0	$1.81*10^4$	$3.218*10^6$

The force on the poles was calculated in ANSYS 2D model. It is important to use a fine mesh size to calculate this force properly. The value of this force is 0.70 MN and it is attractive towards the nearest horizontal yoke beams.

Also pole force was calculated in the ANSYS 2D by virtual work method, i.e. the pole was shifted by some distance and the energy change was calculated. The pole was shifted by 2 cm and 4 cm toward the center of the magnet. The results are listed in the Table 7. These calculations also shows that the poles will be attracted to the nearest horizontal yoke beams because the energy increases with shifting.

Table 7. The energy change after shifting the one pole toward the center of the magnet.

Shift, cm	0	2	4
Energy, MJ	4.820	4.840	4.863
Force = dE/dx, MN		1	1.1

The main results of the magnetic field calculations are listed below.

1. The integrals around the center of the magnet is 1.012 T*m for 666 A of the current in last design of the field clamps.
2. Maximal magnetic field on the coil is ~ 3.6 T at 666 A current.
3. The vertical force on one coil toward the yoke is ~ 3.05 MN at 700 A current. The horizontal forces of de-centered coil are about 20 kN per 5 mm shift that is not much.
4. The force on the poles is about 0.7 MN and it is opposite to the center of the magnet. The neat force toward the center on the horizontal iron beams subtracting the vertical coil force is about 50 tones.
5. The influence the irons B-H parameters on the field integral is listed in the Table 5 and may be considered as not principal.

3.2. Mechanical calculations

The mechanical calculations of the iron yoke were done in ANSYS code.

The calculations were done upon old understanding that the poles are attracted towards to the center of the magnet. The deformation of the iron yoke after applied force from attracting poles to the center of the magnet, is shown Fig. 26. The applied forces values are 3 MN. Four bolts fixing the poles to the horizontal parts of the iron yoke are designed to keep the poles.

The current estimations show that the poles are attracted to the opposite direction, not to the center of the magnet. It looks worth to estimate the thickness of the horizontal iron beams because no significant forces are acting on them except the pole masses.

The iron yoke has not problems with structural loads.

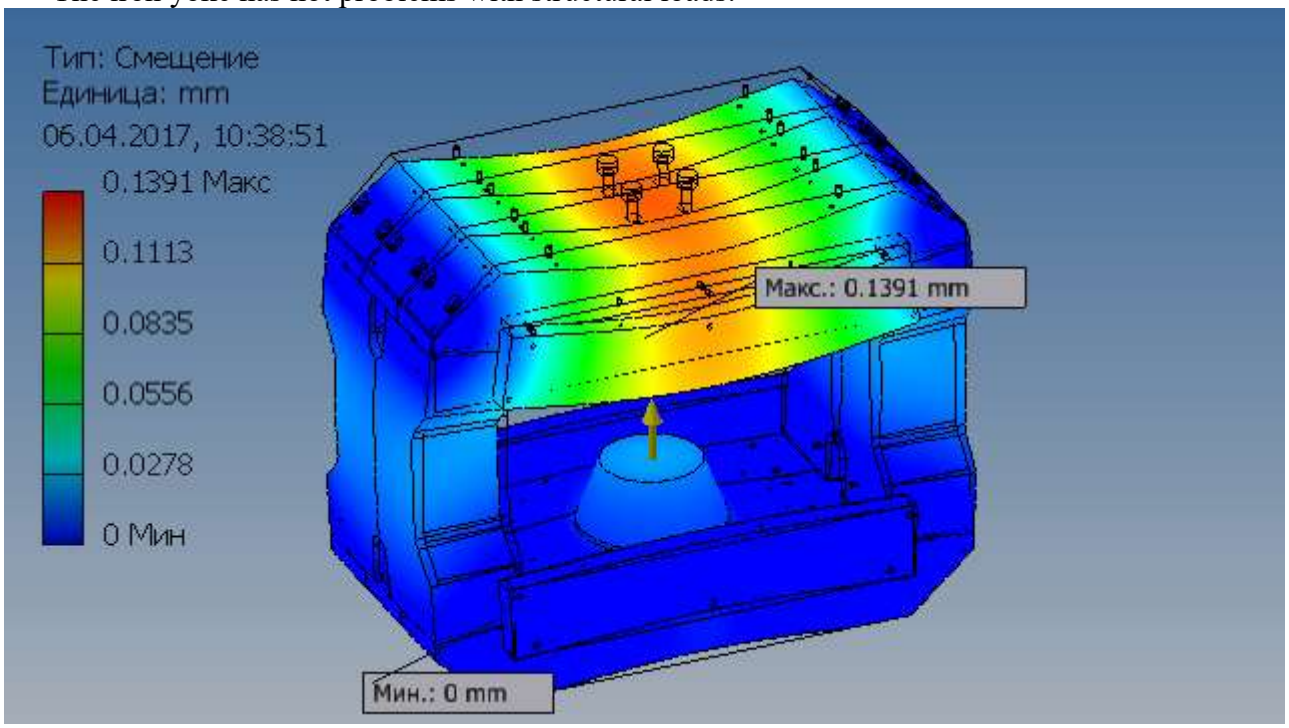

Fig. 26. Deformation of the iron after applying of the attracting forces to the poles. The maximal deformation is 0.14 mm.

Support struts under compressive vertical force

As mentioned above, two designs of the support struts are considered here.

Several models of the support struts (eight struts design) were calculated in ANSYS 3D models. The compressive force of 45 t (360 t of total load) and the temperature gradients were applied to the models as shown on the Fig. 7. Some results are presented in the Fig. 27 and Fig. 28. Weakest parts of the struts are G-10 cylinders having low tensile and shear strengths. The G-10 compressive tensile strength is ~ 300 MPa and ~ 600 MPa for 295 K and 4 K respectively [Carl L. Goodzeit]. The shear strength of G-10 is ~ 50 MPa and 100 MPa for 295 K and 4 K respectively [Carl L. Goodzeit].

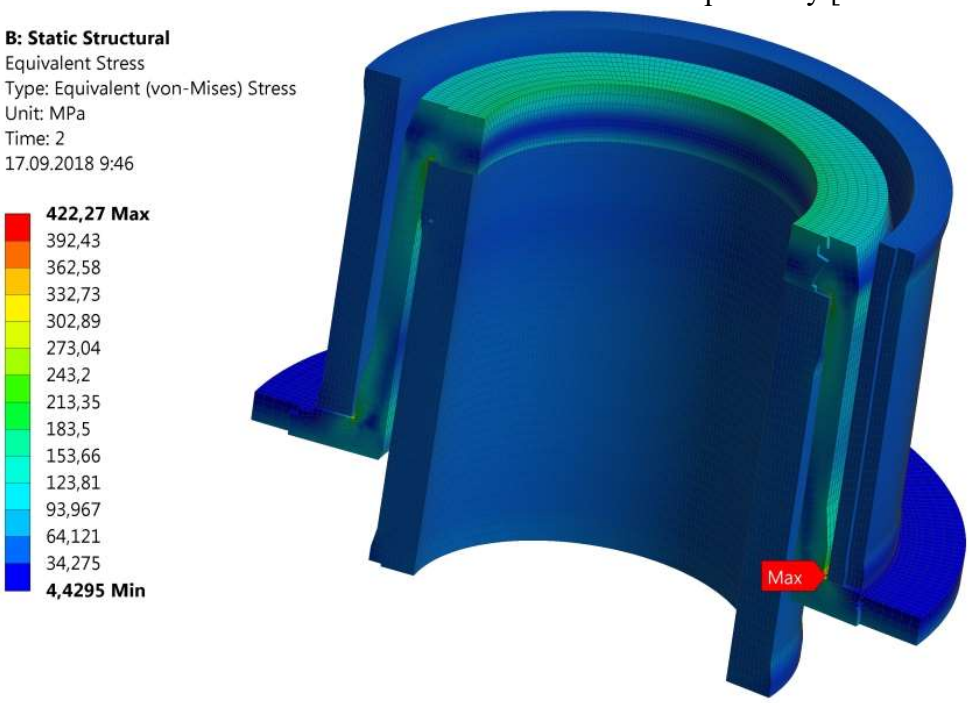

Fig. 27. The stresses in the support strut after of cooling down and application ~ 45 t vertical force.

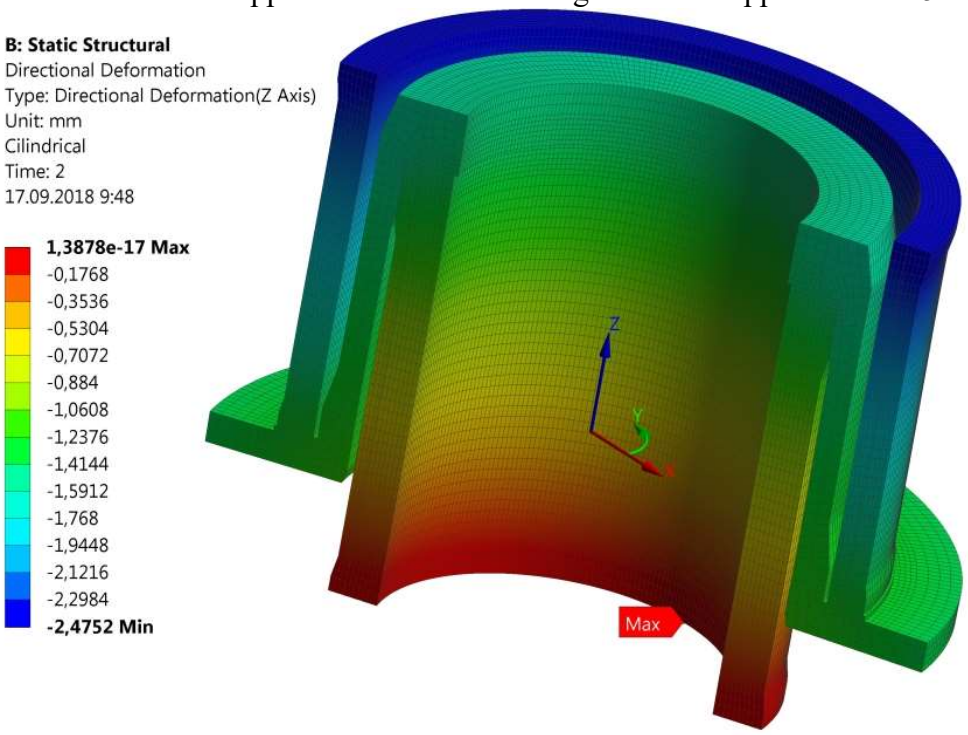

Fig. 28. The deformations in the support strut after of cooling down and application ~ 45 t vertical force.

The calculated maximal shear stresses in outer warm G-10 cylinder are 40 MPa and 60 MPa in warp and normal G-10 glass fibers orientations. So, the safety factor even in the warp model is low. The G-10 plastic may be subjected to delamination working in such conditions. As a conclusion one may say that the safety factor for the shear stress is very low. The thickness of the G-10 cylinder may be slightly increased.

In the single strut design, only 2D ANSYS model was calculated, now. The main idea of the single support design is to place the G-10 ring uniformly around whole coil to avoid its bending between the struts in the 8 struts design. The thickness of the G-10 ring should be approximately the same in both designs, about 10 mm.

The von Mises stress values are presented on the Fig. 29 below. The maximal values in the G-10 rings are on the thick places, about 300 MPa. The shear stresses in the G-10 rings

The comparison the shear stresses between these two designs is presented on the Fig. 30. The maximal shear stress in the eight struts design is in the thinnest part of the cylinder; while the maximal shear stress in the single strut design is on the thick ends of the cylinder. Anyway, the calculations of the single struts design will be continued to have full 3D model calculations as in the Fig. 30 on the left figure.

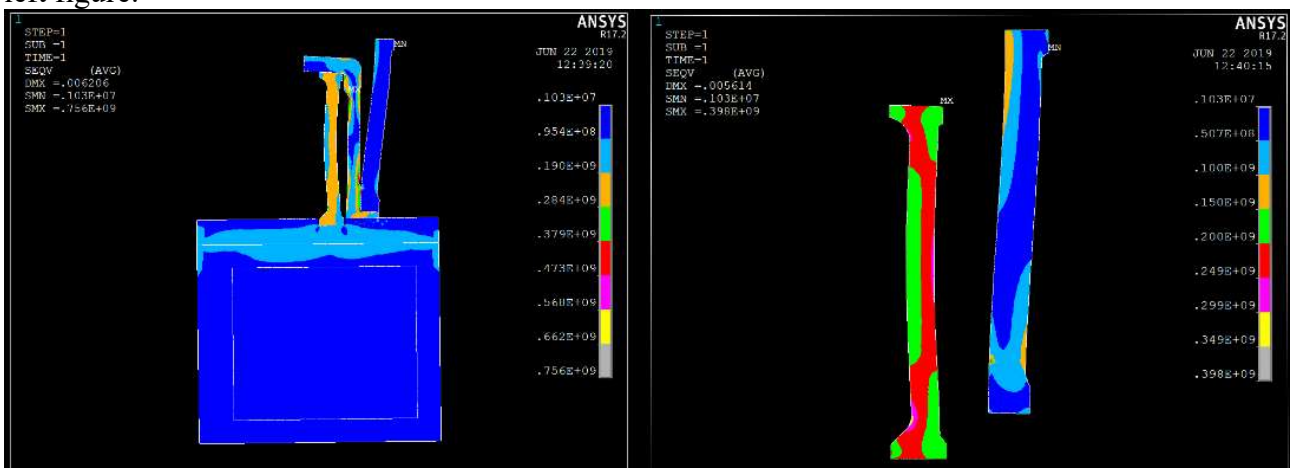

Fig. 29. The von Mises stress in the 2D model of ANSYS calculations. The whole model is on the left, the G-10 cylinders of the support is on the right.

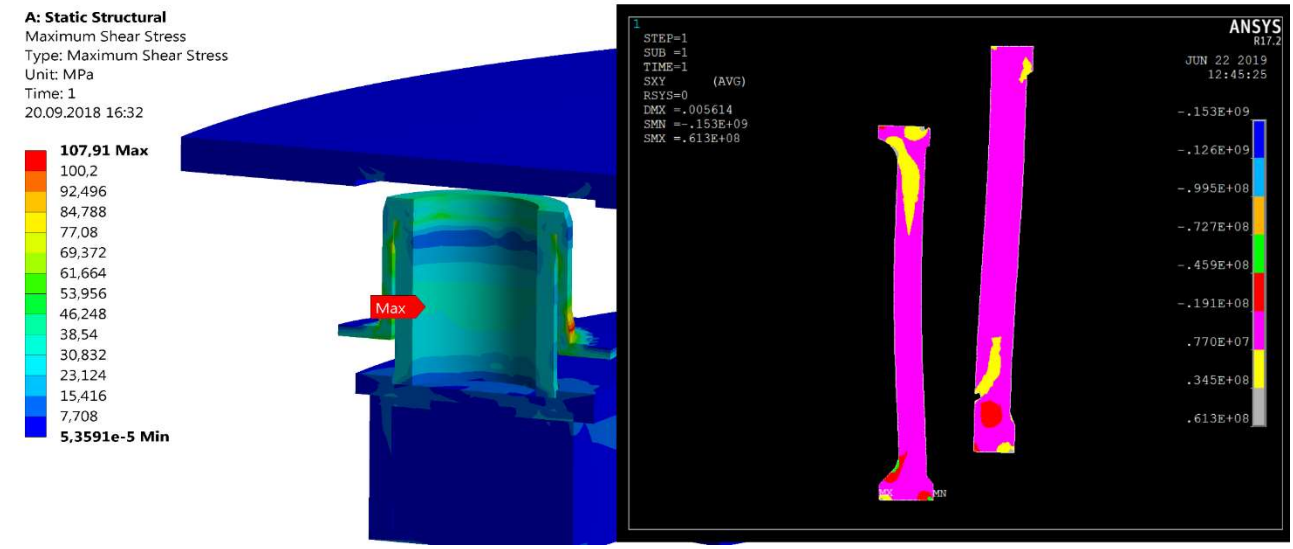

Fig. 30. The shear stresses: left is in the 8 struts design, full 3D model; right is in the G-10 rings in 2D model only.

Coil stress and strain calculations

The cold mass of the coils consists of different materials. The internal stress will appear after

cooling down and magnetic forces application. The purpose of the calculations is to obtain stress and deformation of the CBM coil structure under the following loads:
- strains and stresses after cooling down from room temperature to 4.5 K temperature;
- strain and stresses after application of the Lorentz force, which were taken as 3 or 3.5 MN of axial direction, and of 5 or 6 MPa pressure on the inner radius of the coil.

The ANSYS code was used for these calculations **in the eight struts design**! The magnetic forces were applied as external forces on the coil. The values of the forces were imported from another ANSYS magnetic field 3D calculations. Some results of direct application of magnetic forces are presented below in the simplified model.

The criteria of acceptable stress results are:
- the stress in the stainless steel is below 600 MPa that is the yield stress at low temperatures;
- the stress in the copper is below 450 MPa that is the ultimate stress at low temperatures;
- the stress in the SC cable is below 350 MPa that is the stress of degradation of superconducting property of NbTi by ~ 5%;
- the stress in the winding structure is desired to be below 100 MPa that is the tensile stress of epoxy compounds at low temperatures. The shear stress τ in epoxy is linked with the tensile stress as: $\tau = \sigma/\sqrt{3}$ (that is in conservative von Mises criteria, for the composite materials it might be higher). Therefore, the τ values should be less than ~ 58 MPa. Stresses beyond these values may produce epoxy cracking causing premature quenches. If such stress is exceeding the 100 MPa value but of compressive quality or not making movements of the SC cable then it may be treated as an acceptable stress.

Preamble before making ANSYS stress and strain calculations

Before making a numerical calculations using some code its worth to evaluate the stress in the coils with simple formulas for a better interpretation of the calculated results. The coil stress appears after application of the two Lorentz forces coming from radial and axial magnetic fields. Also the internal stresses from different thermal contraction of the materials should be considered. Finally, the stresses will be evaluated in ANSYS code. The axial magnetic field in the coils acts as pressure, it may be evaluated directly as Bz*I*L or as knowing that B^2 acts as pressure 0.4 MPa corresponding to 1 T. As the Bz ~ 3.5 T, the pressure will be ~ 5 MPa. This pressure leads to hoop stress in the coils which is estimated as $\sigma = p*R/h$ (R - radius and h - radial thickness of the coils). So, $\sigma = 5*0.7/0.16 = 22$ MPa – the hoop stress without Cu and stainless steel plate. As these elements have higher Young modulus than the SC winding the code calculations of the whole model should give much lower values of the hoop stress.

The radial magnetic field produces the axial force attracting the coil to the closest iron. Its value was calculated as ~ 2.5 MN. If the coil would be uniformly held in axial direction the axial stress inside the coil would be as $\sigma = F/(2\pi R*h) = 2.5/(6.28*0.8*0.16) = 3.1$ MPa – very low value. But in our design the coil will be fixed with six support struts, so the stresses from the axial force will be localized around these struts due to bending of the coil arcs in axial direction. Such bending effect may be estimated as for bending a beam having one end fixed and the other end free. This stress is evaluated according:

$\sigma = \frac{M}{J_x} * y$, where M – force momentum [N*m], Jx – momentum of inertia [m^4], y – half length of the coil axial size. For a rectangular shape beam the $Jx = a*b^3/12$, as a ~ b = 0.2 m, then $Jx = 1.33*10^{-4}$ m^4. $M = F/24 * 2\pi R/12 = 4.4*10^4$ N*m. The half-length y ~ 0.1 m. The result is:

$\sigma = 4.4*10^4*0.1/1.33*10^{-4} = 33$ MPa.

Firstly this value should be considered as highest as the bending beam has not free end. Secondly, the maximal stress will be in the stainless steel plate, and thirdly this value is well low.

The final stress will be with addition of the thermal contraction stresses.

The calculations presented below should be interpreted upon rough estimation given in this preamble.

End of preamble

The 3D model of the coil used in the calculations was consisted of the following materials visible in Fig. 10: stainless steel plate, copper case, G-10 sheets of 2 mm thickness surrounding the SC winding, the SC winding was a composite material containing ~ 50% of G-10 material. Anisotropic properties of the materials were also accounted. All relevant parameters of the materials are listed in the Table 8. There was a friction boundary condition between the copper case and the stainless plate. The stainless steel plate will be bolted to the copper place.

The calculated model was represented by 1/4 length of the real model.

The first set of the calculated results is shown on the Fig. 31 - Fig. 37. These results were obtained at applied vertical force of 3.6 MN and internal pressure of 6 MPa on the winding. As far as the coils are intended to be tested at 1.05 factor of the current the forces must by higher by ~ 10%. The forces were applied uniformly! The material properties of the winding were taken summary of the contraction coefficients winding materials that is listed in Table 8.

The influence of different materials was shown in previous CBM magnet reports. It is very important to use epoxy resin filled with fine powders that is well known fact in designing of SC magnets.

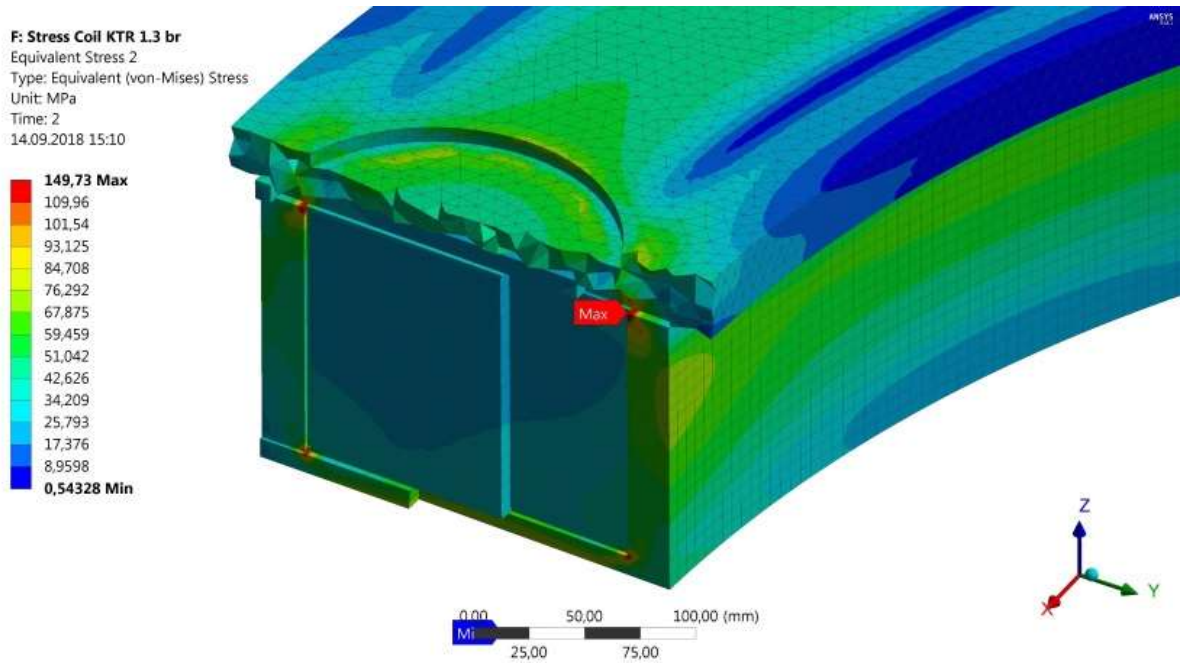

Fig. 31. The total stress in the coil structure after cooling and forces application. The maximal value is about 150 MPa in the stainless steel plate.

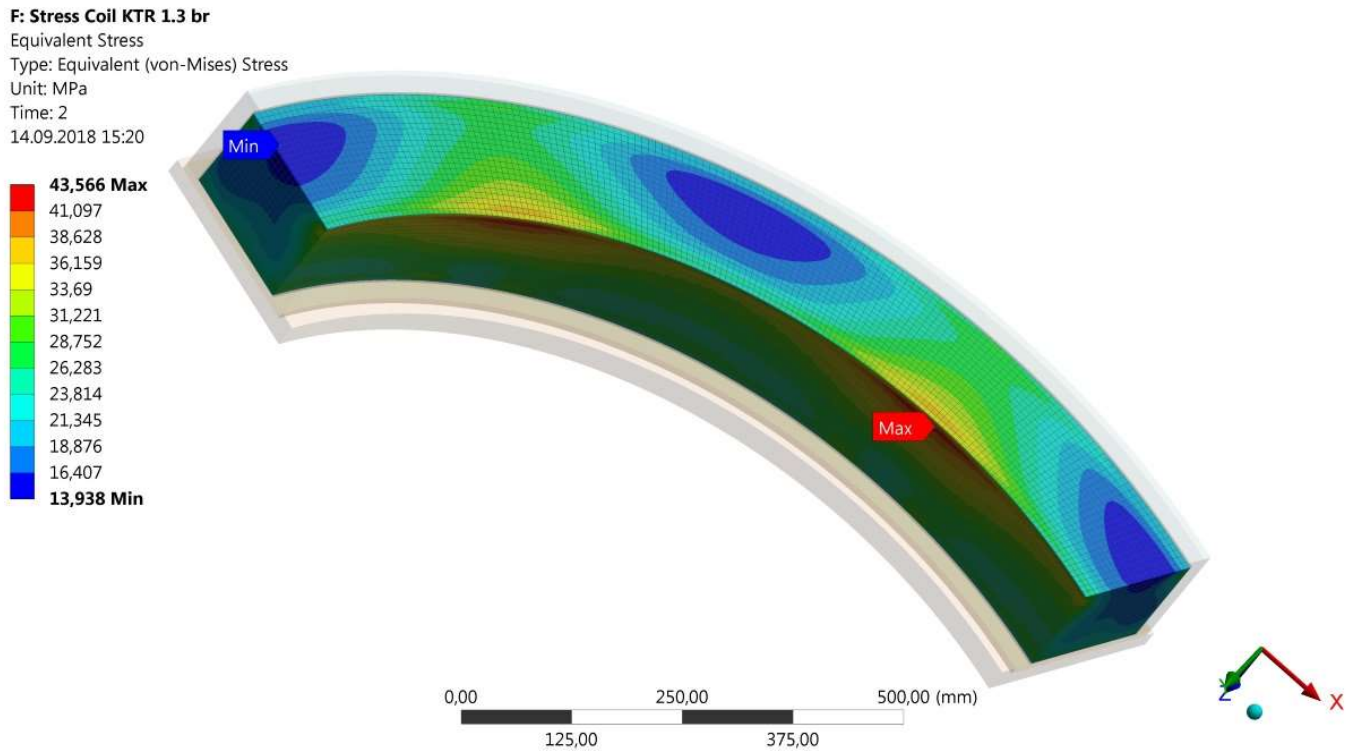

Fig. 32. The von Mises stress in the structure after cooling down and forces application. The maximal value is about 43.6 MPa in the same place. The grey part is the copper case and the st steel plate.

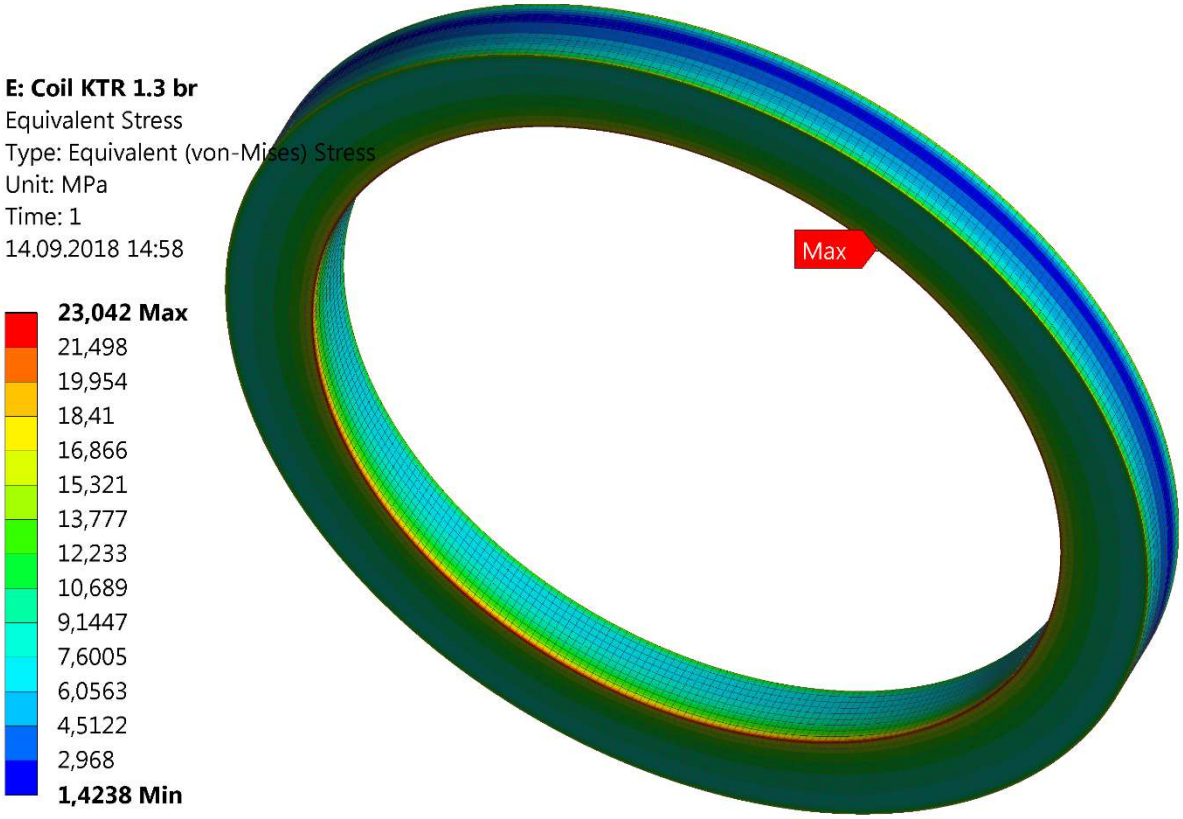

Fig. 33. The von-Mises stress in the coil after cooling down only.

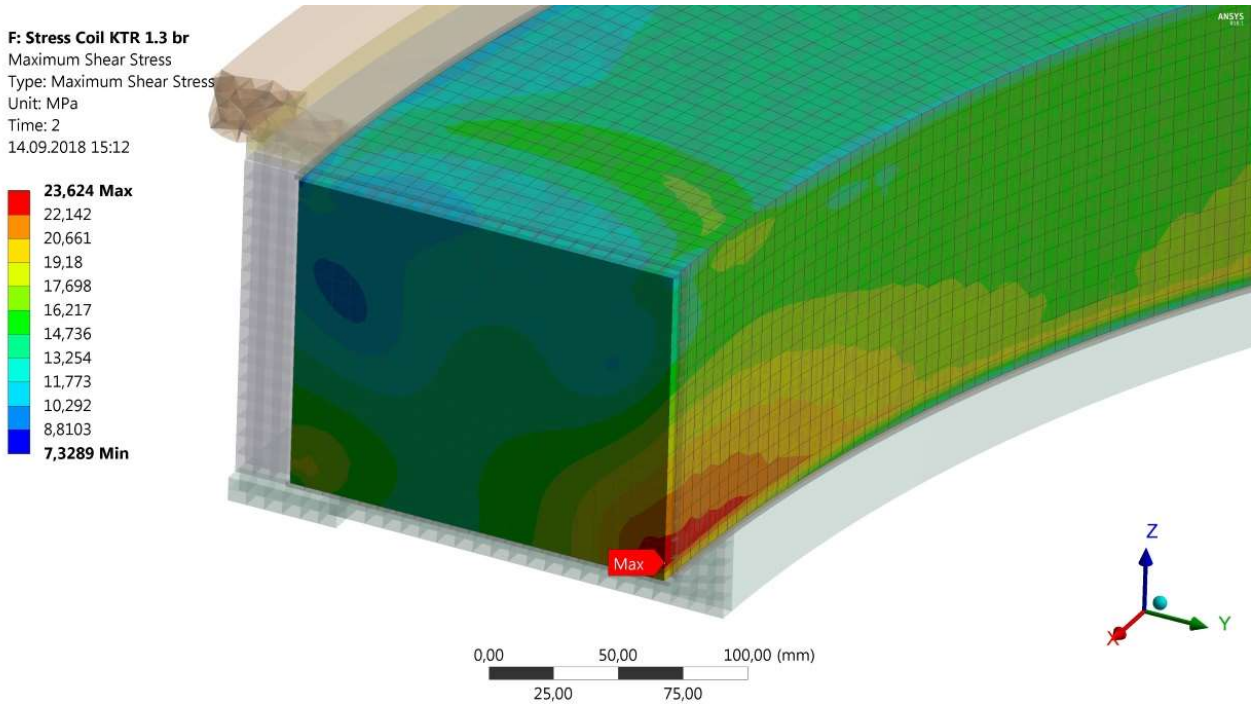

Fig. 34. The shear stress in the coil after cooling down and forces application. The maximal value in the coil is 23.6 MPa.

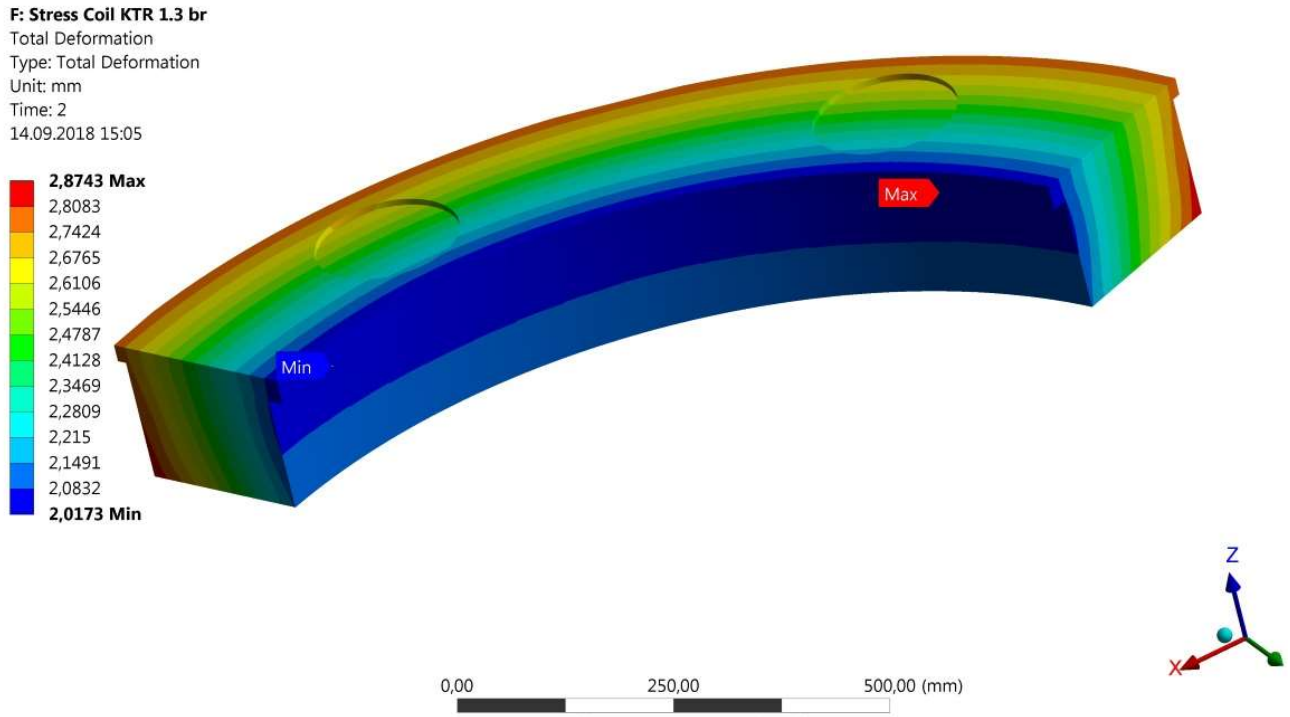

Fig. 35. Total deformation after cooling down and forces application.

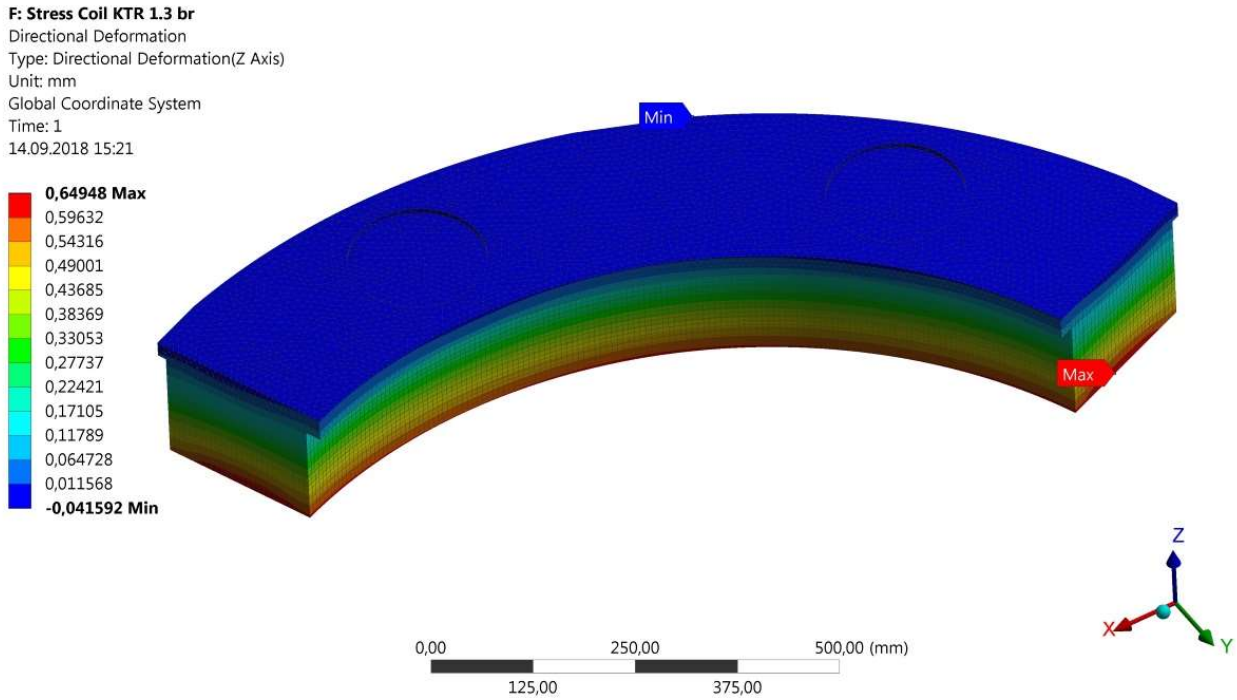

Fig. 36. Total deformation in vertical direction (Z axis) after cooling down.

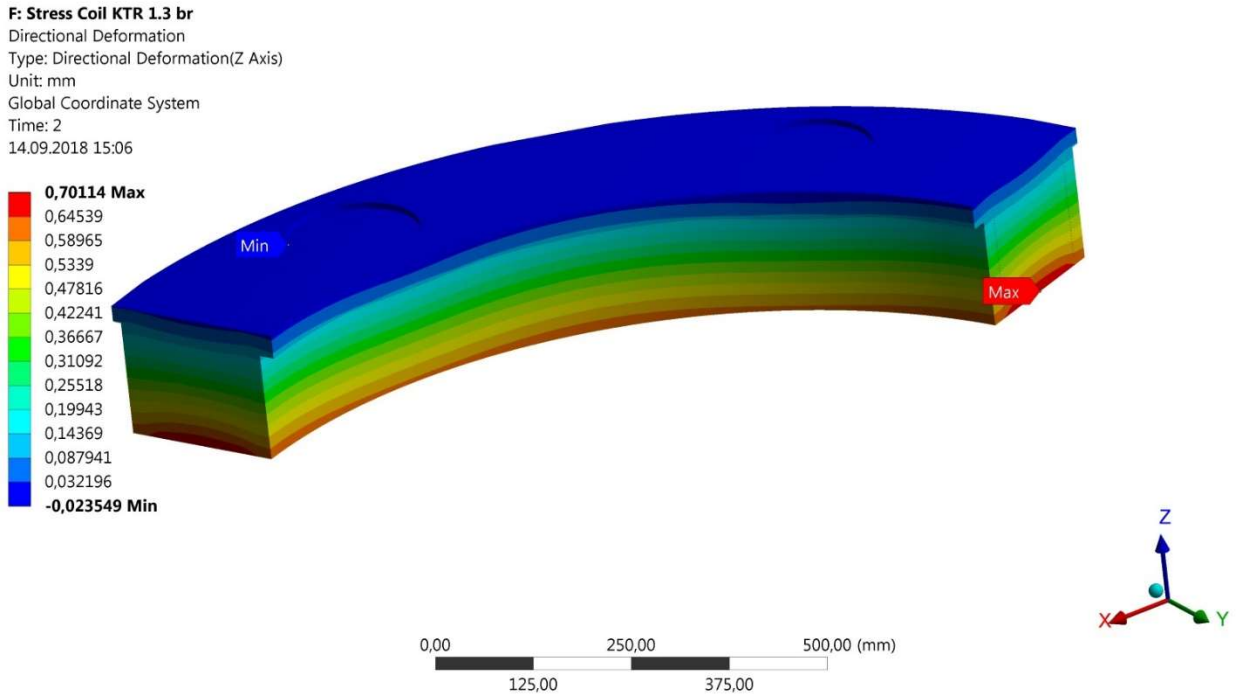

Fig. 37. Total deformation in vertical direction (Z axis) after cooling down and forces application. The superconducting coil will be bended by 0.05 mm after vertical force application.

The stresses in the all magnet model with additional horizontal forces due to misalignment

The magnetic field calculation have shown that there will be forces due to misalignment of the coil with respect to the iron yoke, Table 6. The calculation were done in ANSYS 3D model as shown in the Fig. 38. The main loads are shown on this figure, the applied horizontal force was 30 kN. The main results of the calculations are presented on the Fig. 39 and Fig. 40.

Some other figures of such calculation may be presented but no surprises there was seen.

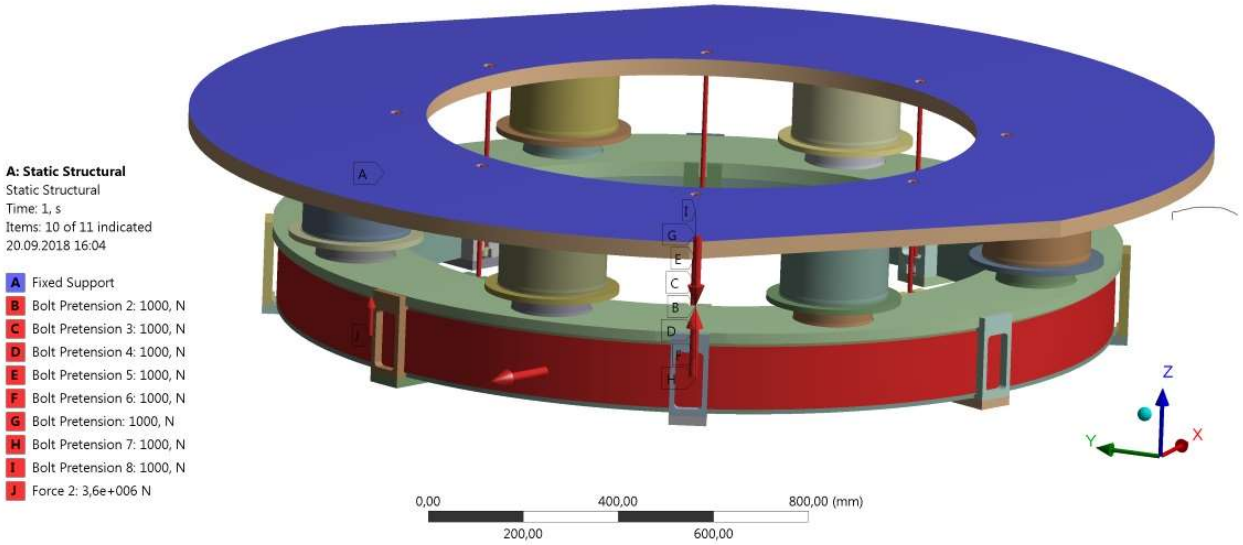

Fig. 38. The model with loads for misalignment calculations.

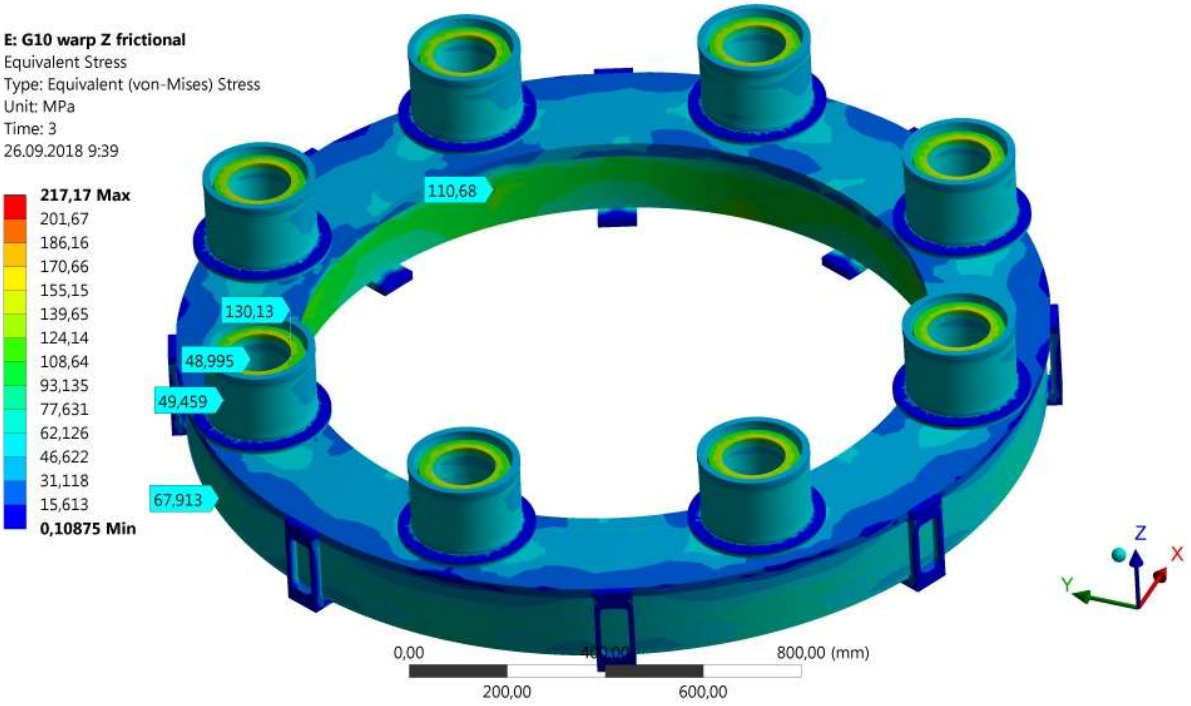

Fig. 39. The von Mises stress after all loads application. The maximal values are on the stainless steel cylinders of the support and the stainless steel plate.

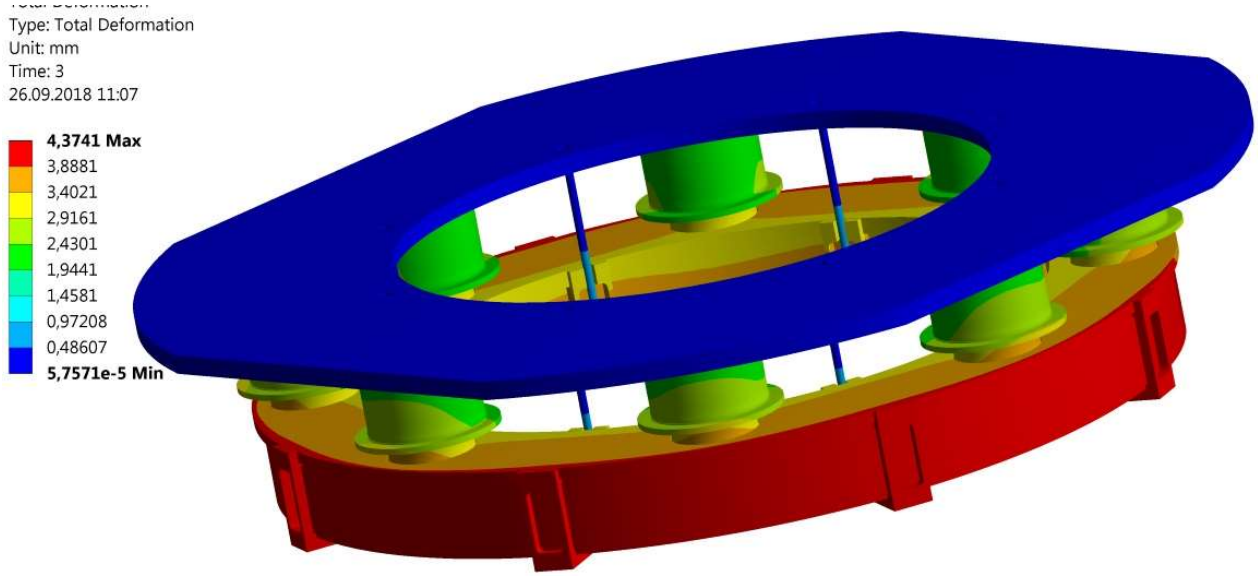

Fig. 40. The total deformation after cool down and of all loads application and 30 kN of horizontal force. The coil has moved by 0.7 mm horizontally.

The combined magnetic-structural analysis in ANSYS 3D model

The magnetic field calculations have shown that the distribution of radial and axial components of the magnetic field is not uniform azimuthally leading to increasing of vertical force by ~ 30%. The non-uniformity of the axial component of the magnetic field is about 8.6%, leading to non-uniformity of internal pressure. For this purpose the combined magneto-structural analysis was done in the simple model shown in the Fig. 41 where the forces from the magnet analysis were transferred to the structural analysis. The model includes the coil, copper case and stainless steel as a solid construction, i.e. without friction.

The results are presented in the Fig. 42 and Fig. 43. No significant difference is seen inside the coil due to non-uniform magnetic field that can be interpreted that the rigid materials surrounding the coil make the stress distribution more uniform in the coil.

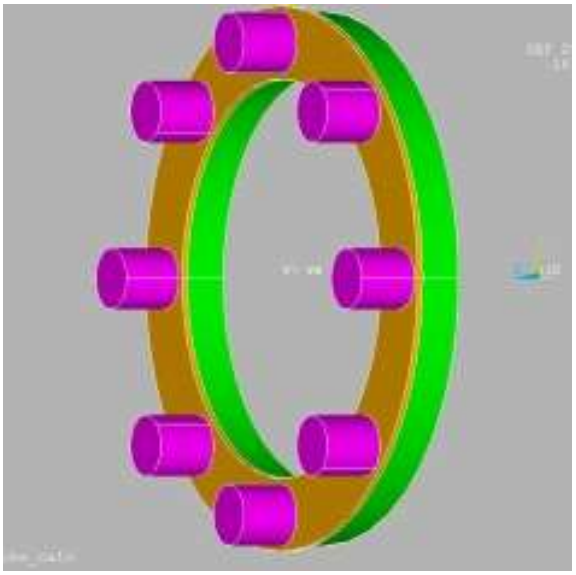

Fig. 41. The 3D model in the magnetic-structural calculations.

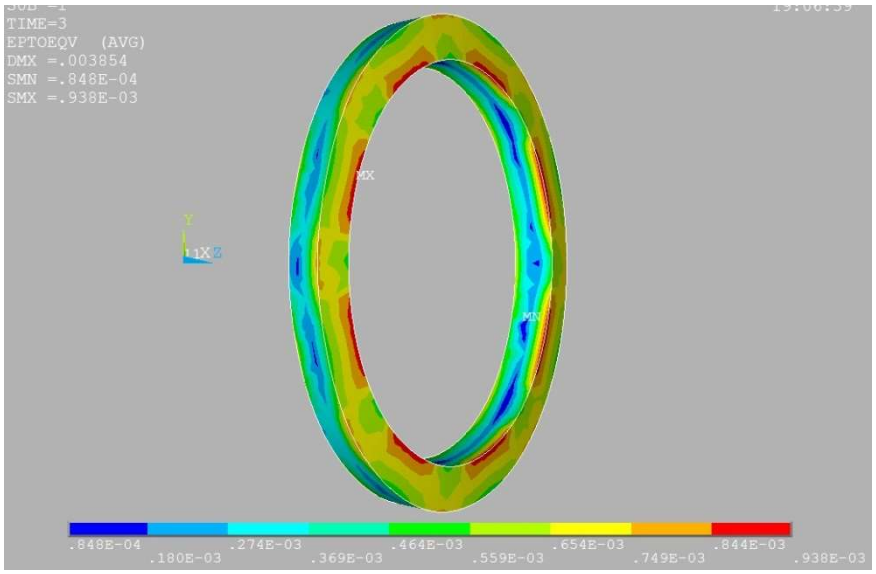

Fig. 42. The von Mises strain in the coil.

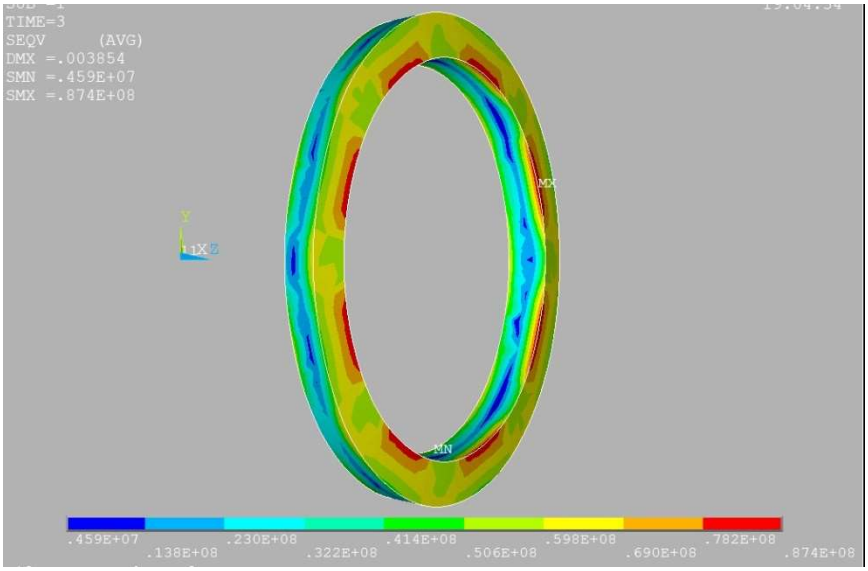

Fig. 43. The von Mises stress distribution in the coil [Pa], maximal value 87 MPa. Local accumulation of the stresses due to non-uniform values of the magnetic field is not high.

The demonstration of non-uniform distribution of the vertical force along azimuth is shown on the Fig. 44 – only here such non-uniformity was presented in this model. Also the ***ellipticity*** of the coil is not seen due to very low difference of the axial component of the magnetic field, only 8.5%. Although, it may be estimated by a formula giving 0.04 mm.

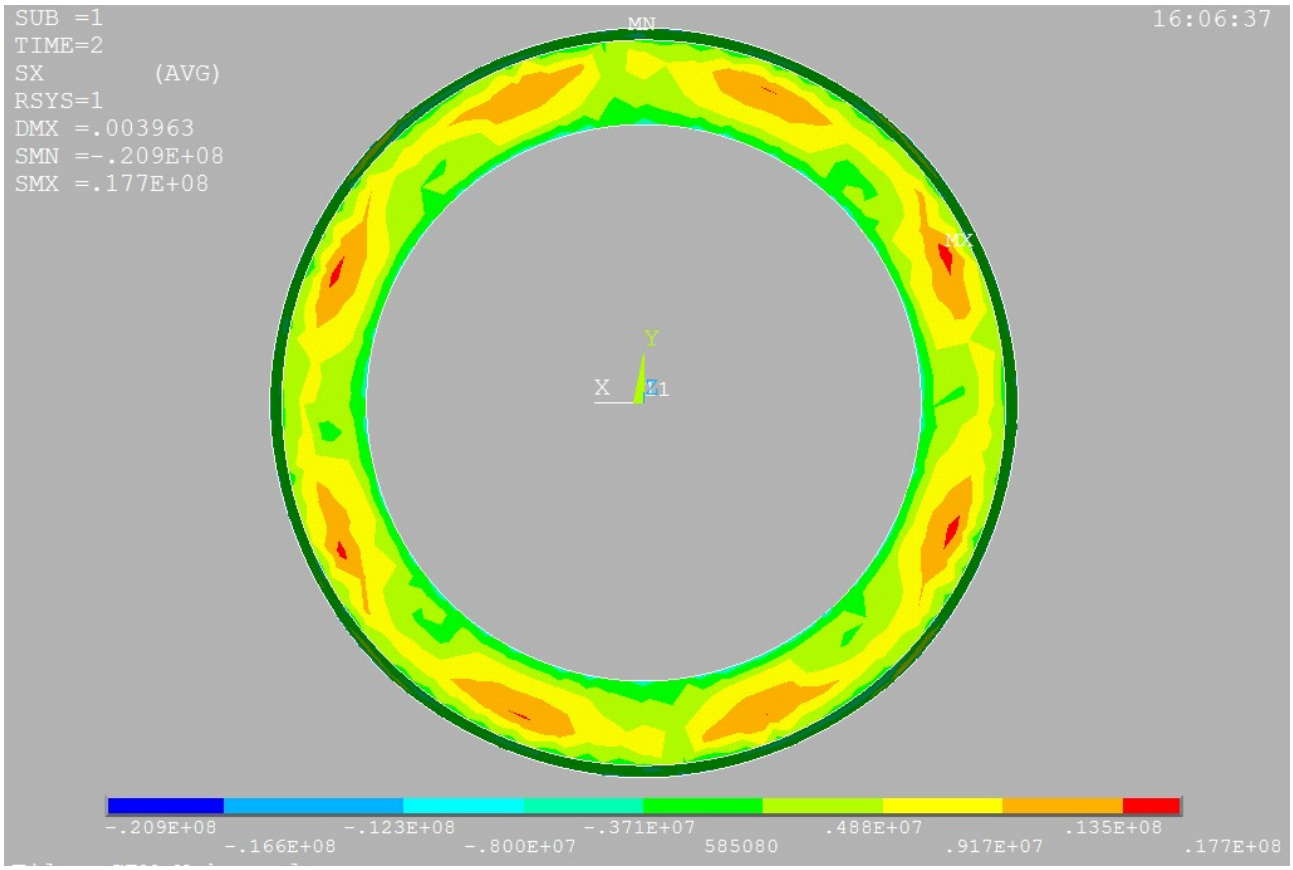

Fig. 44. The radial stress in the copper case. The demonstration of non-uniform distribution of the vertical force along azimuth – that is the red zones.

Table 8. Some materials properties used in the structural analysis.

Property	Stainless steel	GFRP material	Coils	Epoxy	Copper
Thermal expansion coefficient, K^{-1}	$1.11\ 10^{-5}$	$1.2\ 10^{-5}$	$1.2\ 10^{-5}$	$1.2\ 10^{-5}$	$1.25\ 10^{-5}$
Shear modulus in xz plain, Pa	$7.5\ 10^{10}$	$4.0\ 10^{9}$	$1.9\ 10^{10}$	$4.0\ 10^{9}$	$4.0\ 10^{10}$
Young modulus y direction, Pa	$2.0\ 10^{11}$	$1.8\ 10^{10}$	$4.1\ 10^{10}$	$9.0\ 10^{9}$	$1.2\ 10^{11}$
Thermal expansion coefficient y direction, K^{-1}	$1.11\ 10^{-5}$	$1.0\ 10^{-5}$	$1.57\ 10^{-5}$	$6.0\ 10^{-5}$	$1.25\ 10^{-5}$
Thermal expansion coefficient xz plain, K^{-1}	$1.11\ 10^{-5}$	$1.6\ 10^{-5}$	$9.2\ 10^{-6}$	$1.6\ 10^{-5}$	$1.25\ 10^{-5}$
Young modulus xz direction, Pa	$2.0\ 10^{11}$	$2.2\ 10^{10}$	$7.5\ 10^{10}$	$1.8\ 10^{10}$	$1.2\ 10^{11}$

Young modulus for the winding consisting of different materials can be estimated by the following formulas:

In the transverse direction of SC cable it is: $E_{tr} = \frac{E_1 \cdot E_2}{E_1 \cdot f_2 + E_2 \cdot f_1}$, where f1 and f2 – filling factors of the material and E1 and E2 – Young modulus for the corresponding material.

In the direction along the SC cable it is: $E_{nor} = E_1 \cdot f_1 + E_2 \cdot f_2$, with the same parameters as above.

The results and conclusions on the structural analysis

1. The stresses in the total coil structure and in the SC winding are well below stresses in all principal materials: stainless steel, copper, and NbTi superconductor. The problem of epoxy cracking is also not seen there, that happens if the tensile stress value exceeds 100 MPa. The

main principal stress inside the winding is positive and is in circumference direction, i.e. the radial movements of the SC cable will not happen.

2. The stresses after cooling down due to difference of the thermal contraction coefficients give about 50% of the total stress value as seen in Fig. 32 and Fig. 33. In the presented calculations the insulation material had the contraction coefficient higher by 30% than for copper. During manufacturing it is planned to impregnate the winding with epoxy composite containing up to 50% by weight of powders. Such epoxy composites have contraction coefficients very close to the contraction coefficient of metals. The considered possible powders are Al_2O_3 (continuously used in BINP) and BN having more excellent parameters, see Fig. 45. The problem that the powders will not go deep inside the winding looks not principal because the maximal stresses are on the outer surfaces of the winding. This technology will be tested before the impregnation of the real coils as it is always done in the BINP workshop.
3. The main models were calculated at loads with higher values than obtained from the magnetic field calculations, i.e. 5 or 6 MPa of pressure and 3.6 MN of the vertical force. In the last design these values are lower.
4. Ellice shape of the coil after its powering was not visible due to very low total radial stress after powering which is estimated about 0.04 mm (total radial shift after powering).
5. Delamination of the SC winding during cooling down or powering has low probability. During ordinal cooling down this process will go at very low cooling power, about 500 W per coil. If such power will be applied to the presented copper structure it will not destroy it. The transient behavior of such process were calculated but not presented here.
6. The calculations of the single strut design concerning the coil stresses were discussed in additional report distributed on November 2018, Fig. 46. The stresses in the coil were less in this design. The stresses in the support itself are presented in 2D design here. They show tolerable results, although 3D model calculations will be done in August-September 2019. The heat load in both design of the struts is the same, about 5 W per coil.
7. The vertical strain of the coil assembling is 1÷2 mm after cooling and loads application. It should be accounted in the total design in the room temperature dimensions.

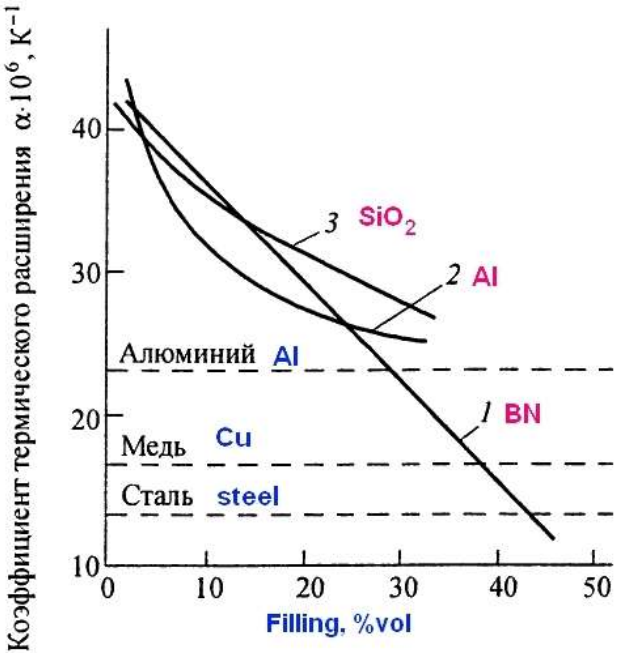

Fig. 45. Influence of filling components in epoxy on thermal expansion coefficient [Yu. Solntsev, p. 679]. The dash lines are the thermal expansion coefficients for metals for comparison.

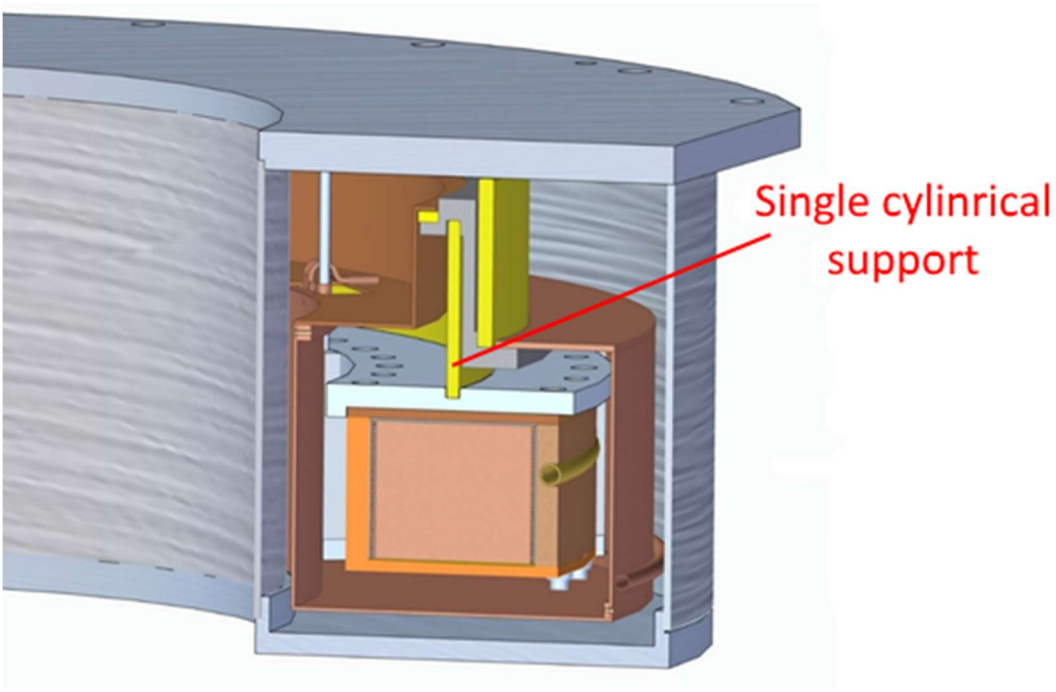

Fig. 46. The design proposal of the single cylindrical support.

3.3. Heat load estimations

The results of the heat loads estimations are presented in the tables below. The view of the temperatures applied to the cold mass is shown on the Fig. 47.

Estimations of the heat loads to 4.5 K helium

The thermal radiation on the LHe coil cases was estimated as:

$Q = \varepsilon S \sigma T^4$, where ε - total emissivity was taken as 0.02, S – surface area of the total coil is 4.2 m^2, T – radiation shield temperature was taken as 60 K.

The heat load from the support struts via stainless steel plates was estimated as:

Q = 16 * 0.51 = 8.2 W – for sixteen struts, where 0.51 is taken from calculations presented below in Fig. 50.

The heat load from the Ti tie rods was estimated as:

$Q = \lambda S^* \Delta T/L$, where λ - thermal conductivity was taken as 0.15 W/(m*K), S – cross-section area is about $1.1*10^{-4}$ m^2, ΔT – temperature difference was taken as 60 K, L – length is about 0.25 m.

Joule heat in the soldered splices was estimated for soldering on 5 cm of length and resistance to be about $5*10^{-8}$ Ohm and at 686 A of current.

Heat loads from the eddy currents during the coils powering is estimated as $Q = U^2/Rco$, where $U = B*S/\Delta t$ and Rco – resistance of the copper case at 4.5 K temperature.

$U = 3T*\pi*0.82^2/3600 = 1.8$ mV – voltage during 1 hour charging rate.

$R = 1.8*10^{-10}$(Ohm*m)*5 m/($5*10^{-3}$ m^2) = $1.8*10^{-7}$ Ohm.

Q_{1h} = 18 W per coil at 1 hour ramping rate. Total power is 36 W.

Q_{4h} = 1.1 W per coil at 4 hour ramping rate. Total power is 2.2 W.

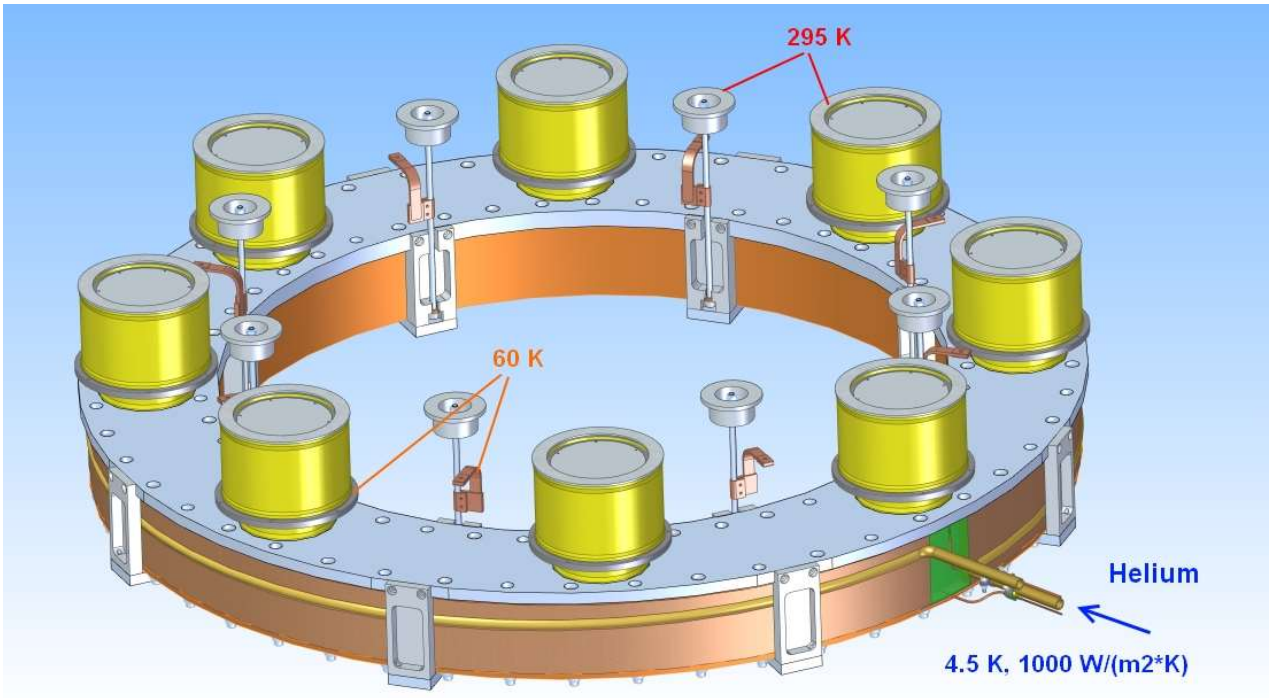

Fig. 47. View of the cold mass of the magnet connected by suspension rods and support struts to the vacuum vessel. The temperatures taken into calculations are shown.

Table 9. Heat loads on 4.5 K helium from both coils and the cryostat.

Heat load sources	**Values**
Thermal radiation on the outer surface of the coil, W	0.12
Support struts, W	< 8.2 expected
Tie rods, W	1.5
Soldering connection of the cable (at least 6 short splices), W	0.12
Thermal radiation on the cryostat, W	0.015
Cryostat suspension, W	<0.1
Current leads, W	0.5
Measurements wires, W	<0.1
Heat bridges of the cryostat neck and others connections, W	<0.1
Eddy currents during the powering for 4 hours, W	*2.2*
Total, W	***~ 10.8*** *(+2.2)*

Hot loads from the support struts and the suspension rods

The support struts give largest part of the magnet heat loads at 4.5 K cold mass. The superconducting winding will press the stainless steel plate exactly opposite these struts. In the current design of the coil the superconducting winding the thick copper wall prevents significant hot spot appearance due to large thickness, about 20 mm.

The presented calculations are to eight struts design. The heat loads from single support design, see Fig. 8, should be close because the total G-10 cylinder thickness is considered to be the same.

The heat loads from the support struts are presented in the Fig. 48 - Fig. 50 as results of $1/10^{th}$ of the support part calculations. The room temperature was fixed at 295 K and the thermal interception by the radiation shields was fixed at 60 K.

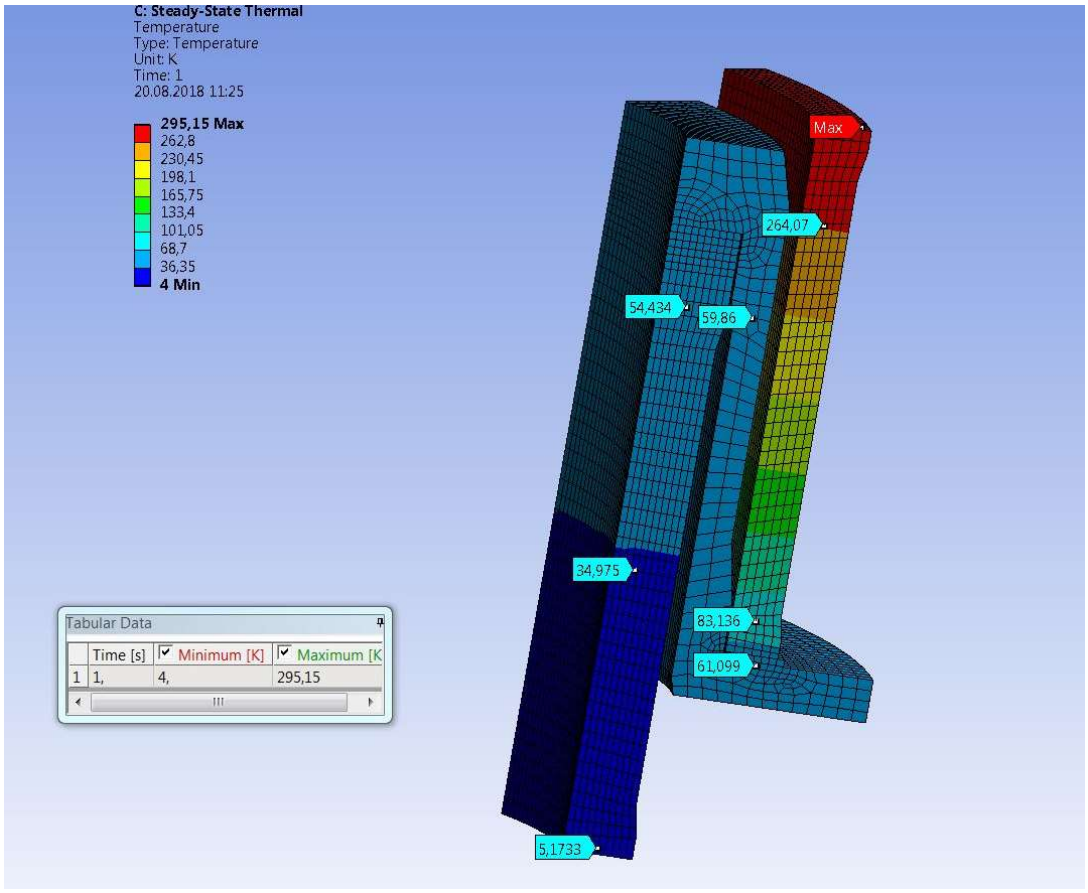

Fig. 48. Temperature distribution in the support strut then the bottom is fixed at temperature 4.5 K, the top at 295 K and the interception at 60 K.

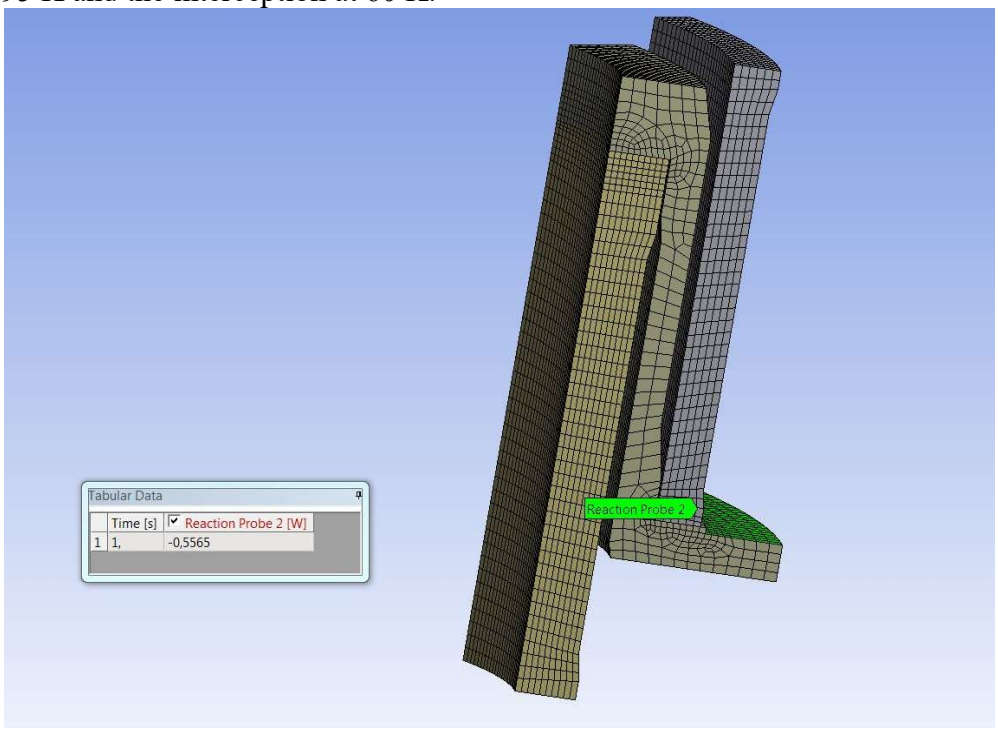

Fig. 49. Heat load on the interception at 60 K is shown, the total value for one strut is 5.6 W.

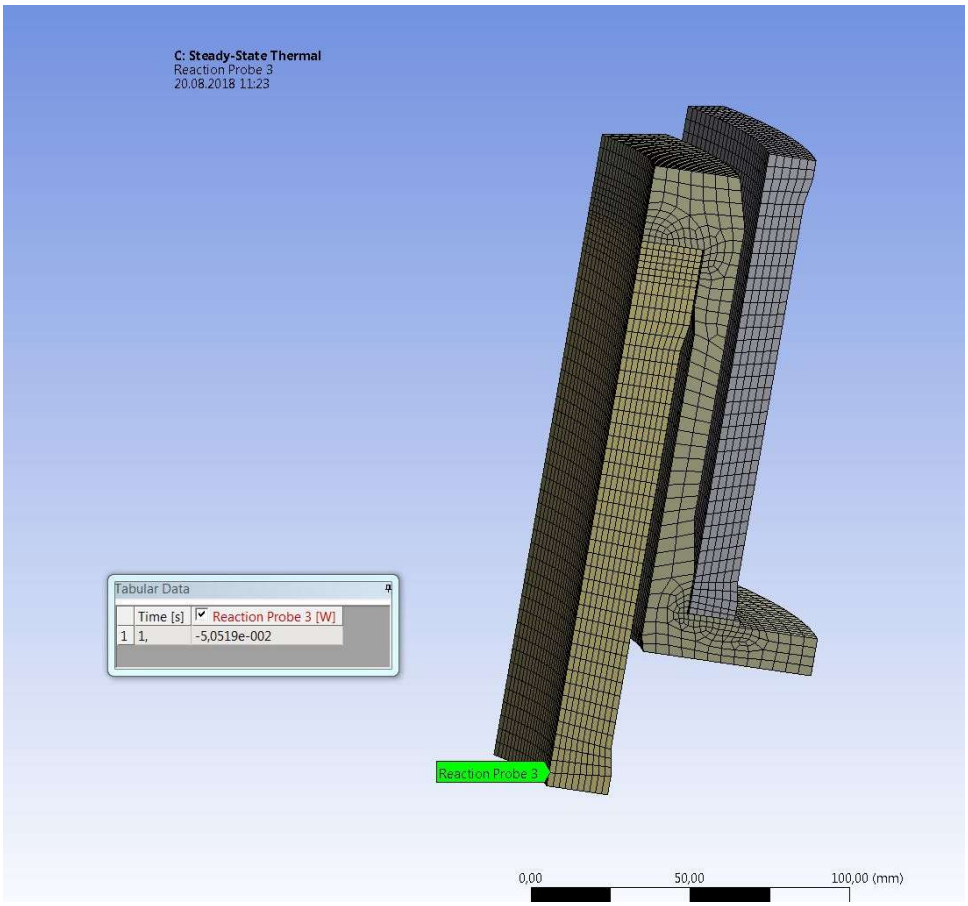

Fig. 50. Heat load on bottom of the strut at 4.5 K is shown, the total value for one strut is 0.51 W.

The temperature map around the coil suspension rod is shown in the Fig. 51. The heat loads to the 4 K and 60 K surfaces are **0.093 W** and **1.4 W** respectively.

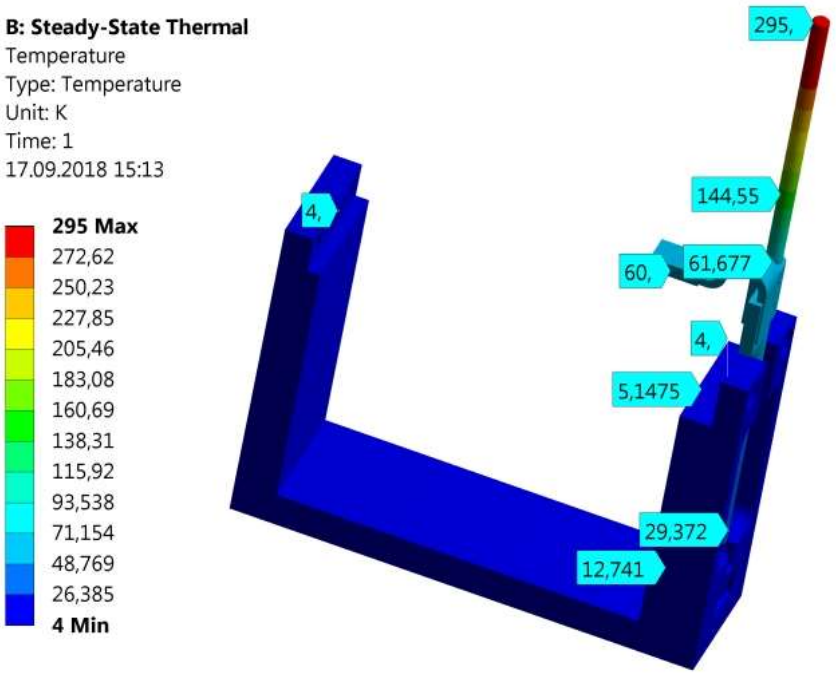

Fig. 51. The temperature map on the suspension rod from 295 K to 4.5 K temperatures. The interception is at 60 K temperature.

Estimations of the heat loads to 50 K helium

The thermal radiation from the vacuum vessel on the radiation shields covered by multilayer insulation may be estimated as:

$Q = q*S$, where, S – surface area of the shields is ~ 5 m^2, q – experimentally determined heat flux, its typical value is about 1 W/m^2.

The heat load from the support struts via stainless steel plates was estimated as from Fig. 49:

$Q = 12*4.12 = 49.5$ for twelve struts.

The heat load from the tie rods was estimated as:

$Q = \lambda S*\Delta T/L$, where λ - thermal conductivity was taken as 0.15 W/(m*K), S – cross-section area is about $1.1*10^{-4}$ m^2, ΔT – temperature difference was taken as 220 K, L – length is about 2*0.15 m (two cylinders).

Table 10 Heat loads on 50 K helium from both coils and the cryostat

Heat load from	**Values**
Thermal radiation on the shields from the vacuum vessel, W	10
Support struts, W	90
Tie rods, W	22
Thermal radiation on the cryostat shield, W	1.5
Cryostat suspension, W	2
Current leads, W	120*
Measurements wires, W	0.5
Heat bridges of the cryostat neck and others connections, W	1
Total, W	~ 247

*) It will be corrected after detailed design of the current leads

The estimation of heat loads from on the Branch Box, the Feed Box and on the transfer line are presented in the Table 11 and Table 12.

The thermal radiation on the surfaces at 4.5-4.6 K was estimated as:

$Q = \varepsilon S\sigma T^4$, where ε - total emissivity was taken as 0.03, S – surface area of the BB, FB and the transfer lines surfaces at 4.5 K is about 7 m^2, T – radiation shield temperature was taken as 60 K.

The heat load from the control valves was estimated on example of Weka valves of DN15 size as: $Q = N*Q_v$, where N – is the number of valves, in our case is 19, Q_v – the heat load from one valve specified by manufacturer, which is in our case about 0.8 W.

The heat load from the check valves was estimated as:

$Q = \lambda S*\Delta T/L$, where λ - thermal conductivity of stainless steel tubes and bellows was taken average as 3 W/(m*K), S – cross-section area is about 10^{-3} m^2, ΔT – temperature difference was taken as 60 K, L – length is about 0.2 m.

Table 11 Heat loads on 4.6 K helium from the Branch Box, the Feed Box and the transfer line

Heat load from	**Values**
Thermal radiation on 4.5 K surfaces from the shields on the FB and BB, W	0.15
Supports and suspensions, W	< 2
Control Valves, W	15.2
Check Valves, W	0.9
Measurement wires, W	< 0.01
Heat bridges of the cryostat neck and others connections, W	< 1
Total, W	19.26

The thermal radiation from the vacuum vessel on the radiation shields covered by multilayer

insulation may be estimated as:

Q = q*S, where, S – surface area of the shields is ~ 7 m^2, q – experimentally determined heat flux from room temperature via multilayer insulation, its typical value is about 1 W/m^2.

The heat load from the check valves was estimated as:

Q = λS*ΔT/L, where λ - thermal conductivity of stainless steel tubes and bellows was taken average as 10 W/(m*K), S – cross-section area is about 10^{-3} m^2, ΔT – temperature difference was taken as 220 K, L – length is about 0.2 m.

Table 12 Heat loads on the 60 K helium (return line) from the Branch Box, the Feed Box and the transfer line

Heat load from	**Values**
Thermal radiation on the shields from the vacuum vessel, W	7
Support and suspensions, W	20
Control valves, W	38
Check valves, W	11
Measurement wires, W	< 1
Heat bridges of the cryostat neck and others connections, W	5
Total, W	82

The temperature maps in the coil are presented in the Fig. 52 and Fig. 53. These calculations were done in ANSYS 3D model containing ¼ part of the coil. The heat loads on the coil are 0.1 W for each titanium suspension rods and 0.7 W for each support struts. The coil is cooled by helium in the cooling tube. The helium parameters are 4.5 K of bulk temperature and the film coefficient of 200 and 10^3 W/(m^2*K). The 10^3 W/(m^2*K) value looks close to real as presented in the Fig. 55 as boiling on copper surface.

It is seen from these figures that the coil design has good thermal conductivity to the external heat loads due to copper case enveloping the superconducting coil. The calculations with 200 W/(m^2*K) film coefficient show the case if liquid helium will contain large fraction of bubbles decreasing this coefficient. The temperature increase by 0.1 K in the coil may be considered as acceptable.

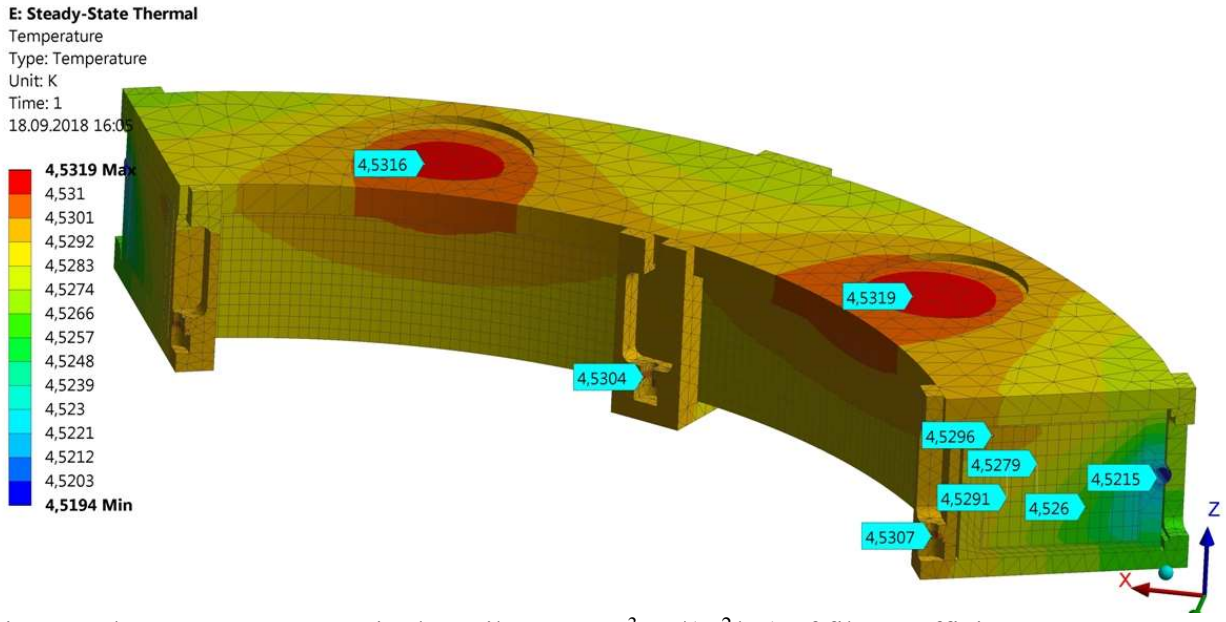

Fig. 52. The temperature map in the coil at α = 10^3 W/(m^2*K) of film coefficient.

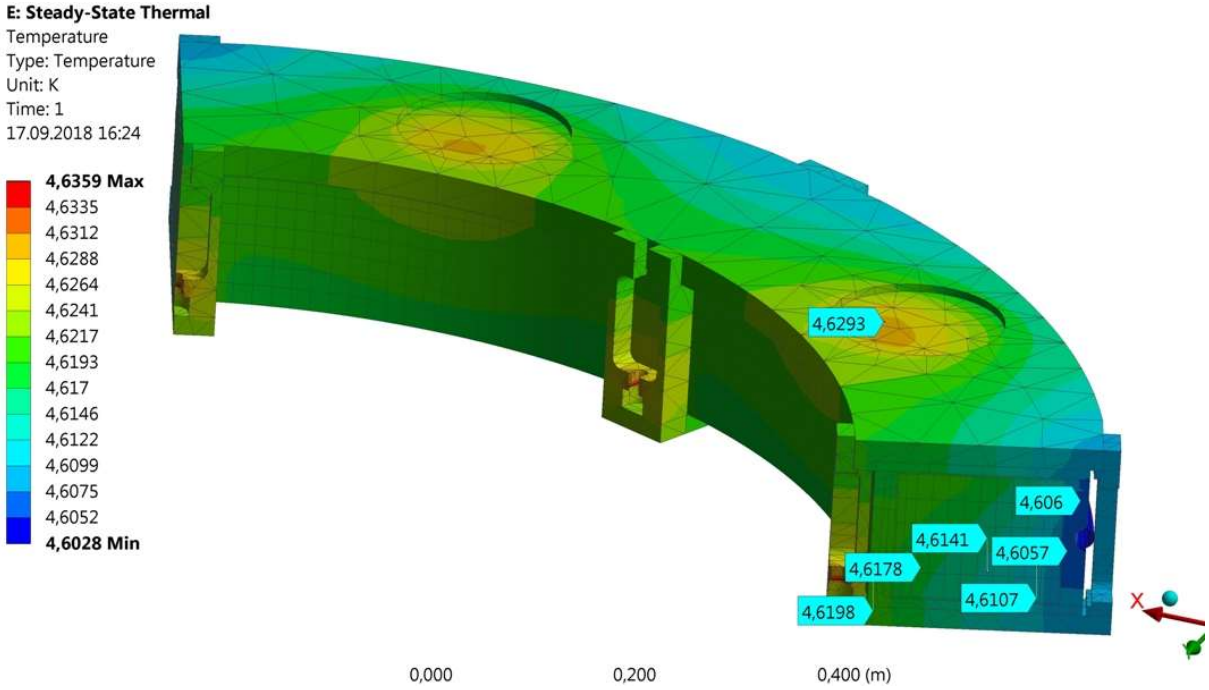

Fig. 53. The temperature map in the coil at α = 200 W/(m^2*K) of film coefficient. This map is interesting to see at low film coefficient.

As a conclusion, total heat load for the CBM detector:

for 4.6 K helium is Q = 24 W; for 50 K helium is Q = 267 W;

The mass rates at normal operation are G = Q/Δh:

G = 1.15 g/s for 4.6 K helium;

G = 2.54 g/s for 50 K helium which is heated from 50 to 69 K, Δh = 105 J/g. Some part of this rate will be excluded for the current leads cooling. In further estimations it will be assumed that all of 2.54 g/s will go through the return cooling line.

3.4 Thermosyphon cooling of the coils

The SC coils of the CBM magnet will be cooled by 4.6 K@3bar helium coming from the cryoplant. The coils should be cooled down by forced flow and in ordinary operation the coils will be cooled by thermosyphon method with helium of 4.5 K@1.3bar. From the cryogenic operation point of view it is convenient to use serial connection of the coils in all stages of the magnet operation.

The superconducting coils of the CBM magnet will be cooled on thermosyphon principle in ordinary operation of the magnet at 4.5 K, see Fig. 54. The liquid helium goes from the cryostat down to the lower coil, after this to the upper coil, and after this the helium returns to the top of the cryostat LHe vessel. There are two physical principle to force the helium go up through two coils. First, the bubble will have some velocity to go up in liquid helium due to buoyancy. Second, significant fraction of vapor inside the liquid phase will create the pressure difference between the liquid helium in the LHe vessel and the tube cooling the coils.

The thermosyphon cooling in horizontal heated channels needs detailed estimations, as there is not much information in literature. In the estimations presented below the homogenous approach was used which was discussed and experimentally proved in [13]. The homogenous approach assumes that there is no separation of bubbles from liquid and average parameters of mixture can be used.

In the SC magnets cooling the main criteria of the thermosyphon operation is to have the vapor quality χ below 0.8 at the outlet of a return tube and in the operating regime it may be in the range 0.4÷0.6 values [12-14].

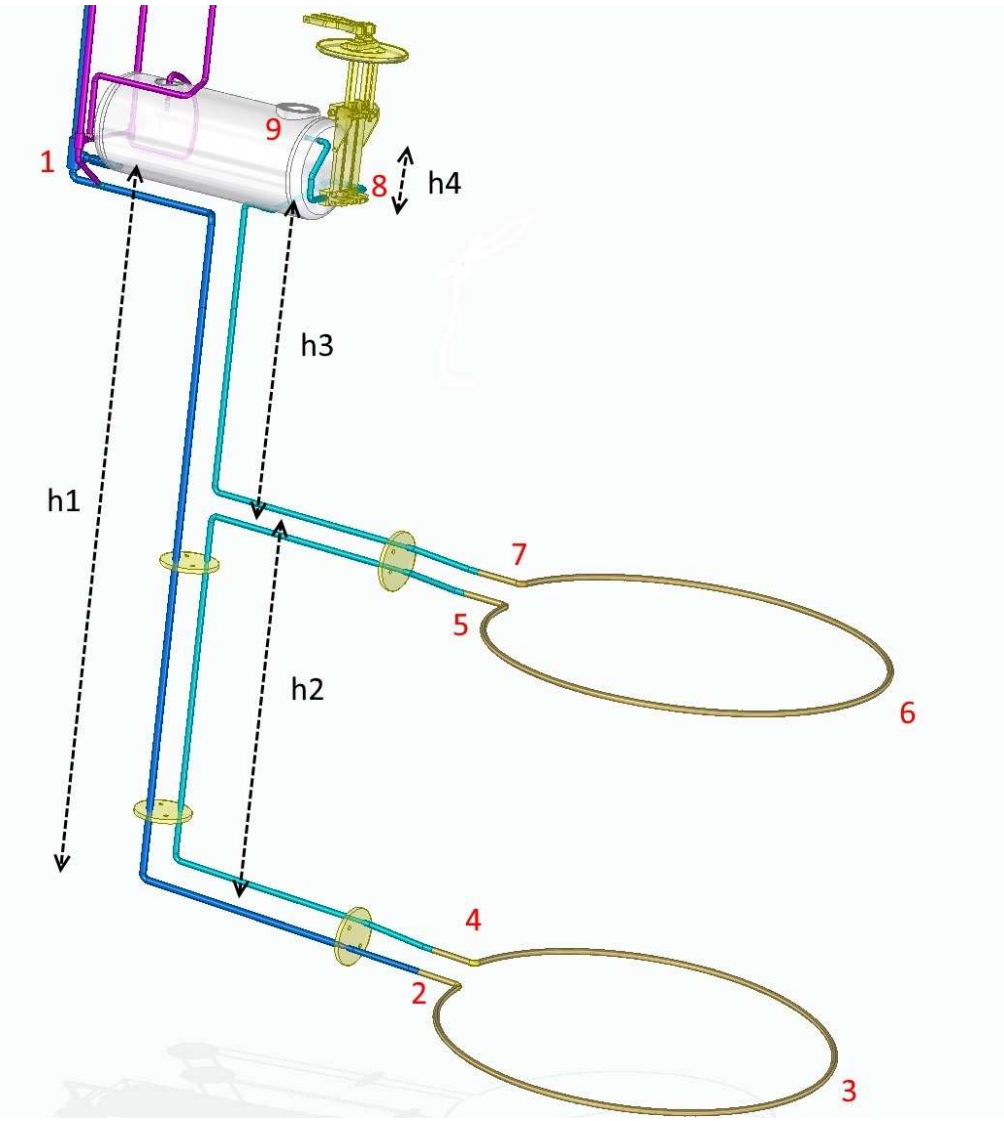

Fig. 54. The cryogenic scheme of the CBM magnet coils with the cryostat. The vertical tube between the LHe vessel and lower coil contain single phase liquid helium. The tubes in the coils have an inclination of about 1°.

The thermosyphon tubes in the CBM design are shown on the Fig. 54. The liquid helium goes down along the height h1 and gas-liquid mixture goes up along the tubes returning to the LHe vessel. The height h2 corresponds to the mixture with χ value after heat loads from the lower coil. The height h3 corresponds to the mixture with 2χ value after heat loads from the upper coil. The height h4 corresponds to the height of the LHe volume after the current leads. The height h1 corresponds to the lowest level of liquid helium in the LHe vessel. So, h2+h3+h4 > h1. There is a difference of densities of liquid in h1 tubes and in mixtures in h2 ÷ h4 tubes. Due to this density difference the gas-liquid mixture in the returning tube raises above the level of liquid helium in the cryostat and it will be returning to the LHe vessel if the vapor quality will be high enough. The values of the heights h1…h4 are 3 m, 2 m, 1 m and 0.5 m correspondingly.

The thermosyphon estimations were based on solving the equations where the pressure difference from the density difference between the inlet and the outlet of the thermosyphon open loop equals the pressure drop on flow friction. The heat loads were applied as follows:

- point 2 2.5 W
- point 3 2.5 W
- point 5 2.5 W

- point 6 2.5 W
- point 8 1.0 W

The equation for the pressure difference due to density difference can be written as result of integration with using average values of densities:

$$\Delta p = \rho_L g h_1 - \rho_{m2} g h_2 - \rho_{m3} g h_3 - \rho_{m4} g h_4$$

The mixture density can be written as $\rho_m = \rho_L \frac{1}{1-\chi+\chi\cdot\rho_L/\rho_g} = \rho_L \frac{1}{1+4.57\cdot\chi}$. For 4.5 K helium there was used the ratio $\rho_L/\rho_g = 5.27$. The ρ_{m2} and ρ_{m3} – average densities in tubes in the heights h2 and h3 respectively.

The equation for the pressure drop on flow friction for a given part of a tube is:

$$\Delta p = \phi_{lo} \cdot \xi \frac{8G^2}{\pi^2 \rho_m} \cdot \frac{L}{d^5},$$

where $\xi = \frac{0.316}{Re^{0.25}}$ - friction coefficient and $\phi_{lo} = \left[1+\chi\left(\frac{\rho_L}{\rho_g}-1\right)\right]\cdot\left[1+\chi\left(\frac{\mu_L}{\mu_g}-1\right)\right]^{-0.25}$ - two-phase multiplier. The pressure drop on friction is integrated on all lengths of the tubes. In homogeneous approach it is convenient to consider three length of the tubes: only liquid phase, two-phase with χ on lower coil and two-phase with $2*\chi$ above the upper coil.

The solved equation looks like:

$$\Delta p = \rho_L g h_1 - \rho_{m2} g h_2 - \rho_{m3} g h_3 - \phi_{lo} \cdot \xi \frac{8G^2}{\pi^2 \rho_m} \cdot \frac{L_{12}}{d^5} - \cdots - \phi_{lo} \cdot \xi \frac{8G^2}{\pi^2 \rho_m} \cdot \frac{L_{89}}{d^5} = 0$$

The mass rate can be written as $G = G_v/\chi$ by definition, where G_v can be included into calculation from 5 W heat load per coil, i.e. $G_v = 2.5*10^{-4}$ kg/s.

The following values were taken in the calculations of the equation: d = 0.0158 m, $\rho_l = 119$ kg/m^3, $\rho_v = 22.5$ kg/m^3, $\mu_l = 3.0$ μPa*s, $\mu_v = 1.25$ μPa*s where the *l* and *v* designations are for liquid and vapor. The rest values were calculated by the formulas below.

The Reynold's number: $Re = \frac{4G}{\pi d \mu_m}$ – there will be the turbulent flow.

$\mu_m = \left(\frac{\chi}{\mu_v} + \frac{1-\chi}{\mu_l}\right)^{-1}$ - the average viscosity of the mixture.

The results of the calculations for the vapour quality and some input parameters are presented in the Table 13 in the outlet of the upper coil is $\chi = 0.0752$, for the pressure difference is 218 Pa, and the mass flow rate is 7.6 g/s. The obtained results may be taken into design of the CBM magnet with accuracy of 10%. Also the results are stable with respect to deviation of most not-well known parameters involved in the above presented formulas. Comparing these results with (Furci, 2015) and (Ken-ichi Tanaka et al., 1996) one may conclude that the void fraction of 0.1 value indicates that the operation of the thermosyphon operation of the CBM magnet has safety factor of about eight.

The detailed results of the pressure drops calculations in parts from L_{12} to L_{89} are presented in the Table 13.

Table 13. The results of the pressure drops calculations in parts of the tubes.

L_{ij} part	L, m	χ	ρ_m, kg/m^3	μ_m 10^{-6} Pa*s	Re	ϕ_{lo}	ξ	**Δp, Pa**
1-2	4	0.0	119	3.0	177000	1.00	0.0146	28
2-3	2.5	0.0188	110					21
3-4	2.5	0.0376						24
4-5	3.5	0.0376						34
5-6	2.5	0.0564						27.5

6-7	2.5	0.0752						32
7-8	2.5	0.0752						32
8-9	1.5	0.0827	86	2.69	197000	1.34	0.0150	19.5

After increasing the total length of the thermosyphon tubes by a factor of 10 (that corresponds increasing the heat power by a factor of 3.2) the results of solving the equation will be: $\chi = 0.167$ and $\Delta p = 750$ Pa (7.4 mbar). These mean that the results of the calculations listed in the Table 13 will be changed not principally if uncertainty of the given parameters is 10-20%.

The stability of the thermosyphon cooling in horizontal channel should be taken into account in the designing, especially at low heat loads. During such instabilities the values of χ are more than 0.8. This effect will be mitigated in the CBM coils by using the inclination of the coils cooling tubes, as shown on the Fig. 5. That gives the total height (within heights h2+h3+h4) with values $\chi>0.8$ for two tubes of about 0.2 m. Any increase of χ in the h2-h3 tubes leads to the rising of helium level in these tubes. So, if the h1-h2-h3-h4 < 0.2 m, then such instability will never happen in the CBM magnet coils (here h1 corresponds to the lowest level of LHe in the vessel). Anyway, some heaters will be placed on the length of h3 tube to completely avoid such effect.

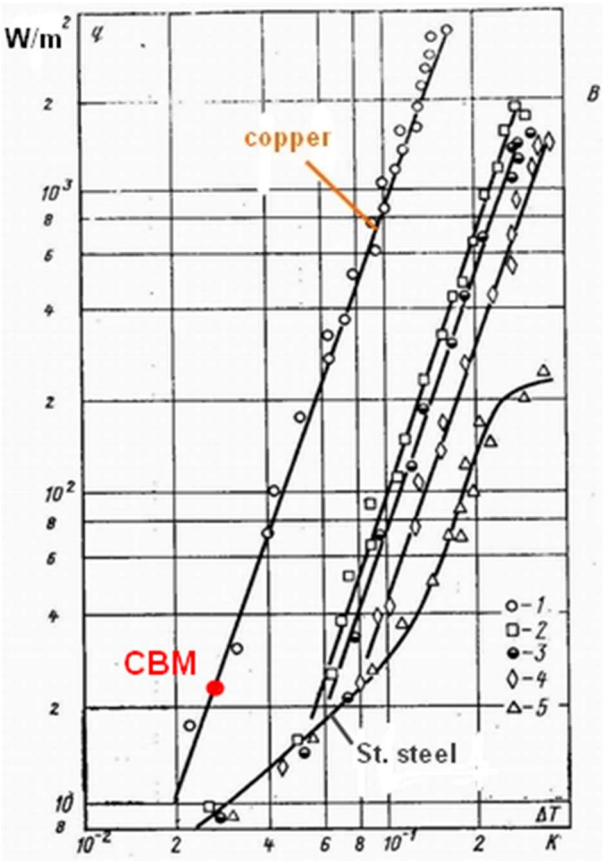

Fig. 55. The nucleate boiling of helium in large volume on different materials. The Y-axis is the heat flux density, the X-axis is the temperature difference between the helium and the surface of the materials.

The obtained results for χ may be considered as low. So, for estimations of heat transfer between the helium and the cooling tubes the heat transfer coefficient may be taken from Fig. 55 as for pool boiling regime. In case if this flux density is below 10 W/m^2 then it will be single phase heat transfer in liquid helium without bubbles appeared.

For total heat in-leak to the one coil is estimated about 5 W as shown in Table 9. The copper cooling tube has following sizes inner diameter ∅16 mm and length 4.4 m. The heat flux density, q,

will be:

$q = Q/(L*\pi d) = 5/(4.4*\pi*0.016) = 23$ W/m^2.

This value of the heat flux density is marked as red dot on the Fig. 55. The temperature difference between helium and copper tube is <0.03 K. It is worth to note that this value is estimated at 5 W of heat in-leaks with guaranty factors. If one take the heat in-leaks values given from direct estimations for the support struts and without the factors then q = 4.6 W/m^2. That is exactly single phase heat transfer regime.

From another hand, the value 23 W/m^2 is by 100 times less than the critical heat flux density. That can be interpreted as if the internal surface of the cooling tube would be covered by 1% of liquid helium the magnet will be cooled in boiling regime with temperature difference about 0.15 K.

This estimation concerns the condition of boiling in large volumes. The criterion of large volume is determined by the sizes of bubbles diameter with respect to the characteristic diameter of the boiling volume. Typical diameters of the helium bubbles are 0.08-0.16 mm [from a paper, circa 1969].

The value of 5 W as heat in-leak to one coil will be left for the following estimations. The working point for the CBM magnet is shown in Fig. 56 to illustrate that this working point is where the isolated bubbles appear on the surfaces. This case may be considered as a bubble goes up in large volume without movement of the liquid helium.

There are experimental results of measuring critical heat flux to the horizontal heated channel at natural convection conditions. The dependence of the ration of vertical unheated length of the channel to the horizontal heated length is presented in Fig. 57. The red dot corresponds to the ratio of vertical and horizontal length as in CBM magnet cooling tubes. It gives the value of the critical flux of about 2 kW/m^2.

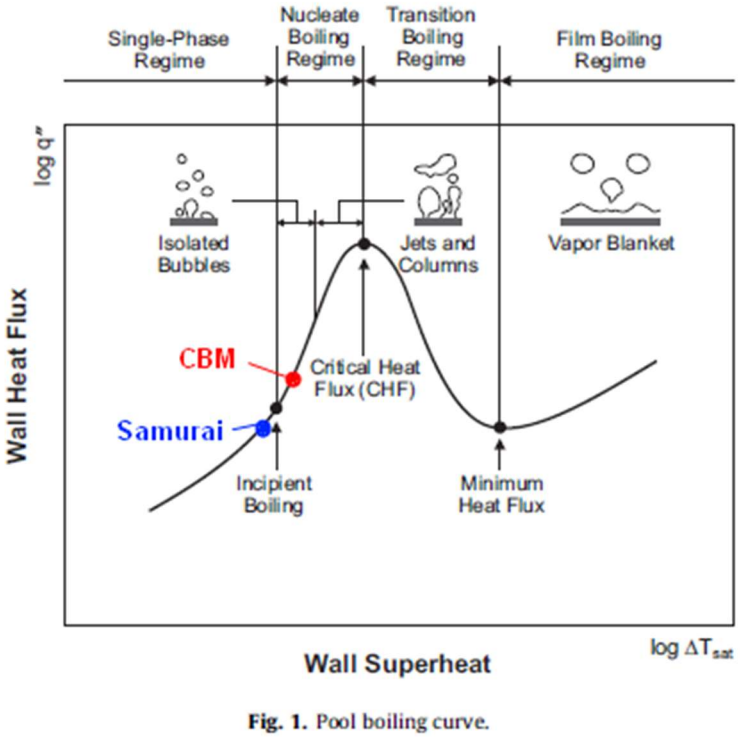

Fig. 1. Pool boiling curve.

Fig. 56. The working point of CBM magnet in basic regimes [taken from a paper].

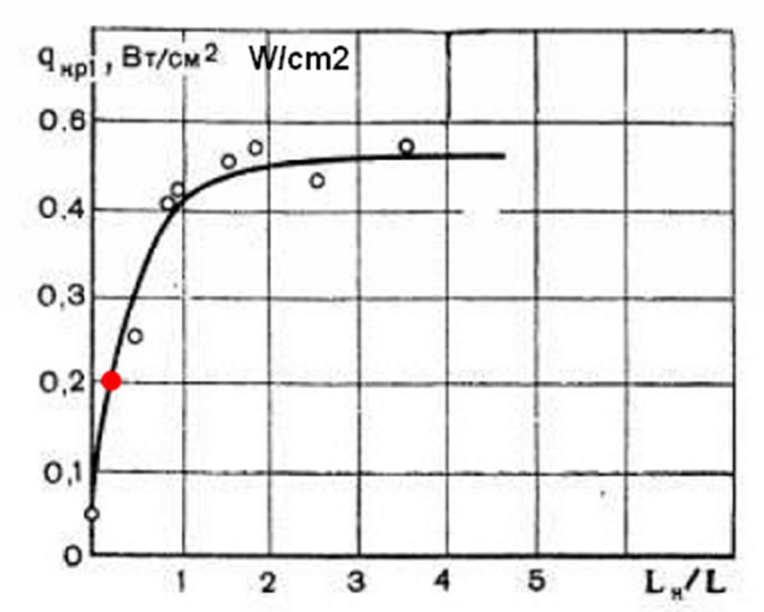

Fig. 57. Influence of vertical unheated channel on critical flux density of helium boiling in horizontal channel at natural conditions. The L_H/L is the ratio of unheated length of vertical channel to the length horizontal channel heated [V. Beliakov].

Conclusions on thermosyphon estimations

1. The thermosyphone cooling of the CBM magnet SC coils has no visible problems in realization. The working point is much closer to the single phase cooling than to critical heat flux.
2. The vapor quality χ in the outlet of the return tube will be about 0.1 that is well below 0.8 as a critical value.
3. The stability of the thermosyphon cooling will be mitigated by inclination of the coil's cooling tubes. The heater will be installed in the h3 part of the cooling tubes.

3.5 Quench calculations

The quench analysis evaluates behavior of the superconducting coils during a quench to give maximal temperature in the hot spot, voltage inside the winding, etc.

Its worth to evaluate *stability parameters* of the CBM coils prior to the quench estimations, they allow to see the impact of the big amount of the copper stabilizer in the SC wire.

The minimal length of the normal zone propagation in a SC wire is

$L = \sqrt{\frac{2\lambda(T_c - T_o)}{\rho J_c^2}}$, where λ - thermal conductivity coefficient of the copper matrix, ρ - electrical resistivity of the copper, Jc – current density, Tc and To – critical and operation temperature of the wire.

$L = \sqrt{\frac{2 \cdot 400 \cdot 4}{10^{-10} \cdot 7.7^2 \cdot 10^{14}}} = 0.073$ m.

Minimal energy for the normal zone propagation:

$E = C\gamma A T_{av} \sqrt{\frac{2\lambda(T_c - T_o)}{\rho J_c^2}}$, where $C\gamma$ - heat capacity [J/(kg*K)], A – cross-section area of the wire, T_{av} – average temperature of the temperature rise.

$E = 2700 \cdot 10^{-5} \cdot 4 \cdot \sqrt{\frac{2 \cdot 400 \cdot 4}{10^{-10} \cdot 7.7^2 \cdot 10^{14}}} = 7.9$ mJ. This is valuable amount of the energy to make

the wire of the CBM magnet coil to be normal, as it is several orders more than in conventional superconducting magnets having wires with NbTi/Cu ratio about 1. So, one may conclude that the training of the coils during the first ramping up will take not much time, or it may not occur at all.

Uniform dissipation energy in one coil

The uniform dissipation of the stored energy in one coil is described in the TDR [1] that is according the current design of the CBM magnet. Heat exchange between the winding and the stainless steel and copper cases was not accounted. In this case we have the following results :

- the E/M ratio is about 6.5 kJ/kg;
- the coil temperature after such uniform quench will be about 91 K;
- the resistance of one winding after such quench is about 4 Ohm;
- the characteristic time of the current decay is about 10 s (L/R);
- the estimated resistive voltage inside the winding, relating the case when a quench started inside the coils (non-uniform quench), is about 0.7 kV;
- the thickness of interlayer insulation is about 0.9 mm, including 0.2 mm of the Kapton insulation and the rest is a kind of the glass fiber insulation. The breaking voltage for the Kapton is more than 100 kV/mm, the breaking voltage for the glass fiber insulation of 10 kV/mm that is among the lowest values for G-10 materials. So, the safety factor will be least (20 + 7)/0.7 ~ 39 for the insulation breaking voltage.

An approach of the quench estimations made in BINP

Main quench calculations were described in the TDR performed by the team from Joint Institute of Dubna and the team from CIEMAT.

The current design of the CBM magnet has the minor changes in the cable parameters and it has the copper case as new element of the coil. The copper case will influence the quench behavior. So, during the last half of the 2017 the quench estimations of the current design of the CBM coils were performed in BINP.

These estimations were performed at the following conditions:

a) the Matlab code was used for this purpose. The current-inductance dependence is presented on the Fig. 58 which was taken from the TDR works;

b) the equations for the two coupled circuits were calculated in this code which are, see Fig. 59:

$$I_1R_1 + L_1\frac{dI_1}{dt} + M\frac{dI_2}{dt} = 0\,;\; I_2R_2 + L_2\frac{dI_2}{dt} + M\frac{dI_1}{dt} = 0\,,$$

where $L_1(I_1)$ and L_2 – inductances of the CBM magnet and the copper cases. $R_1(T)$– resistance of the CBM magnet, $R_2(T)$ – resistance of the copper cases, M – mutual inductance. General considerations on whether to include the coupled circuits into calculations or not are evaluated by analytical formulas comparing the characteristic times of the main magnet - $\tau_1 = \frac{L_1}{R_1}$ and of the secondary circuit - $\tau_2 = \frac{L_2}{R_2}$. It is worth to note that the calculations with the external dump resistor give more induced current in the copper cases than without it. At the beginning I_1 =700 A, I_2 = 0 A.

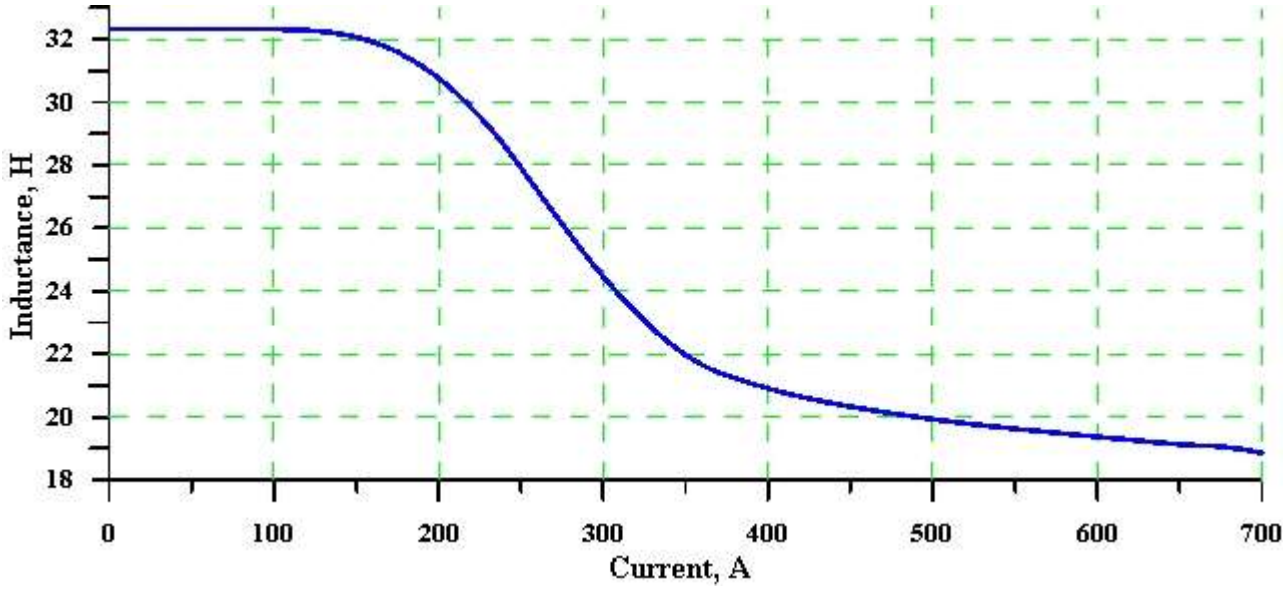

Fig. 58. The dependence of the whole CBM magnet inductance on the current.

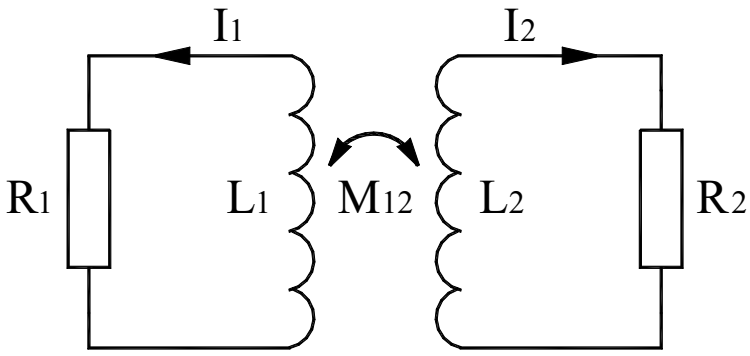

Fig. 59. Scheme of the coupled circuits.

c) the starting conditions for solving these equations were the 10 K for the one coil while the other stayed cool and the 40 K for hot wire for the hot-spot calculations. The validity of these conditions is described below.

d) while the L_1 inductance is dependent of the current the L_2 and M inductances should also have some dependence on the current due to presence of the iron yoke. Nevertheless in the calculations the fixed values of the latter inductance were used such as $L_2 = 1.09*10^{-5}$ H and $M = 1.2*10^{-2}$ H.

e) the $R_2(T)$ resistance of the copper cases was dependent on the temperature. This resistance changes its value from ~ 10^{-7} Ω to $5*10^{-6}$ Ω during a quench.

f) the cylindrical parts (poles) of the iron yoke made of technically pure iron have L-R parameters close to the copper cases. The estimated inductance of one pole with ANSYS is about $7*10^{-7}$ H. The estimated resistance at $\rho = 8.6*10^{-8}$ Ω*m at 273 K for iron is about $R = 6.4*10^{-7}$ Ω. Anyway the poles were not included in the calculations to escape more complexity. They will make benign effect on the quench behavior characteristics: on voltage, hot-spot temperature and as external energy extractors.

g) a quench-back effect due to heating of the copper cases was not accounted.

Normal zone propagation velocities

The velocity of the normal zone propagation along the wire [M. Wilson] is

$v_a = \frac{J_e}{\rho C}\sqrt{\frac{L_o \cdot T_s}{T_c - T_s}}$, where J_e – engineering current density, ρC – heat capacity [J/(m^3*K)], L_0 = $2.45*10^{-8}$ W*Ω/K^2, T_s – average temperature of heat generation, T_c – critical temperature of NbTi.

$v_a = \frac{7.7*10^7 \cdot 10^{-4}}{2700}\sqrt{\frac{2.45 \cdot 7}{9.6-7}}$ = 7.3 m/s, so it will take about 0.67 s for the normal zone to go around one turn of the coil.

The velocity of the normal zone transverse the cable was estimated in 2D model using ANSYS, as shown on the Fig. 60. The heat generation in the normal wire was set as $2.2*10^6$ W/m^3, at was assumed that in the neighbor wire it was the same heat generation at the temperature of 7 K.

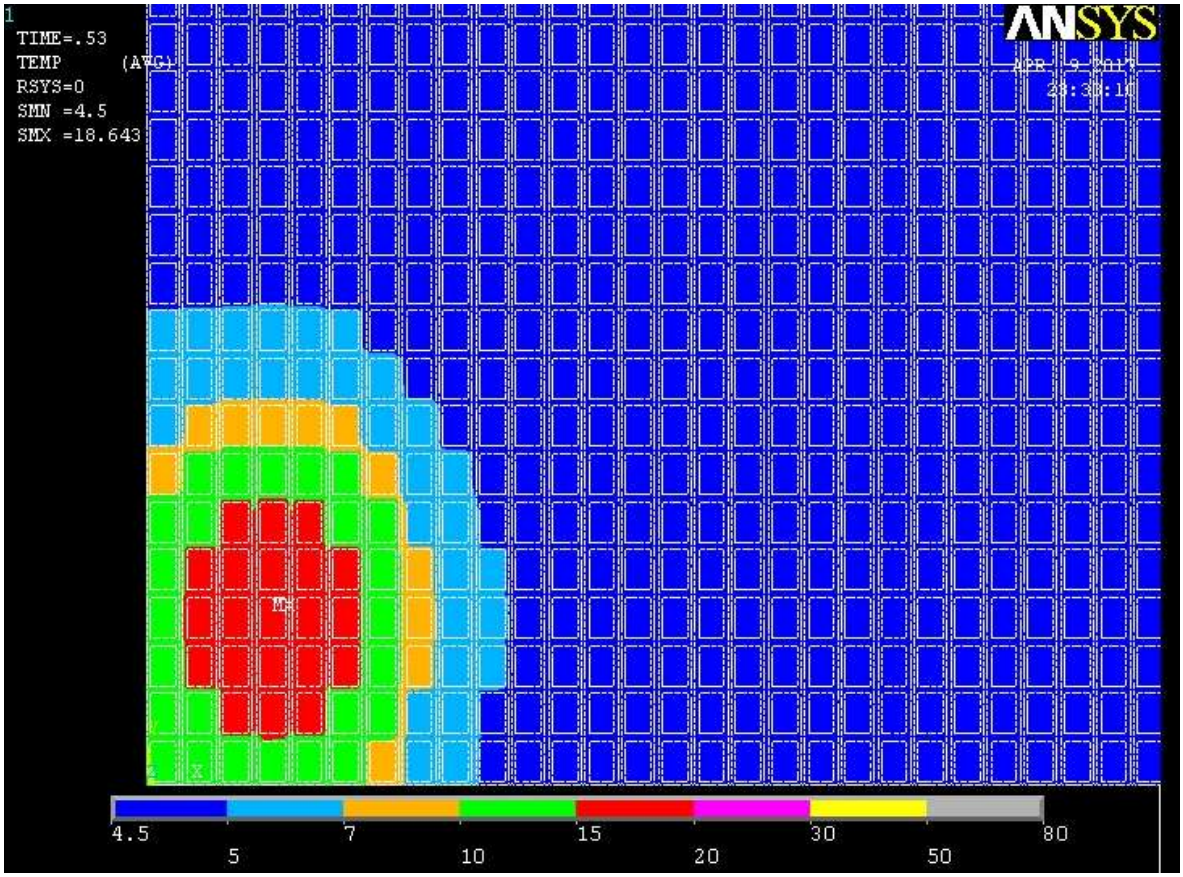

Fig. 60. Normal zone propagation in the winding in 2D calculations. Here time after start of the quench is 0.53 s, the quenched wire is in the center of the red zone and its maximal temperature is 18.6 K.

The velocity across the layers is about 0.05 m/s. This is low value, because typically such velocity has some 1-3% from the v_a value, as it mentioned in literature for convenient superconducting magnets. The reason is to high amount of the insulation between the layers of the winding. This velocity is also slightly faster for a direction along the layer. The maximal time for a normal zone going from the 1st layer to the 53rd is 0.159/0.05 = 3.2 s.

Such a low value of the transverse velocity leads to slow build-up of the winding resistivity. It helps to extract most part of the stored energy into the external resistor. The disadvantage of such a low value is that the hot spot temperature will be respectively higher.

These 2D model calculations also show that after ~ 3 s the hot-spot temperature in the winding will be ~ 40 K. That temperature value was taken in the BINP quench calculations as mentioned above.

It is worth to note that if the normal zone starts to propagate in the 1st or 53rd layer, depending on the coil, the normal zone will reach the neighbor coil.

Quench estimation in ordinary conditions with 2.1 Ω of the dump resistor

The CBM magnet has an active protection system based on energy extraction on the dump resistor

having 2.1 Ω. It is demanded that the most part of the stored energy should be extracted on this resistor. After happening of a quench the quench detection system after ~ 50 ms should switch on the powering circuit to a kind of L-R electrical circuit.

These calculations were presented in the TDR report and that results are presented on the Fig. 61. The quench was detected by 0.6 V threshold, the dump resistor was activated after 50 ms. The maximal voltage is around the current leads bus bars. The magnet and the hot spot temperatures are about 45 K and 70 K respectively.

The energy extracted by the dump resistor is 3.74 MJ that is ~ 75% of the stored energy.

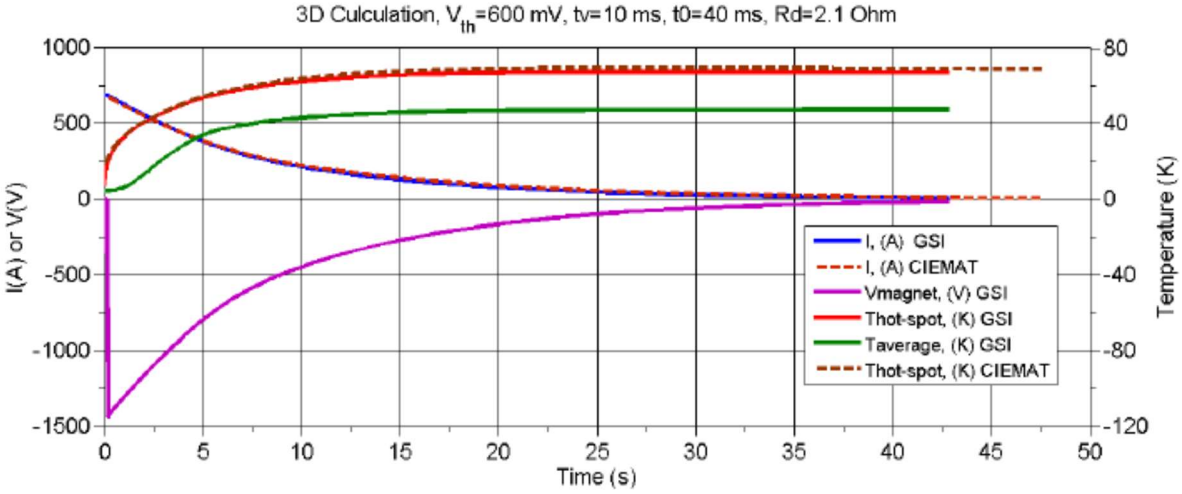

Figure 34. 3D quench calculation of the CBM dipole - magnet current, magnet voltage and the maximum (hot spot) coil temperature.

Fig. 61 The quench calculations with activated dump resistor taken from the TDR.

The BINP calculations based on the conditions described above with the dump resistor are presented on the Fig. 62 - Fig. 64. The winding temperature after such quench is about 52 K that is due to more time delay of the dump resistor activation and slightly higher current. During a quench the resistance of the copper cases changes by more than 10 times due to heating. It influences on the magnet current decay as it is seen on the Fig. 62 where the current from the copper cases "returns" to the magnet current.

The maximal temperature as in TDR as in BINP calculations are close corresponding to ~ 70 K and ~ 79 K respectively.

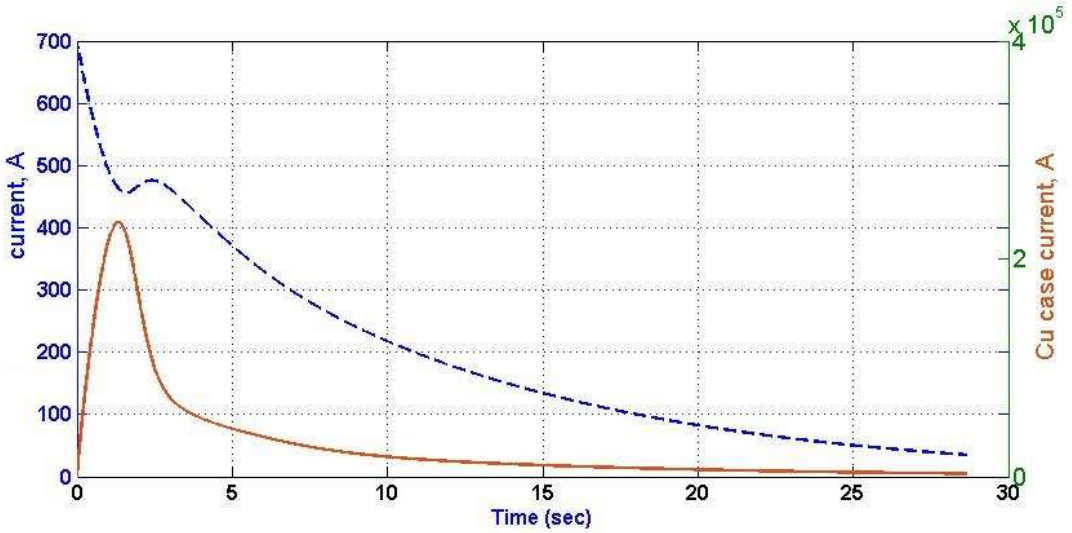

Fig. 62 The currents behavior during the quench with the dump resistor of 2.1 Ω.

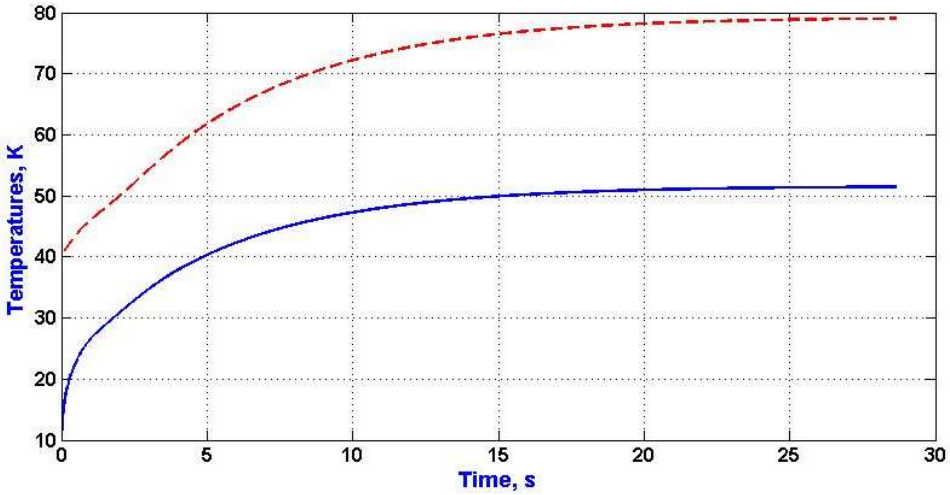

Fig. 63 The temperatures behavior during the quench with the dump resistor of 2.1 Ω. The blue line is for the magnet, the red line is for the hot-spot temperature. It assumed that the dump resistor was switched on after 3 s.

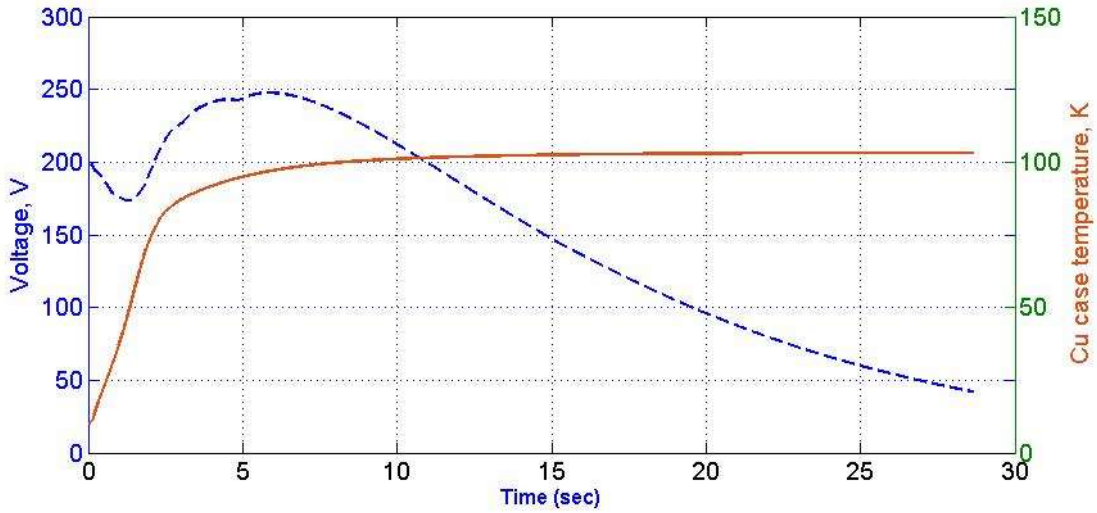

Fig. 64 The resistive voltage of the winding and temperature of the copper cases behavior during the quench with the dump resistor of 2.1 Ω.

Quench estimation with 1.0 Ω of the dump resistor

The estimations were made identical to the previous only the external resistor value was taken as 1.0 Ω.

The results of these calculations are presented in the Fig. 65 and Fig. 66. The maximal voltage is around the current leads bus bars. The maximal resistive voltage of the winding is ~ 472 V. The magnet and the hot spot temperatures are about 68 K and 106 K respectively.

The energy extracted by the dump resistor is 2.53 MJ that is ~ 50% of the stored energy.

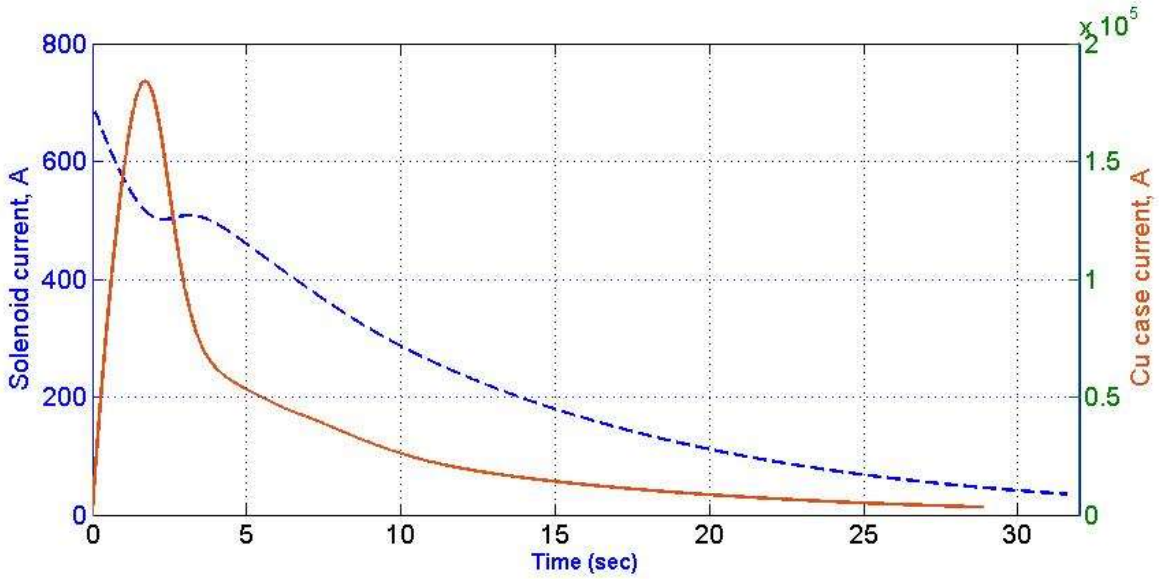

Fig. 65. The currents behavior during the quench with the dump resistor of 1.0 Ω.

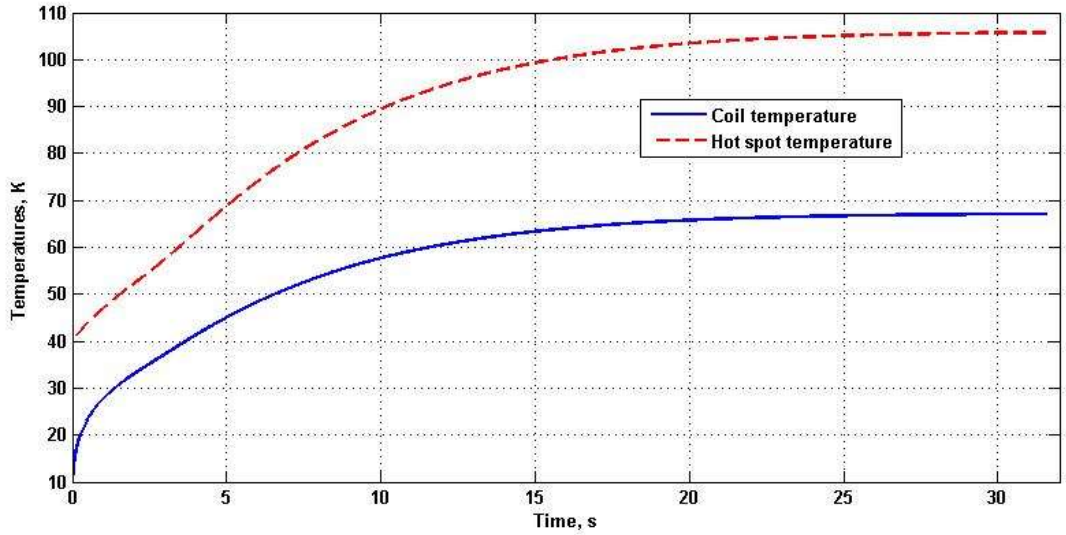

Fig. 66. The temperatures behavior during the quench with the dump resistor of 1.0 Ω. It assumed that the dump resistor was switched on after 3 s

Quench estimation of short-circuited magnet and copper cases influence on it

Although it is not considered to make the quenches without the dump resistor the quench calculations under such condition were performed as in the TDR as well as in the BINP project. The magnet should be self-protected even if the dump resistor is not switched on. The BINP calculations approach is described above. The points of interests of such calculations are the hot-spot temperature and internal voltage of the magnet. In both cases the stored energy is dissipated only in one coil of the magnet.

The results of the TDR calculations are presented on the Fig. 67. The maximal resistive voltage during this quench is about 1200 V that corresponds to the ~ 600 V of the internal voltage compensated by inductive voltage.

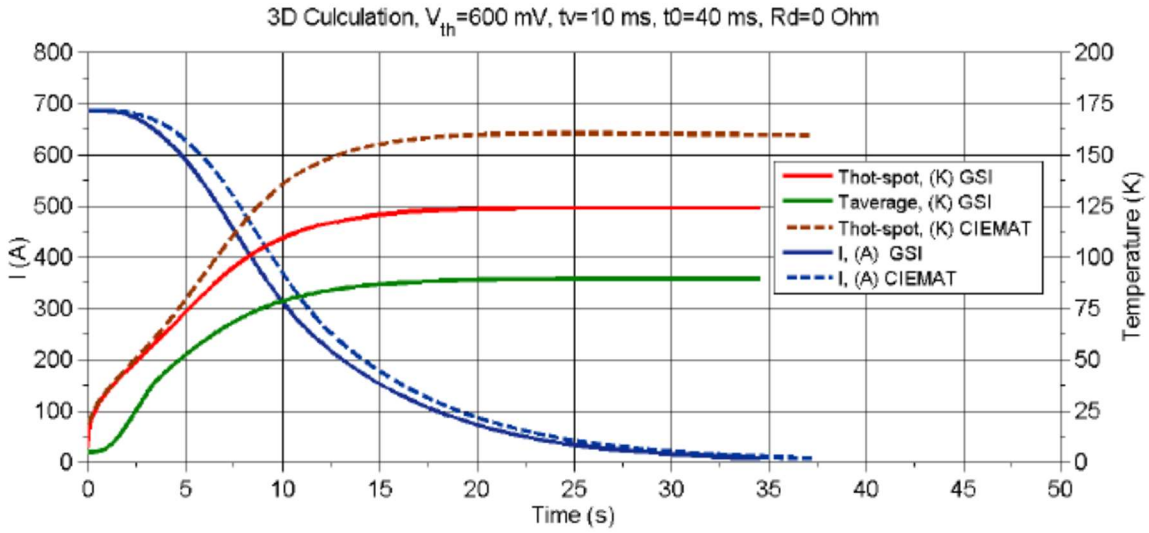

Figure 32. 3D quench calculation of the CBM dipole - the magnet current, hot-spot temperature and the average coil temperature.

Fig. 67 The results of the quench calculations extracted from the TDR.

The results of the BINP calculations are presented in Fig. 68 - Fig. 70. They are close to the TDR results if compared with Fig. 67.

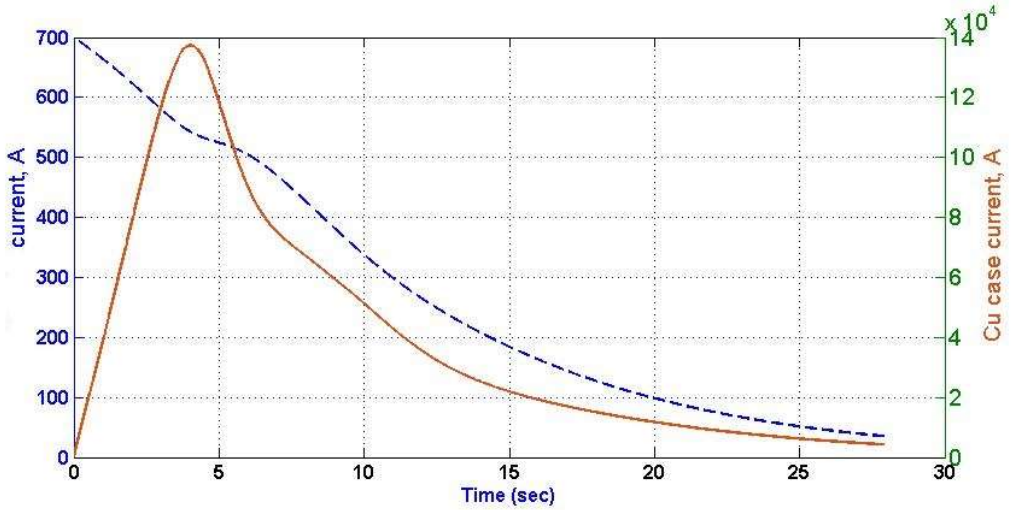

Fig. 68 The currents behavior during the quench of the short-circuited magnet.

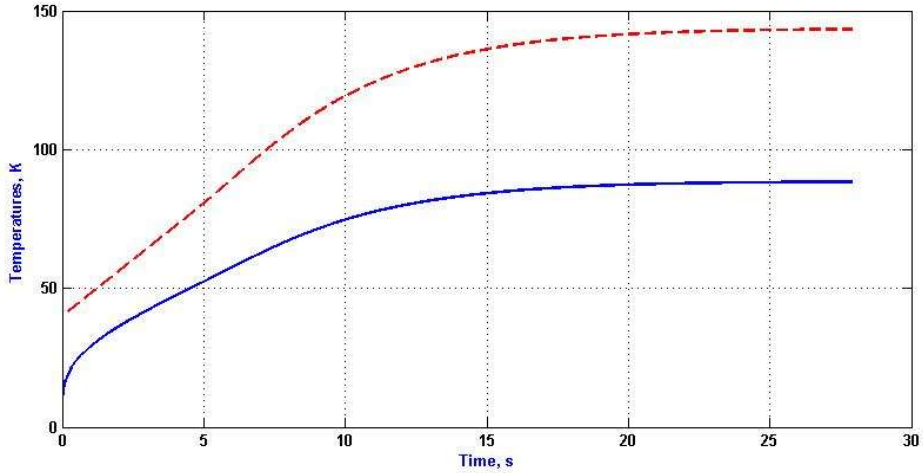

Fig. 69 The temperatures behavior during the quench of the short-circuited magnet. The blue line is

for the magnet, the red line is for the hot-spot temperature.

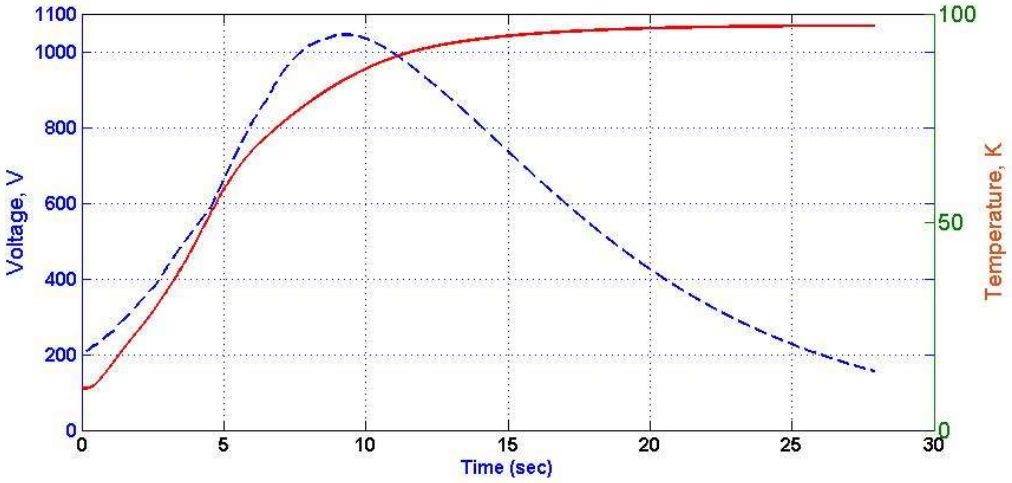

Fig. 70 The resistive voltage of the winding and temperature of the copper cases behavior during the quench of the short-circuited magnet.

The influence of the copper cases on quench behavior as the secondary protective circuit is demonstrated on the Fig. 71 - Fig. 73.

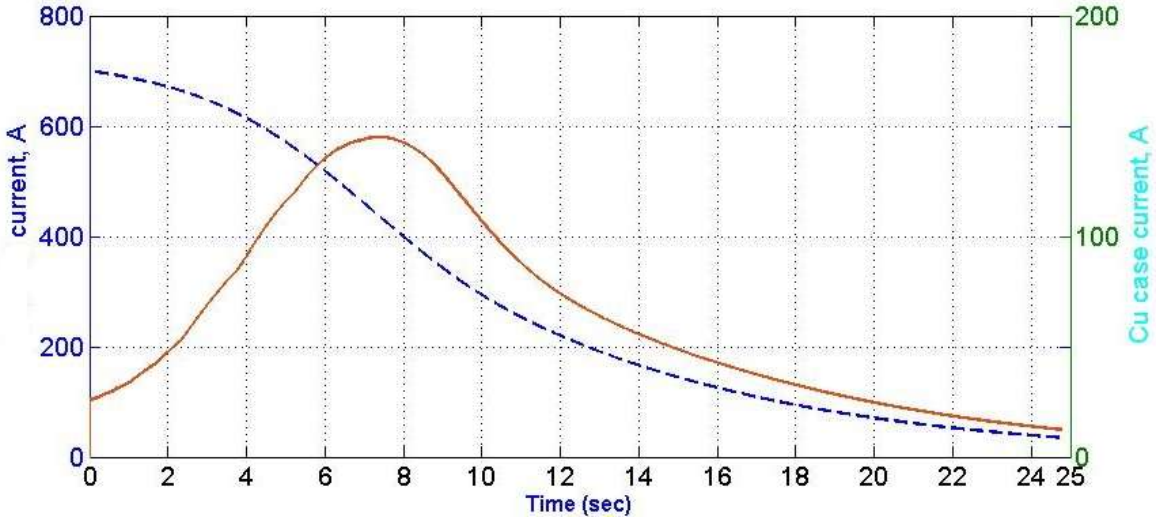

Fig. 71 The currents behavior during the quench of the short-circuited magnet and with R2 having the resistance several orders higher than for the copper case.

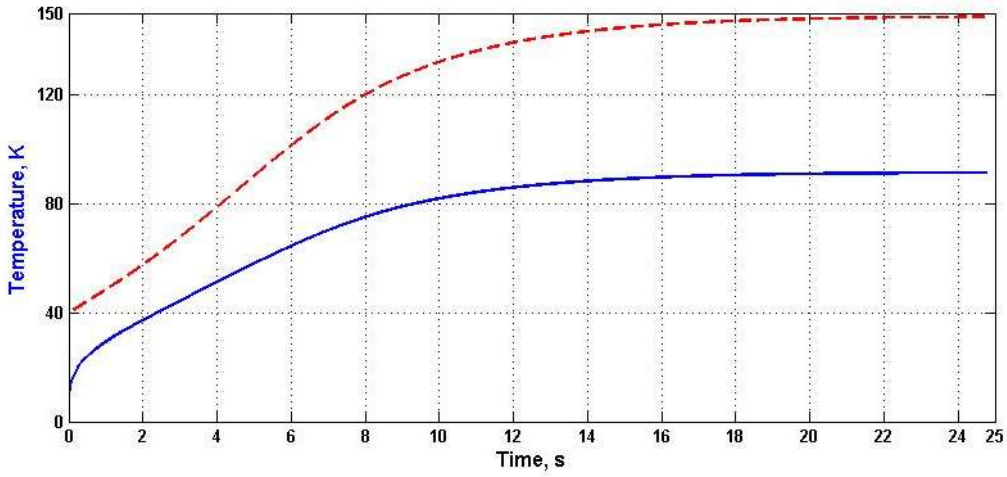

Fig. 72. The temperatures behavior during the quench of the short-circuited magnet and with high

R2 value. The blue line is for the magnet, the red line is for the hot-spot temperature.

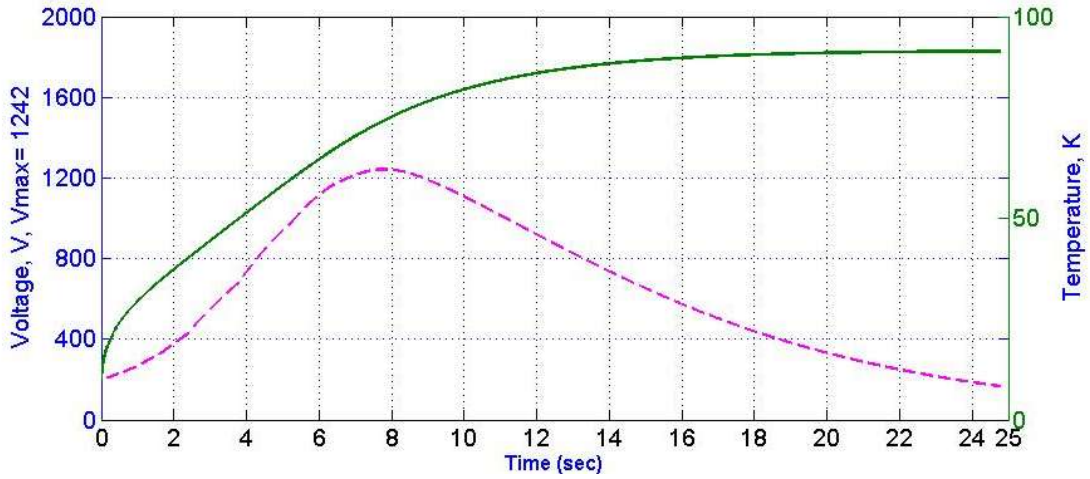

Fig. 73. The resistive voltage of the winding and the temperature of the coil winding behavior during the quench of the short-circuited magnet and with high R2 value.

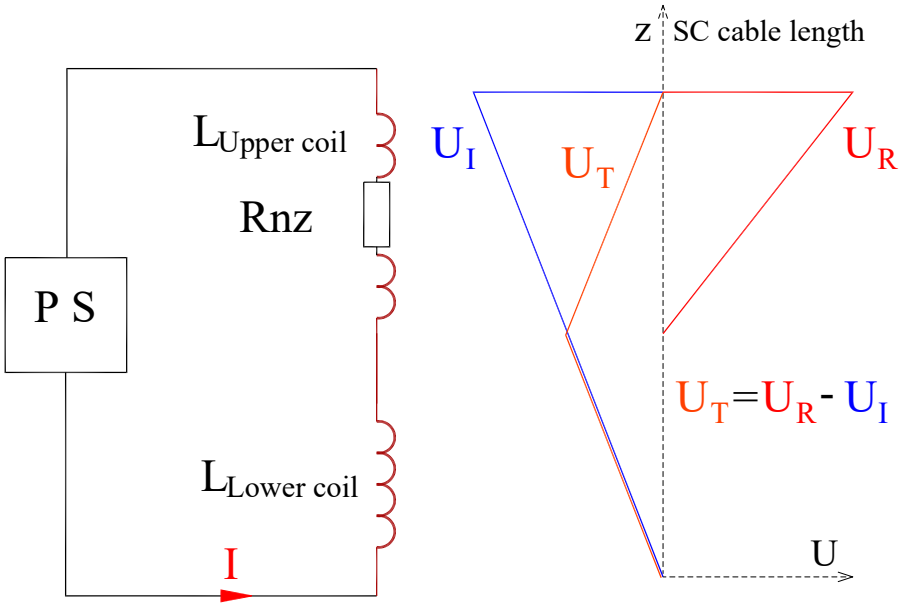

Fig. 74. The illustration of voltage distribution inside the CBM magnet. The total voltage U_T is the subtraction of inductive and resistive voltages. The inductive voltage is uniformly distributed across the whole magnet.

Results of the quench calculation:

1. In ordinary conditions the most part of the stored energy will be extracted on the dump resistor. It will extract about 83-86% of the stored energy, as presented in the TDR. The average temperature in the quenched coil will be below 50 K taking into account the stainless steel plate. The hot-spot temperature will be well below 80 K. The maximal voltage will be on the current leads bus bars.
2. The calculations of the short-circuited magnet shows the hot-spot temperature about 150 K and the internal voltage around 600 V. The maximal voltage will be between the coils.
3. The copper cases of the coils have some influence on the quench but not high. The resistance of the copper cases changes by ~ 14 times during a quench. The cylindrical iron poles will also affect the quench behavior but less than the copper cases.

4. In total the CBM magnet coils looks protected from quench effects. Attention should be paid to bus bars insulations especially in the cold mass zone.

3.6 Power supply and quench protection system

The proposed quench protection system is based on dissipating the stored energy of the magnet on a dump resistor after detection of a quench. The system consists of quench detection subsystem and energy extraction subsystem.

The powering circuit is shown on the Fig. 75.

Requirements for the quench protection system are:

- The amount of the stored energy to be extracted is 5.1MJ.
- Stored energy should be extracted to the external dump resistor with the value of 2 Ohm.
- The active elements of the dump resistor should not be hotter than 100° C. Cooling time should be specified;
- Quench detection circuit should provide fast detection of the normal phase appearing. The discrimination time should be about 6ms and the threshold – about 0.6V (0.6V corresponds to 6 wounds in the normal state).
- Number of the voltage tabs and the locations of their connections should be determined.
- Dump resistor should be introduced to the circuit not later than in 40 ms. That gives the demands on the energy extraction switch (current breaker).
- Dump resistor value is 2.1 Ω. The middle point should be introduced and grounded in order to minimize the voltage between coil and the ground.

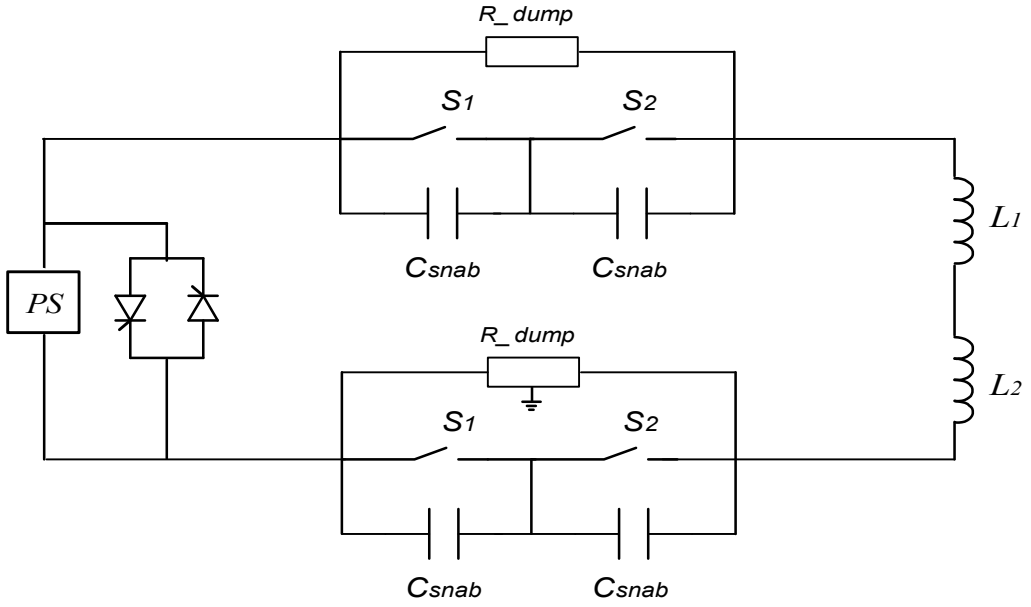

Fig. 75. Powering system of the CBM magnet.

The block diagram of the power supply is shown on the Fig. 76. The main parameters of the power supply are as follows:

Nominal output power 12kW;
Nominal output current 1000A;
Nominal output voltage 12V;
8 hours run Stability - < 0.01% from nominal;
Output ripples in voltage:
0-300Hz - < 10 mV rms,
0-40 kHz – < 100 mV rms;
Control Interface – CAN

Form factor 19” x 4U

The diagram of the quench detection system is shown on the Fig. 77.

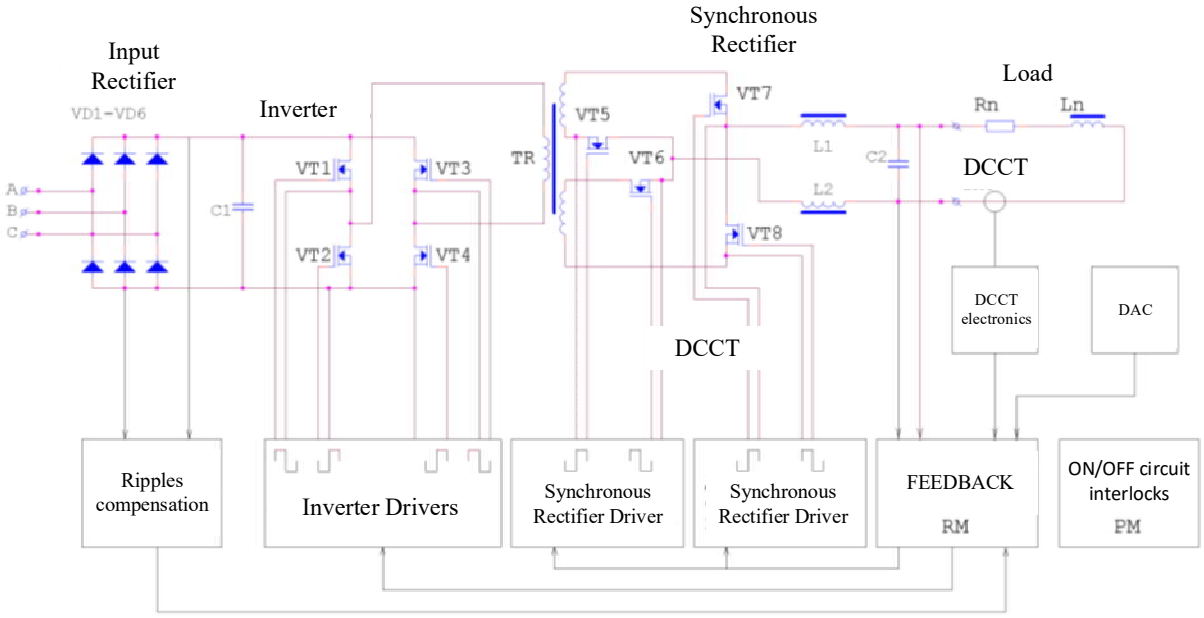

Fig. 76. The power supply block diagram.

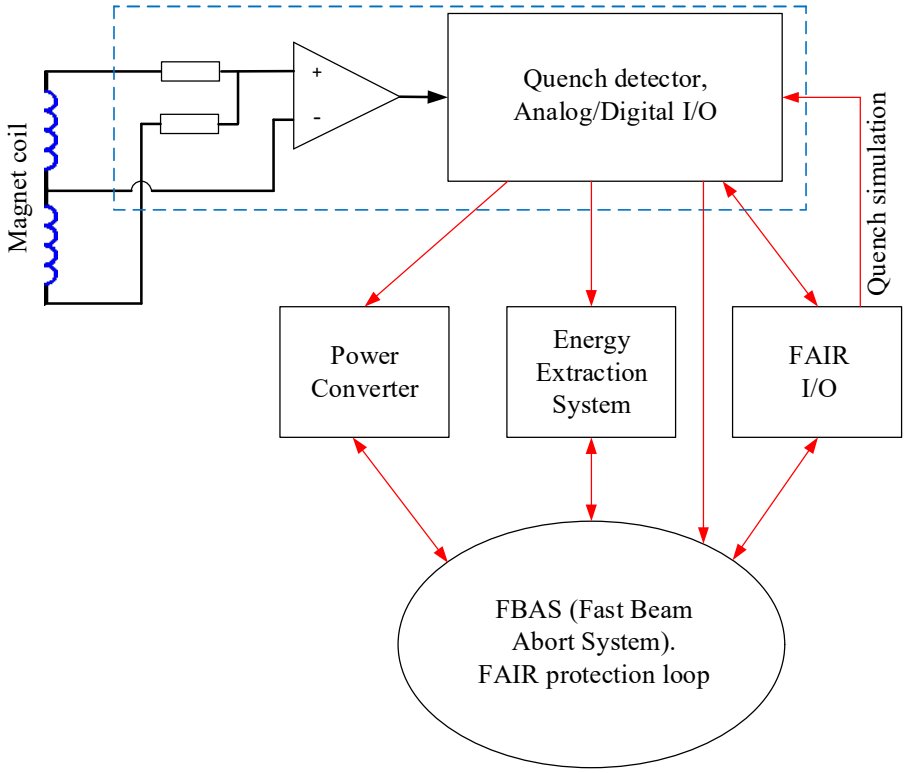

Fig. 77. The quench detection diagram of the CBM magnet.

4. Cryogenics of the CBM detector

4.1 Cryogenic diagram

The cryogenics diagram of the CBM magnet is presented on the Fig. 78. The cryogenics of the CBM detector consists of the Branch Box (BB), the Feed Box (FB), the cryostat of the CBM detector

and the cryogenic transfer lines. The length of the transfer lines between the BB and the FB is about 30 m.

For the transfer line the most tubes were chosen to be DN15 STD, so OD = 21.34 mm, ID = 15.8 mm.

The parameters of the cryogenic valves are listed in the Table 14. The valves are of PN25 type – nominal pressure of 25 bar, they should have a Cu flange for a heat load interception along its stem.

The parameters of the valves are estimated at the following conditions:

- maximal heat loads for the CBM detector 60 W at 4.5 K and 3 bar, so G = 2.8 g/s = 10 kg/h; and 190 W at 50 K and 18 bar, so G = 1.8 g/s = 6.5 kg/h;
- maximal heat loads for the HADES detector 150 W at 4.3 K G = 6.9 g/s = 25 kg/h; and 400 W at 50 K and 3 bar, so G = 3.8 g/s = 13.6 kg/h.

(The mass rate G was estimated via enthalpy difference as Q/Δh.)

Valve coefficient for the control valves $K_V = \frac{G}{514}\sqrt{\frac{T_1}{\rho_g \cdot \Delta p \cdot p_1}}$, and for JT valves is: $K_V = \frac{G}{257 \cdot p_1}\sqrt{\frac{T_1}{\rho_g}}$, where G – mass flow rate [kg/h], p_1 and T_1 – upstream pressure [bar] and temperature [K], Δp – pressure difference between the valves, taken as 0.01 bar; ρ_g – gas density at normal conditions [kg/m^3].

Table 14 Cryogenic valves list.

Valve	Valve purpose, Couplings	Kv, max	Kvs	DN, mm	G_{op}, g/s	Pop, bar	Top, K	Position without electricity
QN1	Open at all operating modes	0.14		15		2.5→1.2	70	Open
QN2		0.051		15		1.3	6	
QN3		1.32		15		2	70	
QN4		0.071		15		2	4.5	
QN5		0.052		15		3	4.6	
QN6	Reduction to 3 bar	0.010		15		18→3	50	Closed
QN7		0.053		15		18	50	
QN8		0.021		15		3	4.6	
QN9		0.081		15		1.3	4.5	
QN10		0.77		15		17	70	
QN11		1.92		15		17	85	
QN12		0.11		15		1.3	5	
QN13		0.053		15		18	50	
QN14		0.076		15		17	70	
QN15		0.072		15		1.3	4.5	
QN16		0.053		15		18	50	
QN17		***0.022***		6		18	4.6	
QD17	Always coupled with QN17			6		18	4.6	
QN18	JT	0.022		15		3	4.5	
QN19		0.39		15		2	300	
QN20				15		18	4.5	
QN21				20		18	4.5	

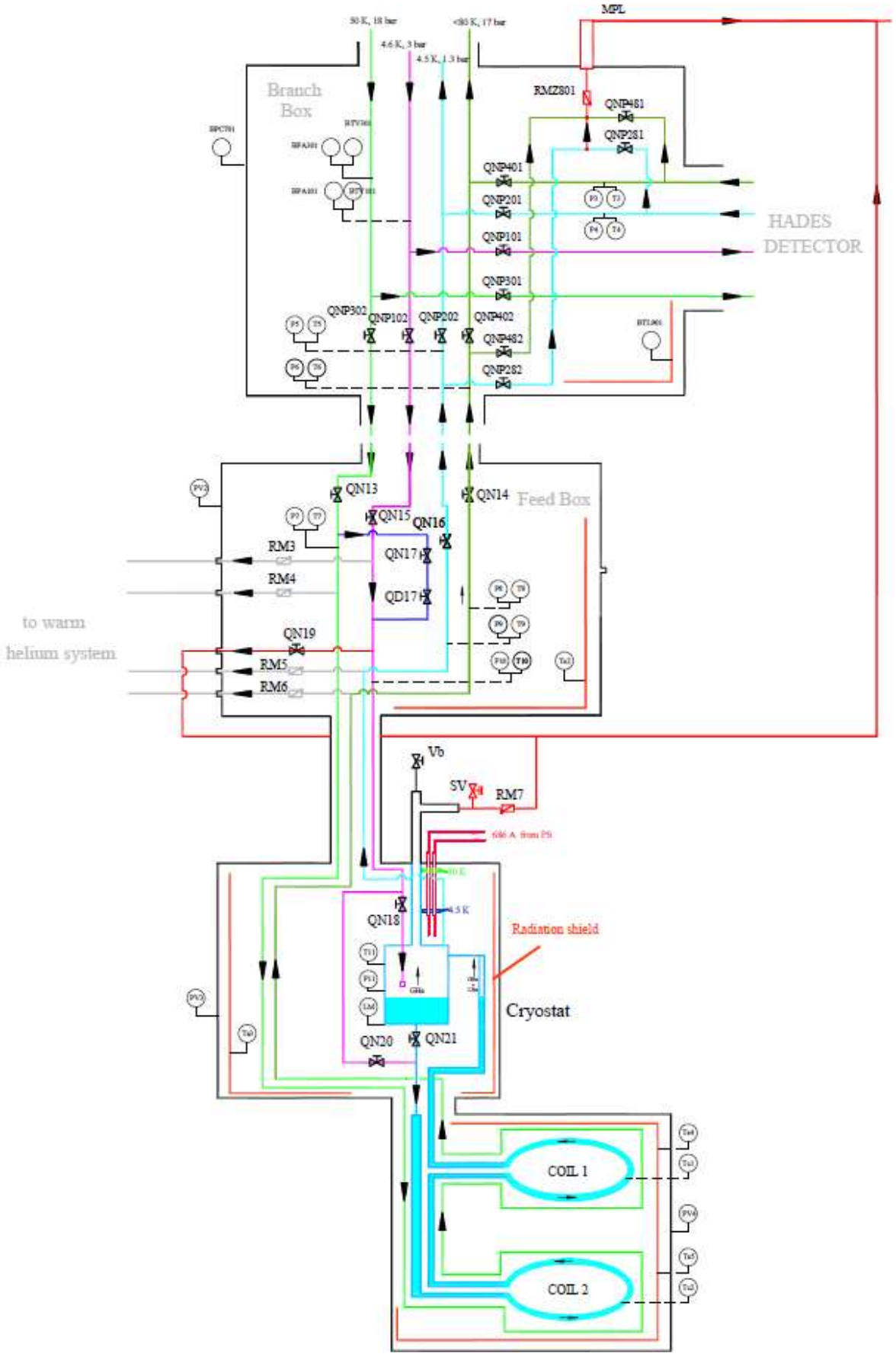

Fig. 78. General view of the CBM detector cryogenic diagram.

General approaches for the cryogenic system are:

- the radiation shields of all cryogenic subsystems should be cooled by return line of 55-60 K helium;
- the Branch Box may has installed vacuum pumps installed;
- vacuum behavior of the systems after a quench as in CBM and HADES detectors or warming up in one detector at operation of another should be taken into account;

The designations on the diagram of the Fig. 78 are: QN – control valves, RM – check valves, P – pressure gauge, T – temperature sensor, PV – vacuum gauge.

The vacuum volume in the cryogenics should divided into independent blocks to be possible find cold leaks during assembling of the system and to exclude deterioration of vacuum during a quench of whether CBM magnet or whether HADES magnet.

4.2 Design of the Feed Box

The design of the Feed Box is shown on the Fig. 79. The cryogenic diagram of the Feed Box is shown on the Fig. 78. The Feed Box should perform all cryogenic operations of the CBM magnet such as cooling down, routine operation at 4.5 K, warming up and quench recovery.

The control valves will give a major part of heat in-leaks, the interception at 60 K temperature should be foreseen at procurement stage of work.

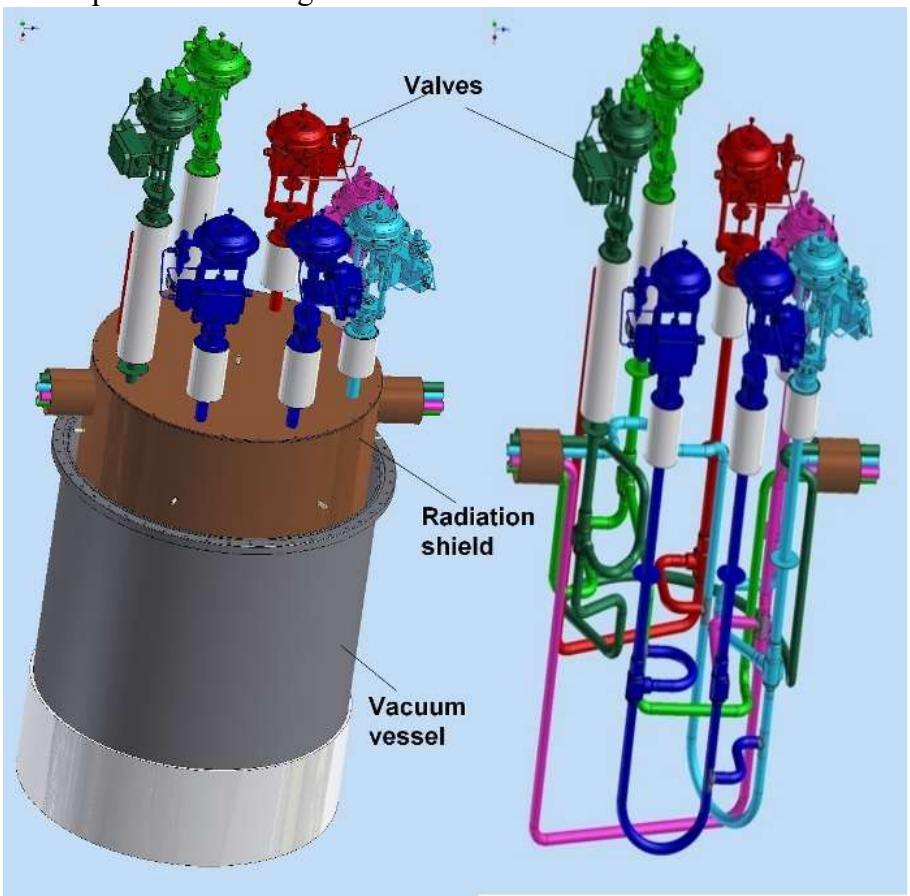

Fig. 79. The preliminary design of the Feed Box.

Items for discussion:

It is demanded to have warm helium purge system and warm helium line for warming up the magnet. It is not clear why the purging can't be performed during installation of the system when the helium lines can be vacuum pumped. After this the cryogenic system can be purged by helium from the cryoplant.

4.3 Design of the Branch Box and the transfer line

The destination of the Branch Box is to supply He gases the CBM and the HADES detectors. All cryogenic operations of these detectors should be performed independently. So, the scheme and the placement of the cryogenic valves in the Branch Box should have symmetry, as it is shown on the cryogenic diagram, Fig. 78. The helium goes from the local cryoplant and after the Branch Box it may go ever to CBM detector ever to the HADES. The return lines of the Branch Box will have sensors of temperature and pressure for controlling parameters of helium. In case of improper parameters of helium the return gas will go to the multipurpose line.

The design of the Branch Box is shown on the Fig. 80.

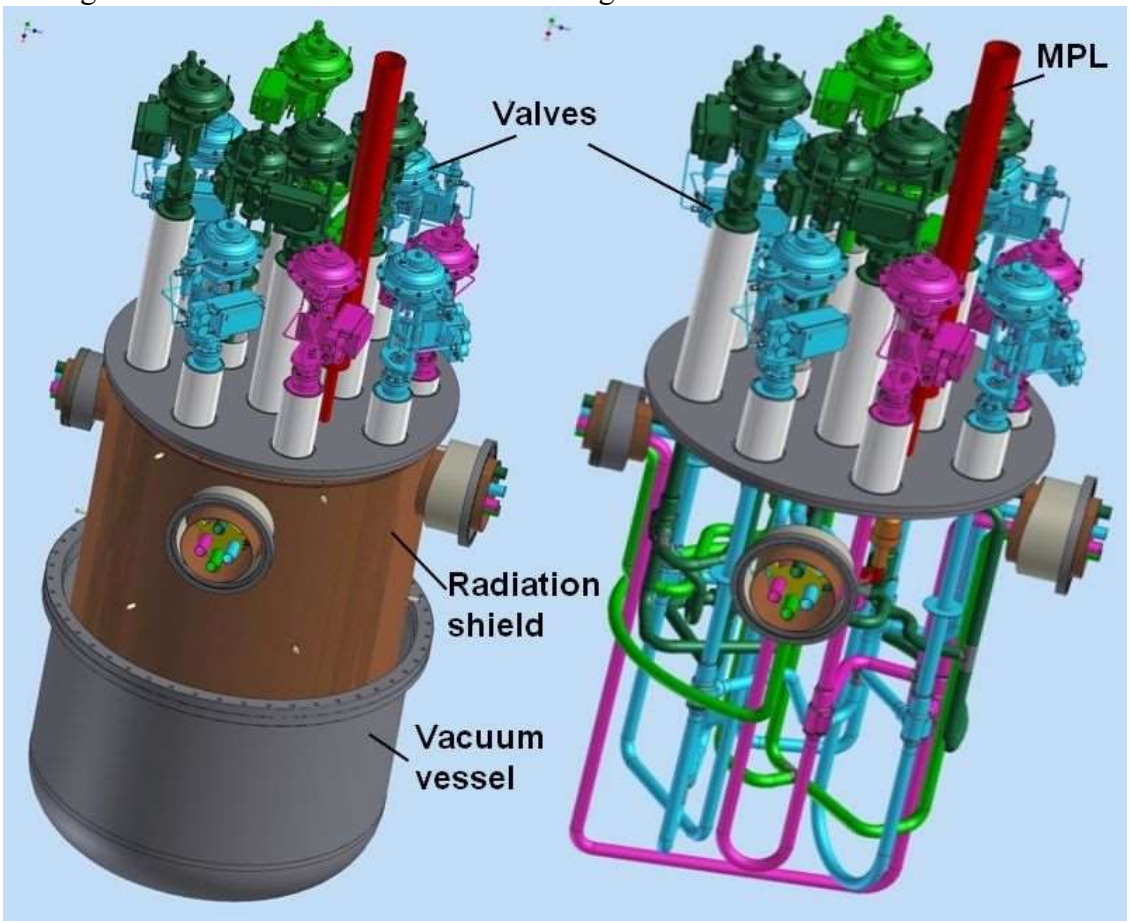

Fig. 80. The preliminary design of the Branch Box. MPL – multipurpose line.

The vacuum volume of the CBM and the HADES cryogenics should be separated around the vacuum vessel of the Branch Box, as stated above. The vacuum ports and measurements flanges should be foreseen.

The common design of the transfer line is shown on the Fig. 81. Details of the thermal contraction compensators are not shown. The design of the separator may be changed to have specific separator for the 50 K tubes and specific separator for the 4.6 K tubes.

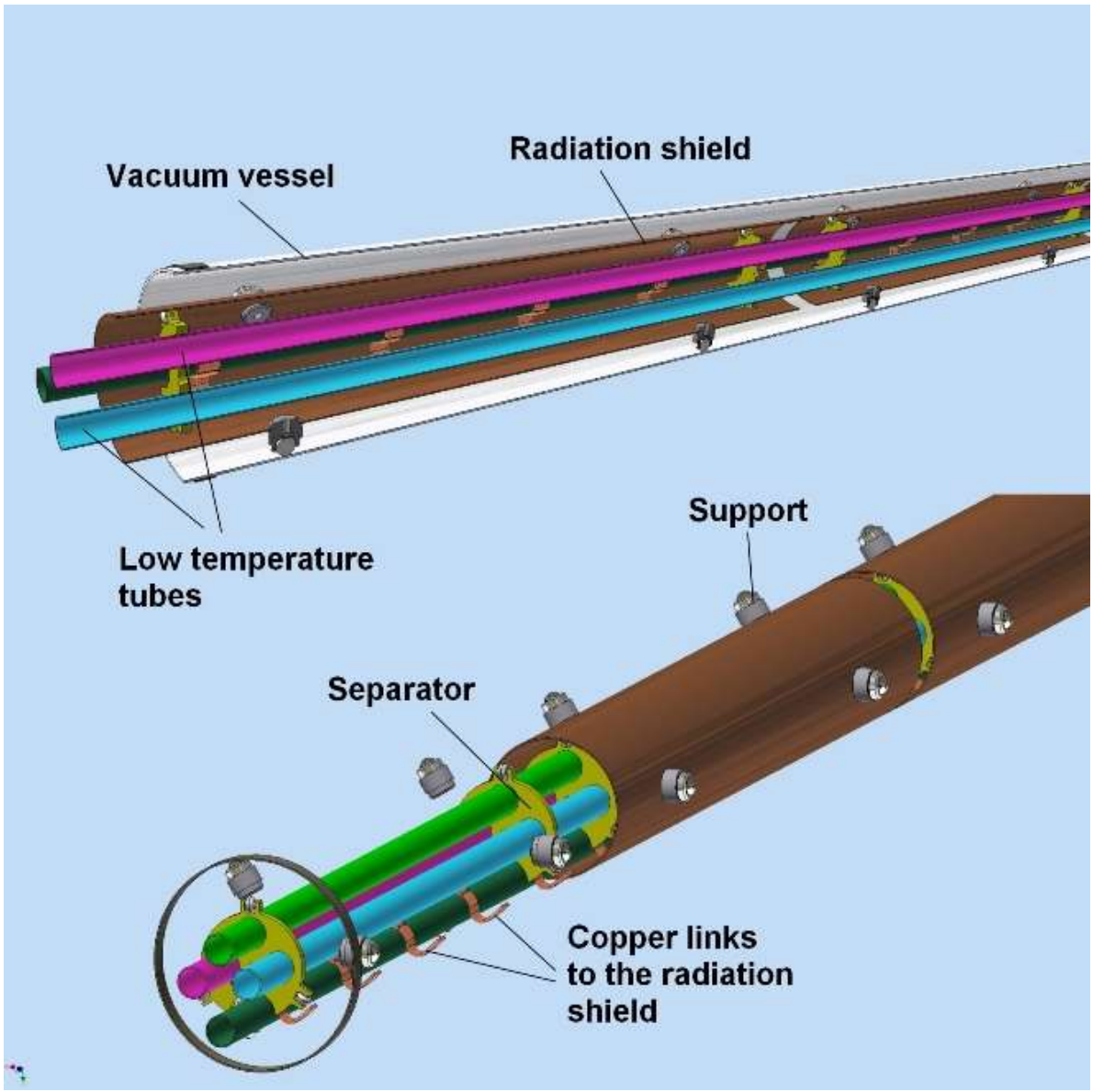

Fig. 81. The design of the transfer line.

4.4 Estimations of pressure drops and heat transfer

These estimations will determine a diameter of a pipe and a mass flow rate for the transfer pipes from the Branch Box to the cryostat and will evaluate the needed mass flow rate for the heat transfer. The pressure drop along the transfer line should be much less than 0.1 bar at ordinary operation of the CBM magnet.

Pressure drop of isothermal gas along a pipe can be evaluated by the following formula:

$\Delta p = \xi \frac{v^2 \rho}{2} \cdot \frac{L}{d}$, where ρ - density, v – velocity, L and d – length and diameter of a pipe, ξ - friction coefficient. Addition pressure drop appears due to acceleration of gas heated along a pipe – not considered here.

With a mass flow rate $G = v*\rho*d^2*\pi/4$ it will be more convenient:

$\Delta p = \xi \frac{8G^2}{\pi^2 \rho} \cdot \frac{L}{d^5}$.

Reynolds number $\mathrm{Re} = \frac{4G}{\pi d \eta}$ determines the flow mode, where η - viscosity [Pa*s].

At turbulent flow, when Re = $2.3*10^3 \div 10^5$, the friction coefficient is calculated as $\xi = \frac{0.316}{\mathrm{Re}^{0.25}}$.

The input parameters of the pipe are inner diameter ID = 15.8 mm and the length of the pipe L = 120 m. The length of the pipe includes the length itself and additional length from the valves, and bellows parts. The parameters of helium at various temperature and pressure are listed in the Table 15 that will be used in the following estimations.

For the 4.6 K helium lines at G = $1.7*10^{-3}$ kg/s we have:

$$\mathrm{Re} = \frac{4G}{\pi d \eta} = \frac{4 \cdot 1.7 \cdot 10^{-3}}{\pi \cdot 0.0158 \cdot 3.4 \cdot 10^{-6}} = 40000 \text{ – turbulent flow.}$$

Friction coefficient $\xi = \frac{0.316}{\mathrm{Re}^{0.25}} = 0.022.$

Pressure drop: $\Delta p = \xi \frac{8G^2}{\pi^2 \rho} \cdot \frac{L}{d^5} = 0.022 \cdot \frac{8 \cdot 2.89 \cdot 10^{-6}}{\pi^2 \cdot 128} \cdot \frac{120}{0.0158^5} = 49$ Pa = 0.00049 bar.

In the ordinary operation the pressure drop along the transfer lines is very low.

For the 50 K helium lines at G = $1.8*10^{-3}$ kg/s we have:

$$\mathrm{Re} = \frac{4G}{\pi d \eta} = \frac{4 \cdot 1.8 \cdot 10^{-3}}{\pi \cdot 0.0158 \cdot 7.4 \cdot 10^{-6}} = 20000 \text{ – turbulent flow.}$$

Friction coefficient $\xi = \frac{0.316}{\mathrm{Re}^{0.25}} = 0.027.$

Pressure drop: $\Delta p = \xi \frac{8G^2}{\pi^2 \rho} \cdot \frac{L}{d^5} = 0.027 \cdot \frac{8 \cdot 3.24 \cdot 10^{-6}}{\pi^2 \cdot 14} \cdot \frac{120}{0.0158^5} = 617$ Pa = 0.006 bar

In the ordinary operation the pressure drop along the transfer lines is also very low.

Heat transfer between helium and tubes for cooling

The return helium at 50-70 K of temperature should cool the heat in leaks presented in the Table 10 and Table 12. The temperature differences should be estimated between the helium and the cooling tubes of radiation shields in all components of the CBM magnet cryogenics.

The heat transfer between the helium and the pipe wall is estimated as:

Q = αS*ΔT, where α - heat transfer coefficient, S – heat transfer surface, ΔT – temperature difference between helium and a pipe wall.

The heat transfer coefficient is estimated as $\alpha = \frac{\lambda \cdot \mathrm{Nu}}{d}$, where λ - thermo conductivity coefficient of helium, Nu – Nusselt number, d – inner diameter of a tube.

The reduced heat transfer coefficient may be taken into account if tube wall is thick and has low thermal conductivity (w – wall parameters):

$\frac{1}{\alpha_r} = \frac{1}{\alpha} + \frac{h_w}{\lambda_w}$, where h_w – wall thickness.

For turbulent flow Nusselt number is estimated as: $\mathrm{Nu} = 0.023*\mathrm{Re}^{0.8}\mathrm{Pr}^{0.33}$, where $\mathrm{Pr} = \frac{\eta c_p}{\lambda}$ - Prandtl number, where c_p – heat capacity.

For 60 K helium Nu = 56, so $\alpha = \frac{0.055 \cdot 56}{0.0158} = 195$ W/(m²*K).

Heat load for one coil from support struts and the radiation shield is about Q = 25 W. The cooling

tube going around the radiation shield has cooling surface $S = \pi d*L = 3.14*0.0158*5 = 0.25$ m^2. So, the temperature difference between helium and tube wall will be:

$\Delta T = Q/\alpha S = 25/(195*0.25) = 0.5$ K.

The cooling helium will be heated, its temperature can be estimated as:

$Q = G*c_p*\Delta T_h$, then $\Delta T_h = Q/(G* c_p) = 25/(1.8*5.3) = 2.6$ K. So, helium entering the lower coil at 50 K will go to the upper coil at temperature 52.6 K that is acceptable.

Table 15. Parameters of helium at given T and p.

T, K	**p, MPa**	**ρ, kg/m^3**	**λ ,W/(m*K)**	**10^{-6} μ, Pa*s**	**h, kJ/(kg)**	**Pr**
4.6	0.1	13.6 (20 at 1.3)	0.009	1.3	33.5	1.15
4.6	0.2	121.5	0.02	3.2	11.8	
4.6	0.3	127.8	0.02	3.4	11.9	
4.5	0.1	14.2	0.009	1.25	32.7	1.15
4.5	0.2	124.2	0.019	3.2	11.2	
4.5	0.3	129.8	0.02	3.4	11.4	
50	1.0	9.5	0.048	6.5	266.1	
50	1.5	14.0	0.049	6.6	275.3	
50	2.0	18.4	0.05	6.7	275.8	
60	1.0	7.9	0.054	7.3	318.5	
60	1.5	11.7	0.055	7.35	328.3	
60	2.0	15.4	0.055	7.4	329.1	0.69
70	0.1	0.7	0.058	7.83	369.0	
70	1.0	6.8	0.059	7.0	371.0	
70	1.5	10.0	0.060	8.0	380.9	
70	2.0	13.3	0.061	8.1	381.9	
80	1.0	6.0	0.065	8.7	423.2	
80	1.5	8.8	0.065	8.7	433.4	
80	2.0	11.7	0.066	8.8	434.5	
100	0.1	0.48	0.074	9.8	534.3	0.67
100	0.2	0.96	0.074	9.8	534.5	
100	1.5	7.1	0.075	10.0	537.8	
100	2.0	9.4	0.076	10.0	539.1	
140	0.1	0.34	0.093	11.9	742.1	
140	0.2	0.69	0.093	11.9	743.3	
140	1.5	5.1	0.094	12.1	746.0	
140	2.0	6.7	0.094	12.1	747.5	
200	0.1	0.24	0.118	15.1	1053.7	0.67
200	0.2	0.48	0.118	15.1	1054.0	
200	1.5	3.57	0.119	15.3	1057.8	
200	2.0	4.75	0.120	15.3	1059.3	
240	0.1	0.2	0.134	17.1	1261.4	
240	0.2	0.4	0.134	17.1	1261.7	
240	1.5	3.0	0.135	17.2	1265.5	
240	2.0	4.0	0.135	17.2	1267.0	
273	0.1	0.175	0.146	18.6	1423.2	
273	0.2	0.35	0.146	18.7	1423.6	

4.5 Operation modes of the CBM magnet cryogenics

The cryogenic system of the CBM magnet should work at the following operating conditions:
- cooling down the system during two weeks;
- ordinary operation of cooled magnet at 4.5 K;
- warming up of the magnet for demanded time;
- quench recovery.

Cooling down of the system

The biggest cold mass of the system is the superconducting magnet having about 3.6 tonnes and the internal energy is about 320 MJ. The rest cold components of the cryogenic system will be cooled down much faster and may be not considered here. Three stages of the cooling down will be proposed:
- first stage – the magnet is cooled to ~ 200 K;
- second stage – the magnet is cooled to ~ 80 K;
- third stage – the magnet is cooled to 4.5 K – operating conditions.

First stage – cooling down to ~ 200 K

Before cooling down, the system should have vacuum in the range $10^{-2} \div 10^{-3}$ Pa. The vacuum pump will be attached by the cryostat where it will have effective pumping capacity of about 500 l/s.

For cooling a magnet from room temperature to ~ 200 K one needs to take off about 50% of the internal energy. In our case it will be 160 MJ and the cooling time is 48 hours. So, the desired cooling capacity is 930 W.

It is assumed in the TDR that the cooling rate should be about 2 K/hour, the high cooling rate may lead to high mechanical stress inside the superconducting structure. From another hand, if a magnet is cooled uniformly this rate may be higher. If firstly the radiation shields of the coils will be cooled down to about 200 K the heat transfer via radiation and support struts conduction will take place. The effect of these factors can be estimated as follows.

The cooling by the radiation shields is

$Q = \varepsilon S \sigma (T^4 - 200^4)$ where ε - total emissivity was taken as 0.06, S – surface area of the two outer surfaces of the coils is 8.5 m^2, T – magnet temperature.

The results are Q = 85 W for T = 260 K, and Q = 21 W for T = 220 K.

The cooling by the support struts via G-10 elements is estimated as:

$Q = \lambda S^* \Delta T / L$, where λ - thermal conductivity was taken as 0.8 W/(m*K), S – cross-section area of one support is 9.1^*10^{-3} m^2, ΔT – temperature difference was taken as 100 K, L – length is about 0.16 m.

The result is Q = 55 W for ΔT = 100 K on the length of the support struts.

So, the cooling down the shields only will give cooling capacity from ~150 W at the beginning to about 50 W in the first stage.

BINP proposes to control the cooling process by measuring the temperature difference in the winding structure in order to be less than 10 K during the cooling down process. This is direct way for controlling the safe conditions during the cooling down process. The cooling diagram is shown on the Fig. 82.

Cooling to ~ 80-100 K

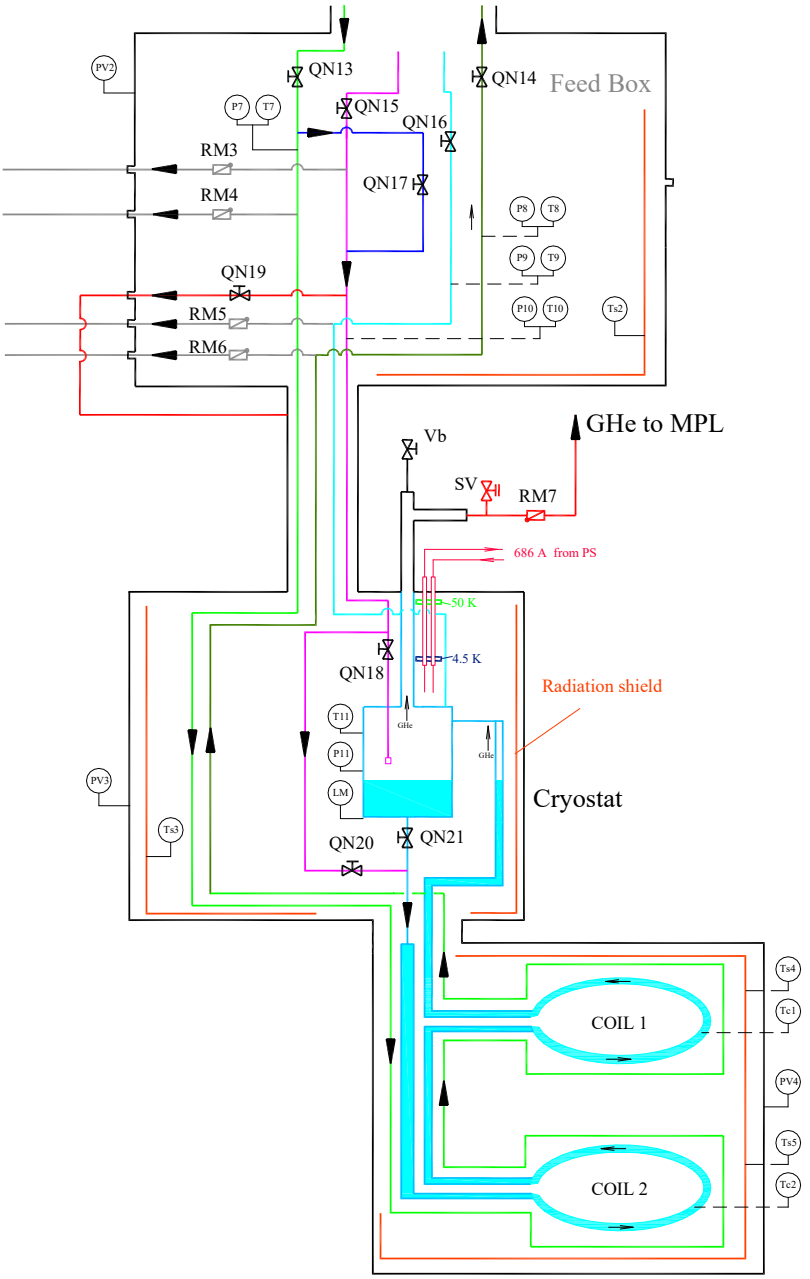

Fig. 82. The diagram of the cooling down procedure of the first and the second stages. The arrows show the helium running helium. The closed valves are QN15, QN16, QN18, and QN21. The open valves are QN17, QN20, RM7.

The coils are cooled by helium from 50 K line. The flow is divided between shields and coils by the QN13 and QN17 valves. The mass flow rate of 0.9 g/s value or lower is enough in this stage.

The cooling helium has large cooling capacity due to high heat transfer coefficient, big cooling surface ~ 1.5 m^2 for every coil, even taking into account reduced heat transfer coefficient due to presence of G-10 around the coil.

The cooling is controlled by thermal sensors which are shown on the Fig. 82. If the temperature difference became more than 10 K the helium flow may be decreased by closing the QN13 valve. Temperature difference in solid body is dissipated with characteristic time as:

$t = \frac{C_v \cdot \langle L \rangle^2}{\lambda \cdot \pi^2}$, where C_v – volumetric heat capacity, λ - thermal conductivity, L – characteristic length of temperature difference. In the first stage of cooling down this time is about one hour.

The estimations of helium efficiency during cooling down

During cooling down of the coils from room temperature, the forced flow of 50 K helium will be used. The mass flow rate *G* is expected in the range from 0.2 g/s to 2 g/s depending on the decreasing temperatures of the coils.

The cooling helium will be warmed up while passing through the cooling tubes. The estimations are based upon average temperature of the helium Tav.

At Tav = 150 K and G = $1*10^{-3}$ kg/s (about 30 l/h) we have:

$$\mathrm{Re} = \frac{4G}{\pi d \eta} = \frac{4 \cdot 1 \cdot 10^{-3}}{\pi \cdot 0.0158 \cdot 1.2 \cdot 10^{-5}} = 6720$$ – turbulent flow.

Cooling capacity of flowing helium at G = $1*10^{-3}$ kg/s is **Qc** = G*Δh, where Δh – is the enthalpy difference.

For helium between the 50 K and 273 K it will be Δh = 1148 J/g. So the Qc = 1148 W. So, G= $1*10^{-3}$ kg/s is more than needed at the beginning of cooling.

For helium between the 50 K and 100 K it will be Δh = 259 J/g. So the Qc = 259 W. So, the cooling capacity of the helium decreases faster the decreasing of specific heat capacity of solid materials. One should expect increasing the mass rate in order to keep the fact cooling rate of the magnet, about 2 K/h.

The heat transfer between the helium and the pipe wall is estimated as:

$\mathbf{Q_{ht}} = \alpha S*\Delta T_{hw}$, where α - heat transfer coefficient, S – heat cooling tube about 0.25 m^2, ΔT_{hw} – temperature difference between helium and the cooling tube wall.

The heat transfer coefficient is estimated as: $\alpha = \frac{\lambda \cdot Nu}{d}$, where λ - thermo conductivity coefficient of helium, Nu – Nusselt number, d – inner diameter of a tube.

For turbulent flow Nusselt number is estimated as: $Nu = 0.023*Re^{0.8}Pr^{0.33}$, where Pr - Prandtl number which is almost always 0.67 in the T> 50 K. For Tav = 150 K it will be Nu = 23.

For 140 K helium Nu = 23, so $\alpha = \frac{0.093 \cdot 23}{0.0158} = 135$ W/(m^2*K).

$Q_{ht} = \alpha S*\Delta T_{hw} = 135*0.25*\Delta T_{hw} = 33.8*\Delta T_{hw}$, so the heat transfer rate is very high, as the ΔT_{hw} will be more than 30 K at the first stage of cooling down. The values of $\mathbf{Q_{ht}}$ should be compared with $\mathbf{Q_c}$. The helium will go out of the tube with temperature very close to the temperature of the cooling tube wall.

The heat transfer between the helium and the cooling tube of the coils is high, so the helium going out of the lower coil will be warmed very effectively. The upper coil will be cooled by this "warm" helium at the beginning of cooling down regime.

Second stage – the magnet is cooled to ~ 80 K

The cooling diagram in this stage is the same. In the controlling process one needs to increase the mass flow if the cooling down rate becomes too slow due to decreasing of temperature difference between the coil and the cooling helium. The extracted energy in this stage is about 40% from original 160 MJ.

Third stage – the magnet is cooled to 4.5 K

In this stage the line of 4.6 K helium will be used. In is assumed that the line itself already has a temperature not high than 60 K as it was surrounded by operating 50 K lines. The cooling starts with closing QN17 valve and opening QN15 valve.

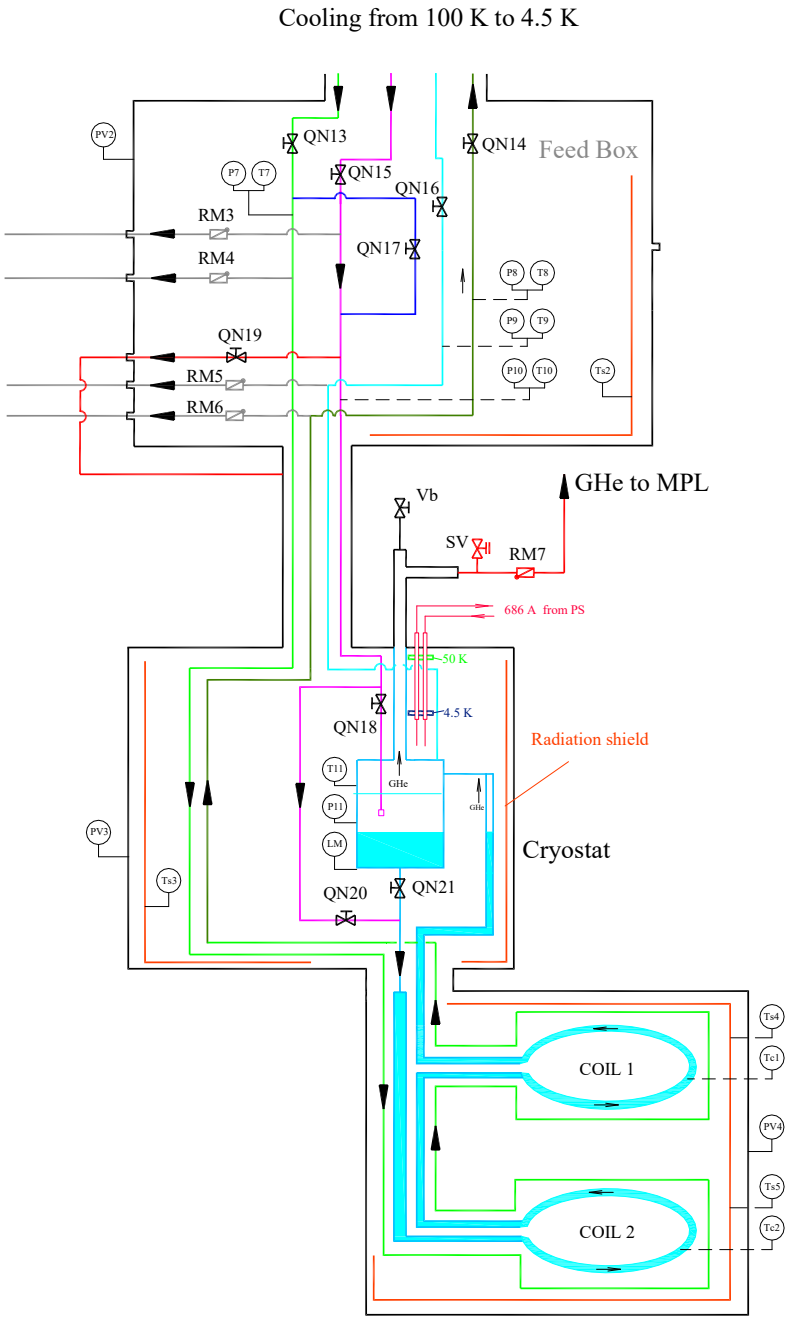

Fig. 83. The diagram of the cooling down procedure of the third stage. The closed valves are QN17, QN20, RM7. The open valves are QN15, QN16, QN18, and QN21.

At the end of the cooling when liquid helium starts accumulating on the lower coil one may close QN20 valve and open QN18 and QN21 valves, then liquid helium will fill the cryostat. The moment of liquid helium accumulation in the low coil may be detected by pressure drop in the cryostat on P11 manometer.

On should find a moment when to close RM7 valve and open QN16 valve.

Total cooling down time will be about 8 days.

Ordinary operation of the cooled magnet at 4.5 K

In the ordinary operation of the cryogenic system the helium flows will be as shown on the Fig. 78. Some part of gaseous helium will go through the current leads; its flow will be controlled by a heater installed in the cryostat.

The liquid helium level will be measured by installed LHe level meter.

One of the possible scenarios of LHe level controlling is to operate at insufficient flow of helium by controlling of QN15 valve, i.e. 1.5 g/s instead of demanded 1.7 g/s of flow rate. When the LHe level becomes too low then the QN18 will be opened to supply 1.8 g/s rate until demanded level of helium in the cryostat.

Warming up of the magnet for demanded time

For accelerated warming up the 300 K line of helium is installed to the Feed Box. This process will be conducted on the same principle as in the cooling down in the first and the second stages. The supply of 50 K helium should be shut. After increasing the lowest temperature in the cryogenic system beyond 27-28 K the vacuum pressure will be increased rapidly.

As a proposal, a number of heaters may be installed on the cold mass of the magnet to give power 200-400 W. Additional power will come from heat transfer between the radiation shields and the magnet due to radiation and gases of vacuum volume. This power will be greater than from the proposed heaters.

Quench recovery

If quench had occurred then the QN15 and QN16 valves should be closed. The rising pressure in the cryostat will open RM7 valve to the multipurpose line. Liquid helium in the cryostat will not go down to the coils. The highest pressure in the system will be not more than 3 bar due to little amount of stored liquid helium in the system.

In the worse case of quench, when the stored energy is fully dissipated in one coil – this coil after a quench will be slowly cooled from ~ 90 K to ~ 50 K due to heat transfer between the winding and the heavy stainless steel plate. After this the cooling down procedure will go as in the third stage of cooling down the magnet.

4.6 Safety analysis

The LHe vessel will be tested and certified by TUV after being manufactured.

Very high pressure may be in the LHe vessel in case of a quench in the magnet or any break of insulating vacuum when air or even helium can leak inside the vacuum volume. This pressure can be estimated as follows. It is assumed that the cryostat is equipped with relief valve allowing helium to go into the multipurpose line.

Formula for pressure buildup in the cryostat:

$\Delta p = \xi \frac{8G^2}{\pi^2 \rho \cdot Y^2} \cdot \frac{L}{d^5}$, where Y – expansion correction coefficient, about 0.8; the rest parameters are the same as for the pressure drop.

The mass rate G is determined by external heat flow to the helium in the coil. Typical heat transfer coefficient is about 10^3 W/(m^2*K) that can be found in literature. It may be reduced by a factor of 2 because heat transfer going through G-10 insulation (quench case) or thick wall of stainless steel (vacuum break). So, the heat flux to helium can be q = 5000 W/m^2 at temperature difference about 10 K – film boiling. The heat transfer surface is about 1.5 m^2 in one coil case. So, total heating power can be about Q = 5000*3 = 15 kW. The mass rate is determined as G = Q/Δh, where Δh – latent heat, about 21 J/g. The length of the pipe is about 3 m, diameter was chosen 0.03 m. G = 0.714 kg/s.

$\Delta p = 0.03 \frac{8 \cdot 0.714^2}{\pi^2 14 \cdot 0.64} \cdot \frac{3}{0.03^5} = 1.7*10^5$ Pa = **1.7 bar**. This is maximal overpressure in the cryostat during a quench at condition that helium goes out through the cryostat neck to the multipurpose line.

It is worth to note that LHe volume in both coils will be not more 30 l, i.e. total mass is 30*124 = 3.7 kg. It means that at given mass rate all liquid helium will go out after 5 s. This time is comparable with the current decay during a quench; it means that helium will start to go out at lower pressure.

The estimated mass flow rate is by a factor of 400 larger than the rate supplied from the cryoplant. The control valves may be closed during several seconds, no problems here seen.

Thermal oscillation may happen in the cryogenic system at various stages of operation. The simple thermal oscillations criteria can be used in designing the system, see Fig. 84.

Characteristic radius is calculated as: $R^*_c = r_0 \cdot \left(\frac{a}{\nu \cdot L} \right)^{1/2}$, where r_0 - tube radius, a - acoustic velocity, m/s, ν - kinematic viscosity, L - length of the pie.

$a = (\gamma \cdot R \cdot \bar{T})^{1/2} = (1.67 \cdot 2078 \cdot 20)^{1/2} = 263.4$ m/s for helium.

$\nu = \eta / \rho$

Another parameter is $\alpha = \frac{T_h}{T_c}$ - ration of warm end of a pipe to cold end of the pipe.

The stability region is at low values of given parameters $R^*_c < 8$ and $\alpha < 6$.

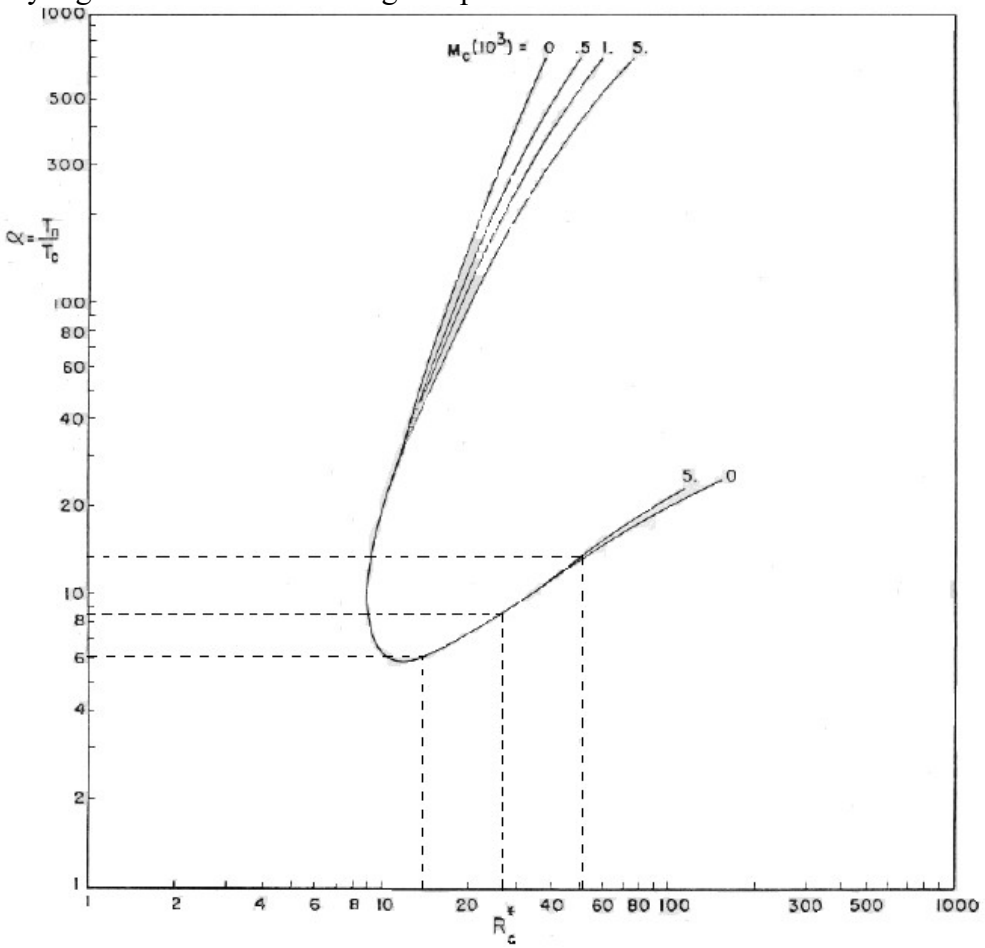

Fig. 84. The graph for the thermal oscillations criteria taken from [J.A. Liburdy].

This criteria show that thermal oscillations will mostly occur during cooling down of the cryogenic system.

Mitigation of faulty fast cooling down

Too fast cooling down may happen in case if the control valves QN17 or QN20 will be fully opened by mistakes of an operator or control code. These valves are placed in by-pass line which diameter can be minimized to the needed only for slow cooling down. The inner diameters of the valves also will be minimal.

5. Assembling of the iron yoke and the coils

The iron yoke should be assembled at least three times: manufacturing plant, BINP site and GSI site. The iron yoke has geodetic platform, geodetic holes and mounting brackets for assembling with demanded accuracy and for alignment procedures, Fig. 85.

The alignment of the magnet will be realized via: 100 t jacks for vertical movements and the gimbals for horizontal movements and rotations.

The magnet assembling steps are shown on the Fig. 87.

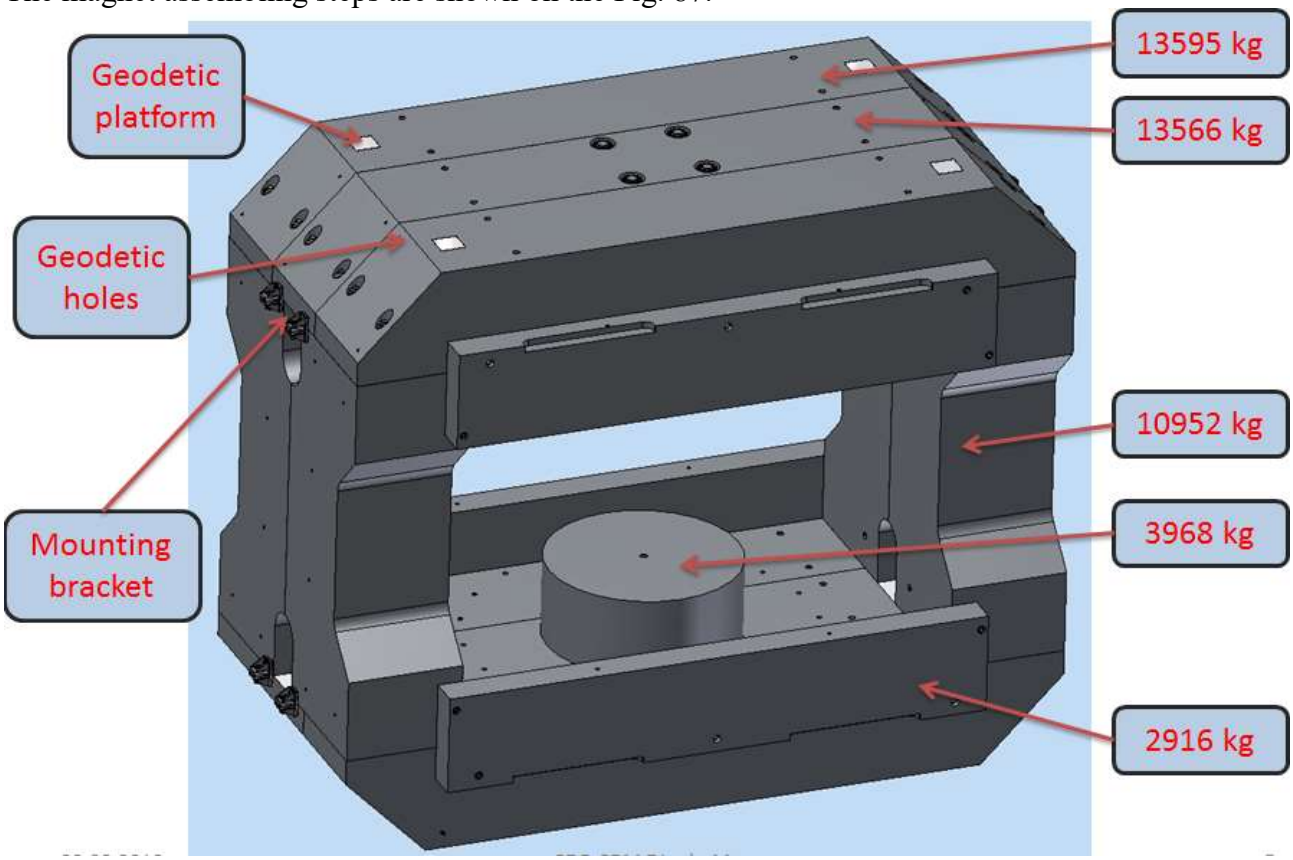

Fig. 85. The iron yoke details.

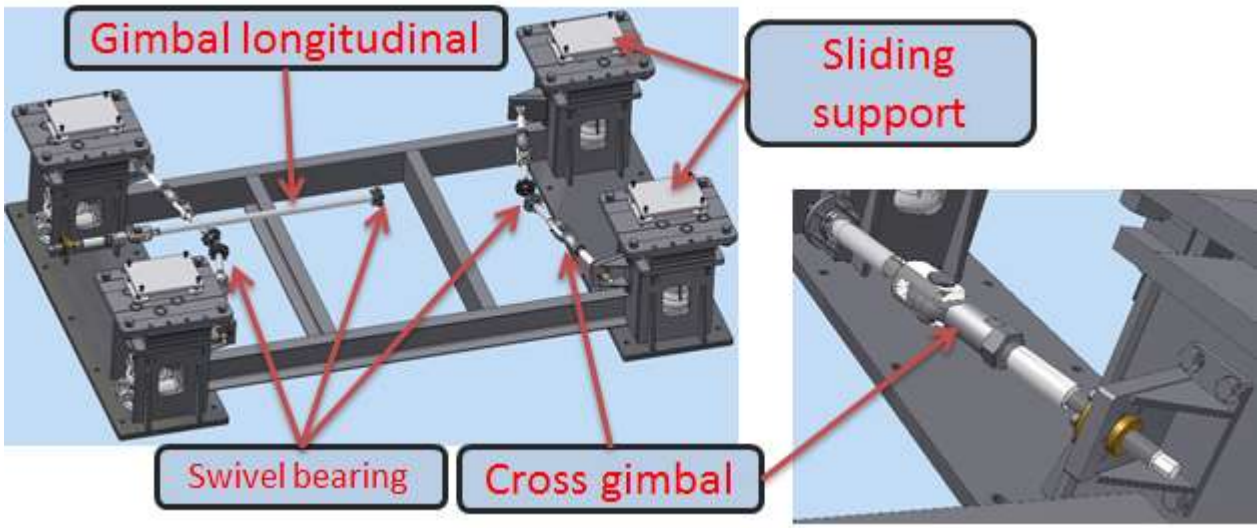

Fig. 86. The support elements for alignment.

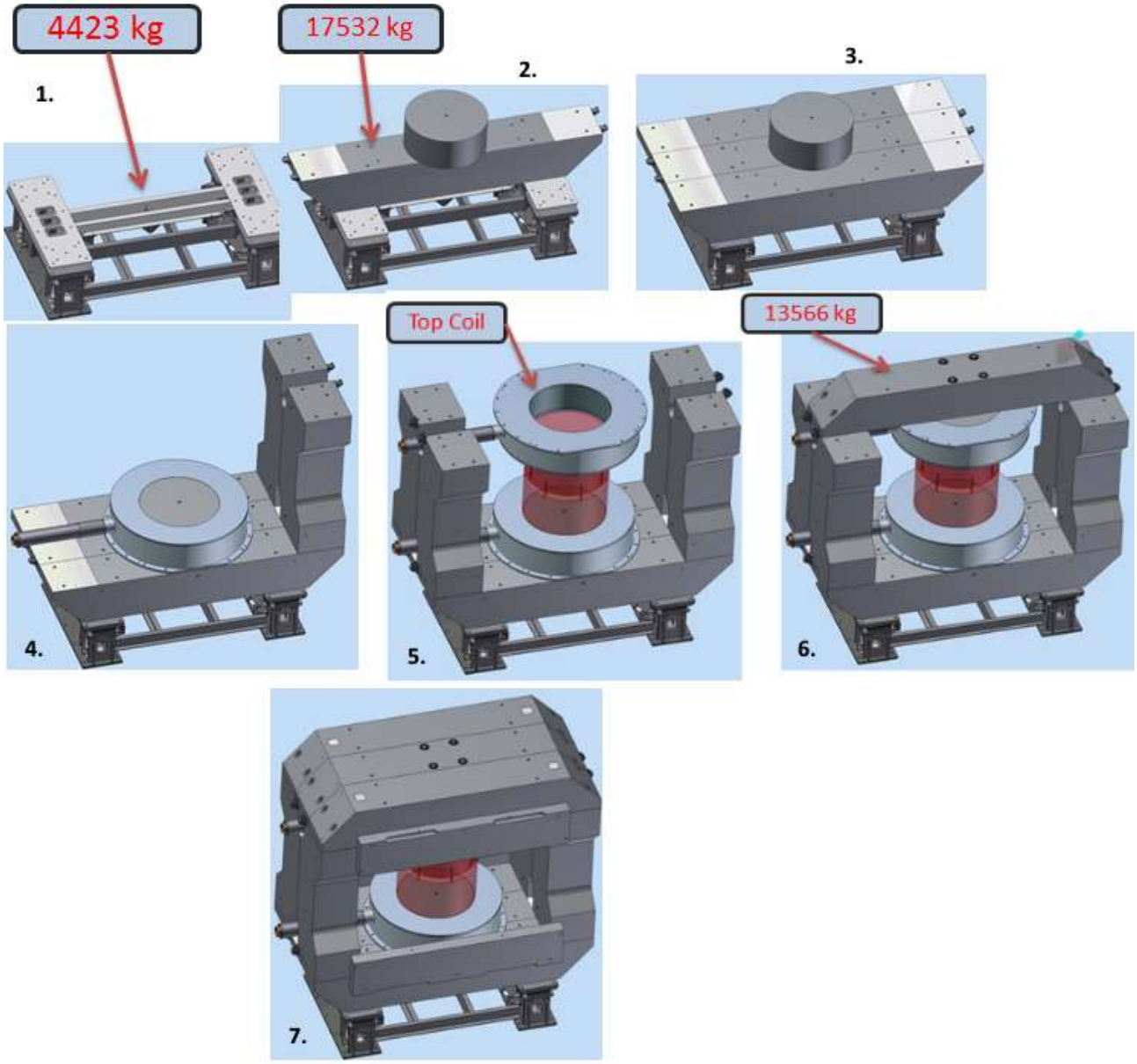

Fig. 87. The assembling steps of the CBM magnet.

6. BINP tests of the CBM magnet (FAT)

The BINP does not have such cryogenic station to provide helium with parameters as of the CBM magnet. Currently it proposed to cool the CBM magnet with liquid helium directly into the cryostat and the radiation shields will be cooled by liquid nitrogen. In this case heat loads to the magnet will be increased.

Quench heaters for quench demonstration should be installed or by interruption of helium cooling?

7. General conclusions finishing CDR work

1. The conceptual design of the CBM magnet including the coil and the cryostat is presented.
2. Magnetic fields calculations were done in ANSYS and Mermaid 3D codes. The main magnetic parameters are satisfied. The magnetic field integral is higher by ~ 1%. The coil design was changed to have 1716 turns, 52 layers and operating current of 666 A.

3. Mechanical calculations of the superconducting coil were presented. The current design satisfies general requirements to superconducting magnets. The support struts design may be improved. The final decision on the support struts design should be taken during the PDR meeting.

4. The quench behavior calculations were presented. The magnet is safe in any quench scenario.

5. Cryogenics of the CBM magnet is described. The thermosyphon cooling estimation was done. The final design of the current leads and the bus bar will be discussed during PDR meeting.

6. The superconducting cable was manufactured. Up to March 2020 it will be insulated.

7. The contract for the iron yoke manufacturing with subcontractor was signed. Some iron yoke changes can be made up to November 2019.

8. References

1. Collaboration Contract CBM-Magnet BINP Annex3 - Technical specifications, 2016.

2. Technical design report

3. M. Wilson, Superconducting magnets

4. Y. Iwasa, Case studies in superconductivity

5. Thermodynamical properties of helium, Sychev V.V. et al, 1984.

6. J.A. Liburdy, J.L. Wofford «Acoustic oscillation phenomena in low-velocity steady flow with heating», Advances in Cryogenic Engineering, 1980, Vol. 25, p. 528.

7. M.A. Green “Quench back in thin superconducting solenoid magnets”. Cryogenics, 1984, Vol. 24, n. 1, p. 3, *and* M.A. Green “The role of quench back in quench protection of a superconducting solenoid”. Cryogenics, 1984, Vol. 24, n. 12, p. 659.

8. Cryogenic data handbook, 1980.

9. J. Weisend “Handbook of cryogenic engineering”, 1998.

10. Yu. Solntsev, “Materials for low and cryogenic temperatures”, S.-Peterburg, 2008 (in Russian).

11. V.P. Beliakov “Cryogenic technique and technology”, Moscow, 1982 (in Russian).

12. H. Furci, A. Four, B. Baudouy “Experimental study of stability and transients in a horizontally heated boiling helium thermosyphon” Materials Science and Engineering 101 (2015) 012062.

13. Baudouy Bertrand, Bessette Anne, Four Aurélien “Modeling of a horizontal circulation open loop in two-phase helium”, Cryogenics 53 (2013) 2–6.

14. Ken-ichi Tanaka, et al “Cryogenic Design of the ATLAS Thin Superconducting Solenoid Magnet”, p.119-122.

15 P.G.Akishin, Yu.V. Gusakov, A.V. Bychkov, P.K. Kurilkin, and V.P. Ladygin “ANSYS and TOSCA calculations for new design of the CBM superconducting dipole magnet”, Dubna report, 2017.